Electronic Supplementary Material (ESI) for ChemComm.

Supporting Information for:

Facile PCET enabled by coordination-induced E–H bond weakening to a redox-active boron center (E = N, O, S)

Anthony Wong,[a] Arunavo Chakraborty,[a] Deependra Bawari,[b] Guang Wu,[a] Roman Dobrovetsky[b] and Gabriel Ménard*[a]

[a] Department of Chemistry and Biochemistry, University of California, Santa Barbara, California 93106, United States

[b] School of Chemistry, Raymond and Beverly Sackler Faculty of Exact Sciences, Tel Aviv University, Tel Aviv 69978, Israel

Table of Contents

1. Materials and Physical Methods

General Considerations. All manipulations were performed under an atmosphere of dry, oxygen-free N_2 or Ar through standard Schlenk or glovebox techniques (MBraun UNIlab Pro SP Eco equipped with a -38 °C freezer). Pentane, diethyl ether, benzene, toluene, tetrahydrofuran (THF), and dichloromethane (DCM) were dried using an Mbraun solvent purification system. 2,2,4-trimethylpentane (iso-octane), acetonitrile, acetonitrile-*d₃*, benzene-*d*₆, bromobenzene, bromobenzene-*d₅*, chloroform, chloroform-*d*, and dichloromethane-*d₂* were purchased from Aldrich or Cambridge Isotope Laboratories, degassed by freeze-pump-thaw, and stored on activated 4 Å molecular sieves prior to use. Anhydrous NH_3, NH_3 (0.4 M in THF), HCl (2.0 M in Et_2O), $PhNH_2$, C_6F_5OH, PhSH, 4,7,13,16,21,24-hexaoxa-1,10-diazabicyclo[8.8.8]hexacosane (Kryptofix-222 = krypt), and TEMPO were purchased from Aldrich, Strem, or other commercial vendors and used as received. $Co(C_5Me_5)_2$ was purchased from Aldrich and filtered through celite using pentane and then freshly crystallized from pentane prior to use. $[CoCp^*_2][(N(CH_2CH_2N(C_6F_5))_3)V(\mu\text{-}N)B(C_6F_5)_2]$ (**1**$^-$), $N(CH_2CH_2N(C_6F_5))_3V(\mu\text{-}N)Li(THF)_3$ (**VNLi**), Gomberg's dimer, and benzyl potassium (KBn) were prepared according to literature procedure.[1-4] Elemental analyses (C, N, H) were performed at the University of California, Berkeley, using a PerkinElmer 2400 Series II combustion analyzer.

Spectroscopic Analyses. NMR spectra were obtained on a Varian Unity Inova 600 MHz, Varian Unity Inova 500 MHz, Bruker Avance NEO 500 MHz, Bruker Avance III HD 400 MHz, or Agilent Technologies 400 MHz spectrometers, and referenced to the residual solvent of acetonitrile-*d₃* (1.94 ppm), benzene-*d*₆ (7.16 ppm), bromobenzene-*d₅* (7.28 ppm for *m*-CH), chloroform-*d* (7.26 ppm), dichloromethane-*d₂* (5.32 ppm), or externally (^{11}B: $BF_3{\cdot}Et_2O$; ^{19}F: $CFCl_3$; ^{51}V: $VOCl_3$; ^{31}P: 85% H_3PO_4). Chemical shifts (δ) are recorded in ppm, and the coupling constants are in Hz.

X-ray crystallography. Data were collected on a Bruker KAPPA APEX II diffractometer equipped with an APEX II CCD detector using a TRIUMPH monochromator with a Mo Kα X-ray source (α = 0.71073 Å). The crystals were mounted on a cryoloop with Paratone-N oil, and all data were collected at 100(2) K using an Oxford nitrogen gas cryostream system. A hemisphere of data was collected using ω scans with 0.5° frame widths. Data collection and cell parameter determination were conducted using the SMART program. Integration of the data frames and final cell parameter refinement were performed using SAINT software. Absorption correction of the data was carried out using SADABS. Structure determination was done using direct or Patterson methods and difference Fourier techniques. All hydrogen atom positions were idealized and rode on the atom of attachment. Structure solution, refinement, graphics, and creation of publication materials were performed using SHELXTL or OLEX2. All POV-Ray depictions of the solid-state molecular structures are shown at the 50 % probability ellipsoid level unless otherwise noted.

Electrochemical Analyses. Cyclic voltammetry was performed on a CH Instruments 630E electrochemical analysis potentiostat, equipped with a 3 mm diameter glassy carbon working electrode, a Ag wire pseudoreference electrode, and a Pt counter electrode with $[Bu_4N][PF_6]$ (0.1 M) supporting electrolyte solution in acetonitrile (CH_3CN). The glassy carbon working electrode was cleaned prior to each experiment by polishing with 1, 0.3, and 0.05 mm alumina (CH Instruments) in descending order, followed by sonication in distilled water for 2 min. All voltammograms were referenced to the Fc/Fc^+ redox couple.

GC-TCD. The headspace from the reactions of **1**$^-$ and PhSH or **1**$^-$ and C_6F_5OH were sampled with a gas-tight syringe and analyzed using an Agilent 6890N GC with a CP Molsieve 5Å column (50 m long, 0.53 mm OD) equipped with a TCD detector to qualitatively test for H_2 formation from these reactions. High purity argon (99.998%) from Praxair was used as the eluent.

Method parameters used for the GC-TCD runs are below.

Parameter	**Value**
Inlet mode	Splitless
Inlet pressure	0.387 bar
Inlet temperature	225°C
Inlet flow rate	31.6 mL/min
Inlet purge flow	20 mL/min@0.5 min
Column mode	Constant flow
Column flow rate	9.5 mL/min
Oven temperature	35°C
Detector temperature	225°C
Makeup flow	0.5 mL/min
Column + Makeup flow	10 mL/min
Reference flow	26.4 mL/min
Detector sampling rate	20 Hz
Computer interfacing software	ChemStation Version N.05.04

100 µL of gas samples were analyzed on the GC-TCD unless otherwise mentioned. All injections were performed manually at ~ 20 µL/s to minimize carrier gas laminar flow at the inlet.

The elution times for O_2 (~12.3 minutes) and N_2 (~25.7 minutes) were determined by injecting 20 µL samples of air into the GC-TCD. To determine the elution time of H_2, we trapped 5 µmol H_2 gas generated by electrolyzing 1 mM aqueous H_2SO_4 using two Pt wire electrodes in a sealed vial with a septum. We sampled the headspace (~10 mL) of this vial and analyzed it to establish the elution time of H_2 to be ~7.3 minutes.

The reactions for headspace analysis were performed in crimp top vials with an approximate total volume of 4 mL and headspace volume of ~ 1 mL. To a frozen bromobenzene solution of $\mathbf{1}^-$ in a crimp top vial was added either PhSH or C_6F_5OH in bromobenzene. The crimp top vial was sealed and the reactions were allowed to warm up to room temperature and react for a designated period. Before analyzing the reaction headspace, we ran samples of the glovebox atmosphere on the GC-TCD to confirm the absence of any extraneous/adventitious H_2 sources. For these samples, we observe N_2 from the glovebox atmosphere as well as a small signal for O_2 from air in the syringe needle and gas lock valve assembly.

Mass Spectrometry. HRMS data was collected on a Waters LCT Premier ESI-MS. The data was worked up using MassLynx software and then plotted.

2. Synthesis of Compounds

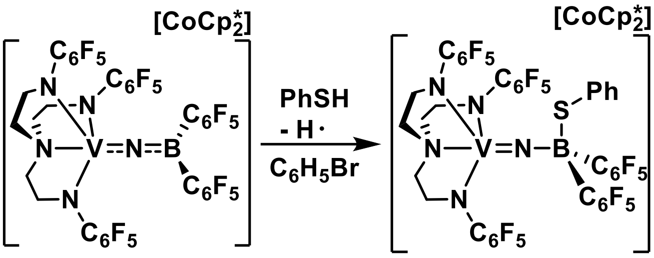

(1⁻) (1-SPh)

Synthesis of $[CoCp^*_2][(N(CH_2CH_2N(C_6F_5))_3)V(\mu\text{-}N)B(SC_6H_5)(C_6F_5)_2]$ (1-SPh). To a frozen solution of **1^-** (0.050 g, 0.0362 mmol) in bromobenzene (2 mL) was added PhSH (0.004 g, 0.0362 mmol) in bromobenzene (0.5 mL) to give an orange solution upon warming up to room temperature. The solution was stirred at room temperature for 1 hour at which point the solution color turned to dark-yellow. The reaction mixture was then treated with pentane (5 mL) to precipitate out an orange oily residue that was washed with more pentane (3 × 1 mL). The residue was treated with diethyl ether after which **1-SPh** precipitated from solution upon standing at room temperature (0.0264 g, 0.0177 mmol, 48.9 % yield). Single crystals suitable for XRD studies were grown from a solution of **1-SPh** in diethyl ether at room temperature. **^{1}H NMR** (400 MHz, CD_3CN, 25 °C): δ = 6.68 (m, 3H; overlapping *m*-C_6H_5 and *p*-C_6H_5), 6.40 (d, $^3J_{HH}$ = 7.1 Hz, 2H; S *o*-C_6H_5), 3.68 (t, $^3J_{HH}$ = 5.6 Hz, 6H; C*H*$_2$), 2.98 (t, $^3J_{HH}$ = 5.6 Hz, 6H; C*H*$_2$), 1.69 (s, 30H; C_{10}*Me*$_{10}$). **^{13}C NMR** (126 MHz, CD_3CN, 25 °C): δ = 131.9 (S *m*-CH), 128.0 (S *p*-CH), 123.4 (S *o*-CH), 95.1 (*C*$_{10}$Me$_{10}$), 60.8 (tren *C*H$_2$), 54.5 (tren *C*H$_2$), 8.3 (C_{10}*Me*$_{10}$). The signal-to-noise ratio was too low for properly identifying the ispo *C* or any C_6F_5 ^{13}C resonance. **^{51}V NMR** (132 MHz, CD_3CN, 25 °C): δ = -272.1 (br). **^{11}B NMR** (128 MHz, CD_3CN, 25 °C): δ = -4.3 (br). **^{19}F NMR** (376 MHz, $CDCl_3$, 25 °C): δ = -130.3 (d, $^3J_{FF}$ = 24.1 Hz, 4F; B *o*-C_6F_5), -148.3 (br, 6F; tren *o*-C_6F_5), -162.7 (t, $^3J_{FF}$ = 20.4 Hz, 2F; B *p*-C_6F_5), -167.5 (m, 10F; overlapping B *m*-C_6F_5 and tren *m*-C_6F_5), -168.1 (t, $^3J_{FF}$ = 22.2 Hz, 3F; tren *p*-C_6F_5). **HRMS (ESI-TOF)** m/z Calcd for $C_{42}H_{17}BF_{25}N_5SV^-$ $[M]^-$: 1160.0345. Found: 1160.0319.

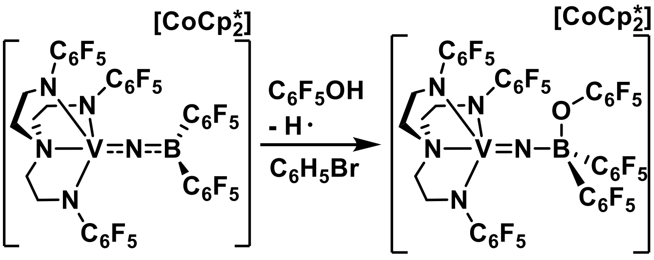

(1⁻) (1-OC$_6$F$_5$)

Synthesis of $[CoCp^*_2][(N(CH_2CH_2N(C_6F_5))_3)V(\mu\text{-}N)B(OC_6F_5)(C_6F_5)_2]$ (1-OC$_6$F$_5$). To a stirring solution of **1^-** (0.030 g, 0.0217 mmol) in DCM (2 mL) was added C_6F_5OH (0.004 g, 0.0217 mmol) in DCM (1 mL) to give an immediate lightening of the solution to orange. The solution was allowed to stir for 2 hours before all volatiles were removed in vacuo. The residue was then washed with pentane (5 × 1 mL) and diethyl ether (5 × 0.5 mL) to give a yellow-orange powder upon removal of the remaining wash solvent in vacuo (0.019 g, 0.0122 mmol, 55.9 % yield). Single crystals suitable for XRD studies were grown from slow vapor diffusion of iso-octane into a saturated solution of **1-OC$_6$F$_5$** in DCM. **^{1}H NMR** (400 MHz, CD_2Cl_2, 25 °C): δ = 3.68 (t, $^3J_{HH}$ = 5.2 Hz, 6H; C*H*$_2$), 2.99 (t, 6H; $^3J_{HH}$ = 5.4 Hz, 6H; C*H*$_2$), 1.69 (s, 30H; C_{10}*Me*$_{10}$). **^{13}C NMR** (100 MHz, CD_2Cl_2, 25 °C): δ = 94.6 (*C*$_{10}$Me$_{10}$), 60.3 (*C*H$_2$), 53.7 (*C*H$_2$), 8.3 (C_{10}*Me*$_{10}$). The signal-to-noise ratio was too low for properly identifying any C_6F_5 ^{13}C resonance. **^{51}V NMR** (105 MHz, CD_2Cl_2, 25 °C): δ = -302.5 (br). **^{11}B NMR** (128 MHz, CD_2Cl_2, 25 °C): δ = -2.2 (br). **^{19}F NMR** (376 MHz, CD_3CN, 25 °C): δ = -133.4 (d, $^3J_{FF}$ = 23.7 Hz, 4F; B *o*-C_6F_5), -148.7 (br, 6F; tren *o*-C_6F_5), -158.9 (d, $^3J_{FF}$ = 20.6 Hz, 2F; O *o*-C_6F_5), -162.5 (t, $^3J_{FF}$ = 19.8 Hz, 2F; B *p*-C_6F_5), -168.5 (t, $^3J_{FF}$ = 20.0 Hz, 4F; B *m*-C_6F_5), -169.6 (br, 6F; tren *m*-C_6F_5), -

169.8 (t, $^3J_{FF}$ = 20.2 Hz, 2F; O *m*-C_6F_5), -170.7 (t, $^3J_{FF}$ = 21.1 Hz, 3F; O tren *p*-C_6F_5), -175.5 (m, 1F; O *p*-C_6F_5). **Elemental analysis** (%) calc. for $C_{62}H_{42}BCoF_{30}N_5OV$: C, 47.62; H, 2.71; N, 4.48. Found: C, 48.00; H, 2.90; N, 5.54.

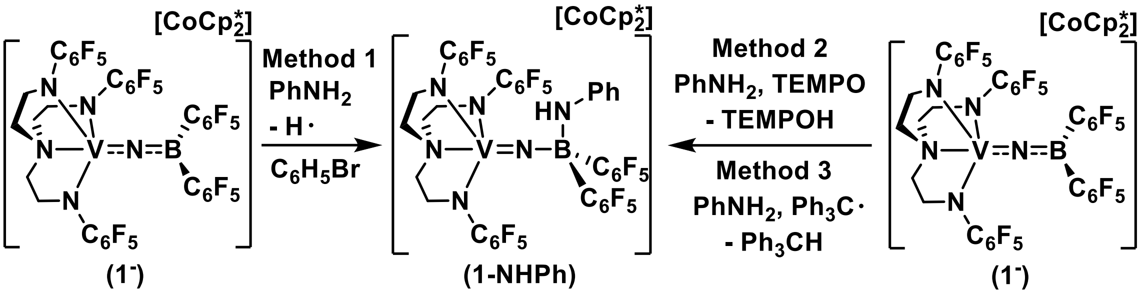

Synthesis of $[CoCp^*_2][(N(CH_2CH_2N(C_6F_5))_3)V(\mu\text{-}N)B(NHC_6H_5)(C_6F_5)_2]$ (1-NHPh). *Method 1:* To a thawing solution of **1**$^-$ (0.010 g, 0.00724 mmol) in bromobenzene-*d*$_5$ (0.4 mL) was added a solution of $PhNH_2$ (0.0007 g, 0.00724 mmol) in bromobenzene-*d*$_5$ (0.2 mL). The resulting solution became dark yellow and analysis of the resulting crude product by NMR spectroscopy revealed a mixture of **1-NHPh**, **2**, and C_6F_5H.

Method 2: To a thawing solution of **1**$^-$ (0.010 g, 0.00724 mmol) and TEMPO (0.0012 g, 0.00724 mmol) in bromobenzene-*d*$_5$ (0.4 mL) was added a solution of $PhNH_2$ (0.0007 g, 0.00724 mmol) in bromobenzene-*d*$_5$ (0.2 mL). The mixture was allowed to stand at room temperature for 1 hour and analysis of the resulting crude NMR spectra revealed the formation of TEMPO–H and **1-NHPh**.

Method 3: To a stirring solution of **1**$^-$ (0.050 g, 0.0362 mmol) and Gomberg's dimer (0.0088 g, 0.0181 mmol) in bromobenzene (1.5 mL) was added $PhNH_2$ (0.0034 g, 0.0362 mmol) in bromobenzene (0.5 mL) to give a gradual lightening of the dark-red solution to pale orange over the course of 1 hour. The solution was then treated with pentane (10 mL) to precipitate out an oily solid that was subsequently washed with more pentane (5 × 0.5 mL), diethyl ether (2 × 0.5 mL), benzene (2 × 0.5 mL), and cold chloroform (1 × 0.25 mL) to remove residual starting material and the triphenylmethane (Ph_3CH) byproduct. The remaining yellow solid was extracted into DCM and filtered through a celite plug before being dried in vacuo to afford the product as a light-yellow solid (0.0418 g, 0.0282 mmol, 77.8 % yield). Single crystals suitable for XRD studies were grown from slow evaporation of a chloroform solution of the product after several days. **^{1}H NMR** (600 MHz, CD_2Cl_2, 25 °C): δ = 6.62 (td, J_{HH} = 7.9, 7.0 Hz, 2H; *m*-C_6H_5), 6.06 (t, $^3J_{HH}$ = 7.0 Hz, 1H; *p*-C_6H_5), 5.71 (d, $^3J_{HH}$ = 8.0 Hz, 2H; *o*-C_6H_5), 3.67 (t, $^3J_{HH}$ = 6.0 Hz, 6H; tren CH_2), 3.65 (s, 1H; N*H*Ph), 2.98 (t, $^3J_{HH}$ = 6.0 Hz, 6H; tren CH_2), 1.68 (s, 30H; $C_{10}Me_{10}$). **^{13}C NMR** (126 MHz, CD_2Cl_2, 25 °C): δ = 151.9 (ipso *C*), 128.2 (*o*-CH), 113.9 (*m*-CH), 111.9(*p*-CH), 94.6 ($C_{10}Me_{10}$), 60.2 (CH_2), 53.2 (CH_2), 8.4 ($C_{10}Me_{10}$). The signal-to-noise ratio was too low for properly identifying any C_6F_5 ^{13}C resonance. **^{51}V NMR** (132 MHz, CD_2Cl_2, 25 °C): δ = -312.2 (br). **^{11}B NMR** (160 MHz, CD_2Cl_2, 25 °C): δ = -6.0 (br). **^{19}F NMR** (376 MHz, CD_2Cl_2, 25 °C): δ = -133.8 (br, 4F; B *o*-C_6F_5), -149.5 (br, 6F; tren *o*-C_6F_5), -163.3 (t, $^3J_{FF}$ = 20.3 Hz, 2F; B *p*-C_6F_5), -167.8 (br, 6F; tren *m*-C_6F_5), -168.1 (t, $^3J_{FF}$ = 22.4 Hz, 4F; B *m*-C_6F_5), -168.5 (t, $^3J_{FF}$ = 21.6 Hz, 3F; tren *p*-C_6F_5). **HRMS (ESI-TOF)** m/z Calcd for $C_{42}H_{18}BF_{25}N_6V^-$ $[M]^-$: 1143.0734. Found: 1143.0734.

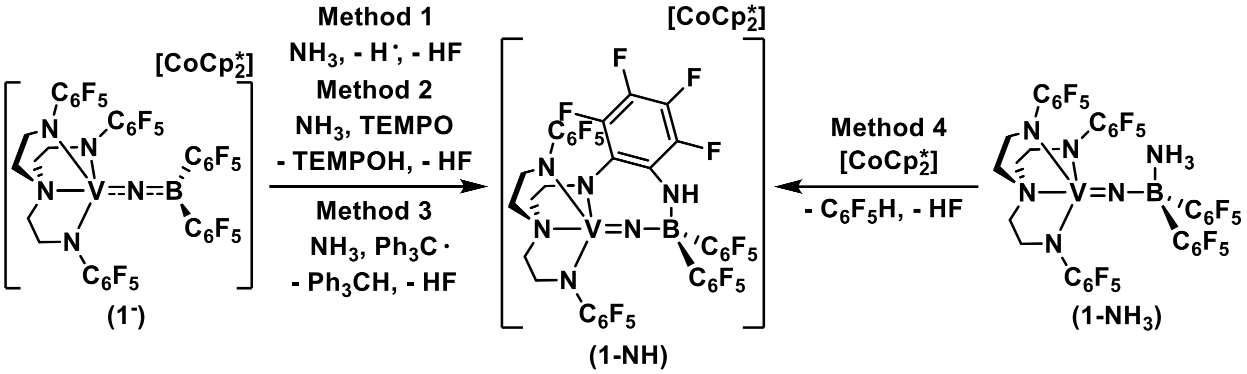

Synthesis of 1-NH. *Method 1:* To a thawing solution of **1**$^-$ (0.020 g, 0.0145 mmol) in bromobenzene-*d*$_5$ (0.5 mL) was added NH_3 (0.4 M in THF) (40.0 µL, 0.0160 mmol) via syringe to give an orange-red solution. The crude NMR spectra revealed a complex mixture of diamagnetic resonances consistent with V^V tren-based products (**1-NH** and **2**) and some C_6F_5H. The reaction mixture was layered with pentane and left to stand at room temperature for several days at which point the title compound precipitated as orange single crystals suitable for XRD studies.

Method 2: Method 2 was carried out in an identical manner to that of Method 1 except TEMPO was added to **1**$^-$ prior to the addition of NH_3. TEMPO–H was observed in the ^{1}H NMR spectrum.

Method 3: Method 3 was carried out in an identical manner to that of Method 1 except Ph_3C• was added to **1**$^-$ prior to the addition of NH_3. Ph_3C–H was observed in the ^{1}H NMR spectrum.

Method 4: To a thawing suspension of **1-NH$_3$** (0.025 g, 0.0234 mmol) in bromobenzene (1.0 mL) was added $Co(C_5Me_5)_2$ (0.0077 g, 0.0234 mmol) in bromobenzene (0.3 mL) to initially give a dark-red solution that faded to orange over the course of 30 minutes. The crude NMR spectra revealed the presence of **1-NH** and C_6F_5H as the main diamagnetic products. The solution was then treated with pentane (10 mL) to precipitate out an oily solid that was subsequently washed with more pentane (5 × 0.5 mL), diethyl ether (2 × 0.5 mL), and benzene (2 × 0.5 mL). After removal of all volatile components in vacuo, **1-NH** was obtained as a light orange solid (0.011 g, 0.0105 mmol, 44.9 % yield). **^{1}H NMR** (600 MHz, C_6D_5Br, 25 °C): δ = 4.23 (br), 3.82 (br), 3.57 (br), 2.83 (br), 2.67 (br), 1.15 (s, 30H; $C_{10}\mathit{Me}_{10}$). **^{13}C NMR** (126 MHz, C_6D_5Br, 25 °C): δ = 93.5 ($\mathit{C}_{10}Me_{10}$), 60.6, 57.1 (br), 54.6, 7.3 ($C_{10}\mathit{Me}_{10}$). The signal-to-noise ratio was too low for properly identifying any C_6F_5 ^{13}C resonance. **^{51}V NMR** (105 MHz, C_6D_5Br, 25 °C): δ = -274.3. **^{11}B NMR** (128 MHz, C_6D_5Br, 25 °C): δ = -4.2. **^{19}F NMR** (376 MHz, C_6D_5Br, 25 °C): δ = -132.8 (br), -148.2 (br), -149.1 (d, $^3J_{FF}$ = 23.4 Hz, 1F; S$_N$Ar tren C_6F_4), -158.8 (d, $^3J_{FF}$ = 26.3 Hz, 1F; S$_N$Ar tren C_6F_4), -161.7 (br), -165.8 (br), -167.0 (br), -171.8 (t, $^3J_{FF}$ = 24.6 Hz, 1F; S$_N$Ar tren C_6F_4), -173.3 (t, $^3J_{FF}$ = 23.0 Hz, 1F; S$_N$Ar tren C_6F_4). **Elemental analysis** (%) Calcd for $C_{56}H_{43}BCoF_{24}N_6V$: C, 48.86; H, 3.15; N, 6.10. Found: C, 48.49; H, 3.44; N, 5.73.

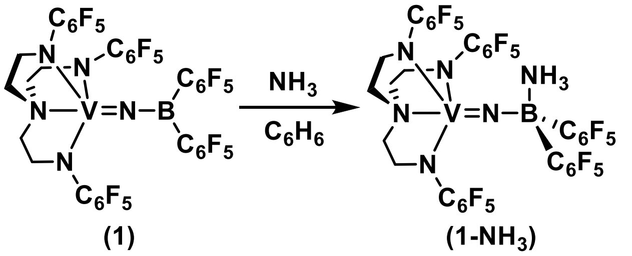

Synthesis of $(N(CH_2CH_2N(C_6F_5))_3)V(\mu\text{-}N)B(NH_3)(C_6F_5)_2$ (1-NH$_3$). In a J. Young NMR tube, a solution of **1** (0.015 g, 0.0143 mmol) in benzene was degassed using three freeze-pump-thaw cycles. Afterwards, the solution was frozen and layered with an atmosphere of NH_3 (excess), and the reaction vessel was subsequently sealed. The solution was allowed to warm to room temperature where the initially dark-green solution lightened to yellow. The reaction stood at room temperature for 15 minutes before being filtered through a celite plug under an inert N_2 atmosphere. The filtrate was collected, all volatiles were removed in vacuo, and the residue was washed with pentane (3 × 1 mL) and diethyl ether (1 × 0.5 mL) to give a bright-yellow powder (0.0128 g, 0.0120 mmol, 84.2 % yield). Single crystals suitable for XRD studies were grown from slow vapor diffusion of iso-octane into a saturated solution of the product in a 1:1 mixture of DCM and benzene. **^{1}H NMR** (400 MHz, C_6D_5Br, 25 °C): δ = 3.61 (bs, 3H; N*H*$_3$), 3.46 (m, 6H; tren C*H*$_2$), 2.64 (t, $^{3}J_{HH}$ = 5.7 Hz, 6H; tren C*H*$_2$). **^{13}C NMR** (126 MHz, $CDCl_3$, 25 °C): δ = 60.0 (*C*H$_2$), 53.2 (*C*H$_2$). The signal-to-noise ratio was too low for properly identifying any C_6F_5 ^{13}C resonance. **^{51}V NMR** (105 MHz, C_6D_6, 25 °C): δ = -303.5 (br). **^{11}B NMR** (128 MHz, C_6D_6, 25 °C): δ = -8.0 (br). **^{19}F NMR** (376 MHz, C_6D_5Br, 25 °C): δ = -134.3 (d, $^{3}J_{FF}$ = 23.1 Hz, 4F; B *o*-C_6F_5), -148.3 (br, 6F; tren *o*-C_6F_5), -154.2 (t, $^{3}J_{FF}$ = 20.6 Hz, 2F; B *p*-C_6F_5), -161.6 (m, 4F; B *m*-C_6F_5), -163.6 (br, 9F; overlapping tren *m*-C_6F_5 and *p*-C_6F_5). **Elemental analysis** (%) Calcd for $C_{36}H_{15}BF_{25}N_6V$: C, 40.48; H, 1.42; N, 7.87. Found: C, 39.10; H, 1.11; N, 7.48.

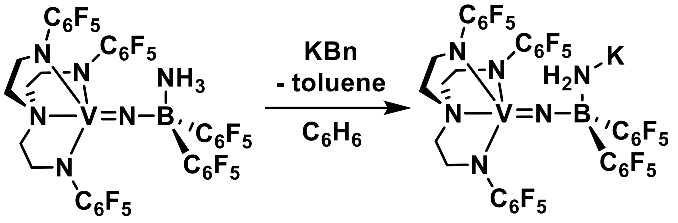

(1-NH$_3$) **(1-NH$_2$K)**

Synthesis of [K][(N(CH$_2$CH$_2$N(C$_6$F$_5$))$_3$)V(μ-N)B(NH$_2$)(C$_6$F$_5$)$_2$] (1-NH$_2$K). A suspension of benzyl potassium (KBn) (0.0061 g, 0.0468 mmol) in benzene (0.5 mL) was added to a stirring solution of **1-NH$_3$** (0.050 g, 0.0468 mmol) in benzene (2 mL) to give a yellow solution and an orange precipitate. The reaction is complete within 15 minutes, as judged by ^{1}H and ^{19}F NMR spectroscopy. The mixture was filtered through a plug of celite and the filter was subsequently washed with benzene (5 × 0.5 mL) and the filtrate was collected. After removal of all volatiles, the orange powder was washed with benzene (2 × 0.25 mL) and then cold pentane (5 × 1 mL). The title compound was isolated as a thermally sensitive light-orange powder (0.034 g, 0.0307 mmol, 65.7 % yield). Orange single crystals suitable for XRD studies were grown by slow vapor diffusion of pentane into a solution of **1-NH$_2$K** in a 2:1 benzene:bromobenzene mixture at room temperature. **^{1}H NMR** (600 MHz, C_6D_6, 25 °C): δ = 3.39 (t, $^{3}J_{HH}$ = 5.6 Hz, 6H; tren C*H*$_2$), 2.31 (t, $^{3}J_{HH}$ = 5.6 Hz, 6H; tren C*H*$_2$), -0.34 (s, 2H; N*H*$_2$). **^{13}C NMR** (100 MHz, C_6D_6, 25 °C): δ = 59.4 (tren *C*H$_2$), 53.2 (tren *C*H$_2$). The signal-to-noise ratio was too low for properly identifying any C_6F_5 ^{13}C resonance. **^{51}V NMR** (105 MHz, C_6D_6, 25 °C): δ = -287.7 (br). **^{11}B NMR** (128 MHz, C_6D_6, 25 °C): δ = -4.9 (s). **^{19}F NMR** (376 MHz, CD_2Cl_2, 25 °C): δ = -135.5 (d, $^{3}J_{FF}$ = 24.6 Hz, 4F; B *o*-C_6F_5), -149.5 (br, 6F; tren *o*-C_6F_5), -161.3 (t, $^{3}J_{FF}$ = 20.1 Hz, 2F; B *p*-C_6F_5), -165.6 (t, $^{3}J_{FF}$ = 20.0 Hz, 4F; B *m*-C_6F_5), -167.8 (br, 6F; tren *m*-C_6F_5), -168.1 (t, $^{3}J_{FF}$ = 21.3 Hz, 3F; tren *p*-C_6F_5). **Elemental analysis** (%) Calcd for $C_{36}H_{14}BF_{25}KN_6V$: C, 39.08; H, 1.28; N, 7.60. Elemental analysis was not attempted due to the thermal sensitivity of the **1-NH$_2$K** compound.

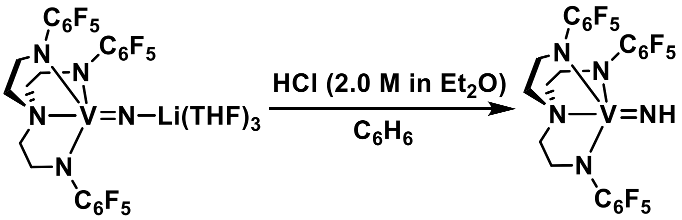

(VNLi) **(2)**

Synthesis of (N(CH$_2$CH$_2$N(C$_6$F$_5$))$_3$)V(μ-N)H (2). To a stirring solution of **VNLi**[1] (0.050 g, 0.0537 mmol) in benzene (4 mL) was added HCl (2.0 M in Et_2O) (26.9 µL, 0.0537 mmol) via a microsyringe resulting in an immediate darkening of the solution to orange. The solution was allowed to stir for 30 minutes before all volatiles were removed in vacuo. The residue was then washed with pentane (5 × 1 mL) and diethyl ether (1 × 1 mL) before being extracted into DCM and filtered through a celite plug to remove LiCl. Upon removal of the solvent, a light-yellow powder was obtained (0.016 g, 0.0226 mmol, 42.1 % yield). Single crystals suitable for XRD studies were grown from slow vapor diffusion of iso-octane into a saturated solution of **2** in DCM. **^{1}H NMR** (400 MHz, C_6D_6, 25 ^{o}C): δ = 3.29 (bs, 6H; C*H*$_2$), 2.18 (bs, 6H; C*H*$_2$). The signal for V=N*H* was not observed. **^{13}C NMR** (126 MHz, $CDCl_3$, 25 ^{o}C): δ = 57.8 (*C*H$_2$), 53.8 (*C*H$_2$). The signal-to-noise ratio was too low for properly identifying any C_6F_5 ^{13}C resonance. **^{51}V NMR** (105 MHz, C_6D_6, 25 ^{o}C): δ = -407.3 (br). **^{19}F NMR** (376 MHz, $CDCl_3$, 25 ^{o}C): δ = -149.8 (d, 6F; *o*-C_6F_5), -165.2 (m, 9F; overlapping tren *m*-C_6F_5 and *p*-C_6F_5). **Elemental analysis** (%) Calcd for $C_{24}H_{13}F_{15}N_5V$: C, 40.75; H, 1.85; N, 9.90. Found: C, 40.41; H, 1.86; N, 9.56.

3. Supplemental Figures for NMR Spectroscopy

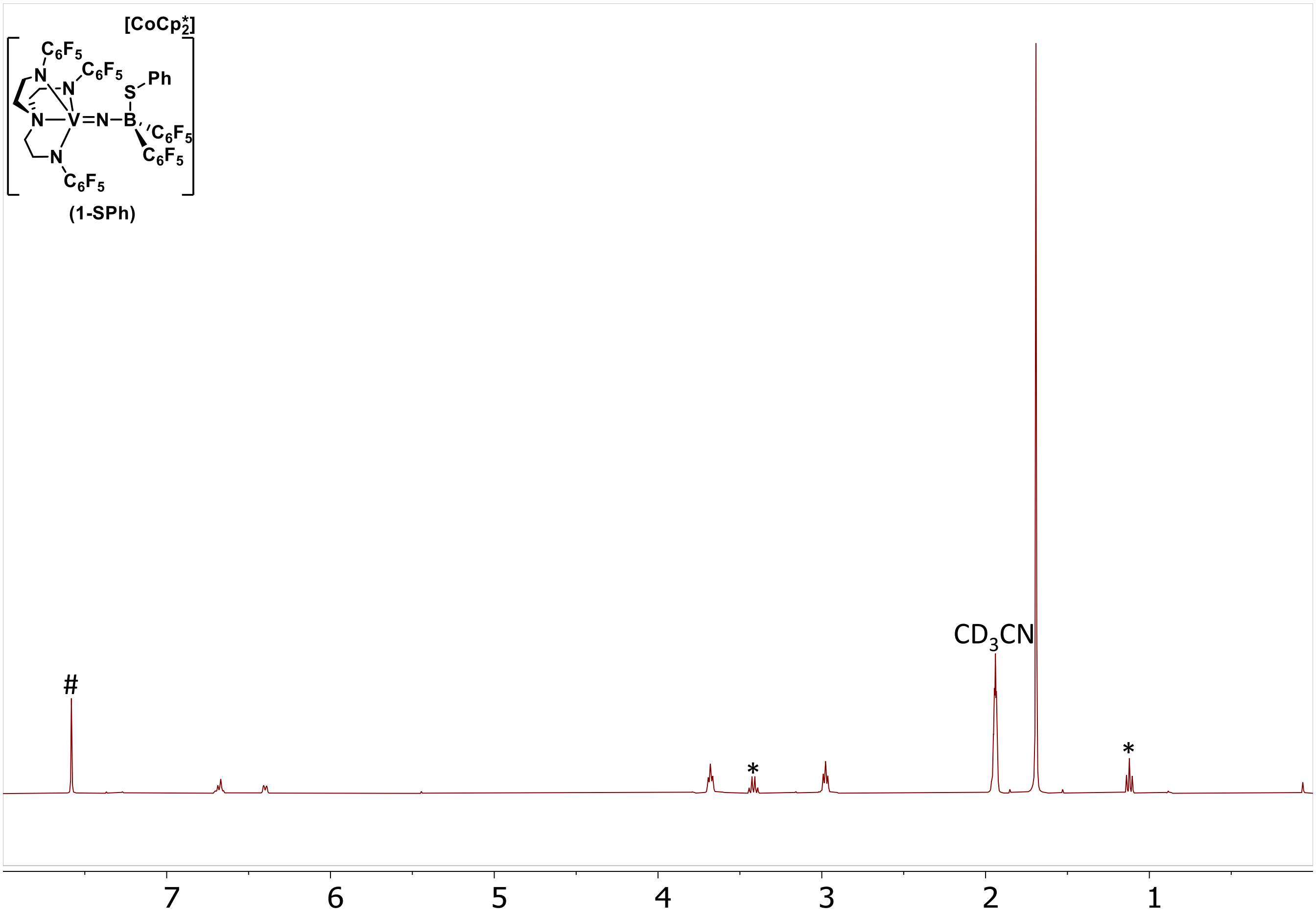

Figure S1. ^{1}H NMR spectrum of **1-SPh** (400 MHz, CD$_3$CN, 25 °C). (* = diethyl ether, # = benzene)

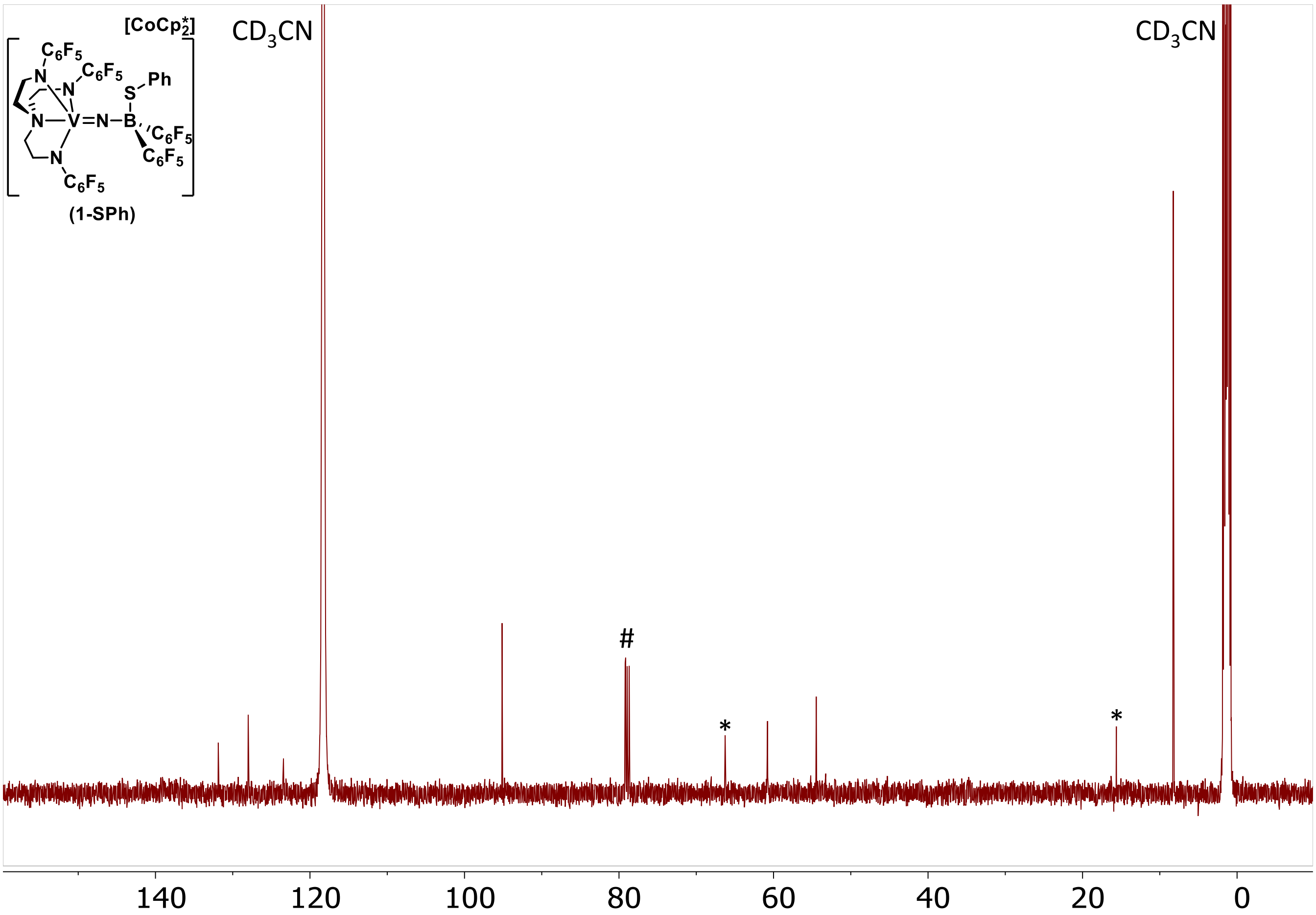

Figure S2. $^{13}C\{^{1}H\}$ NMR spectrum of **1-SPh** (126 MHz, CD_3CN, 25 °C). (* = diethyl ether, # = benzene)

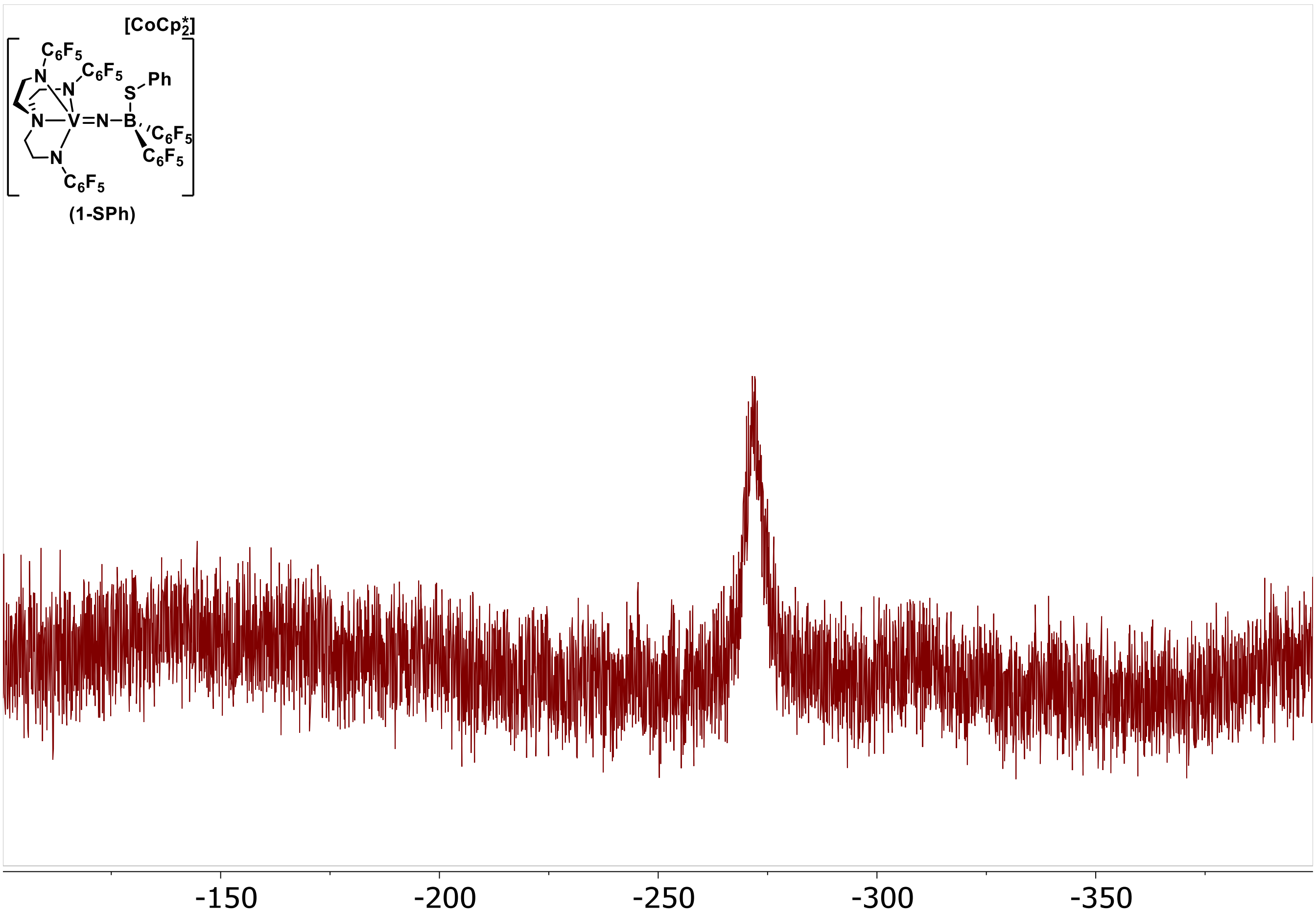

Figure S3. ^{51}V NMR spectrum of **1-SPh** (132 MHz, CD_3CN, 25 °C).

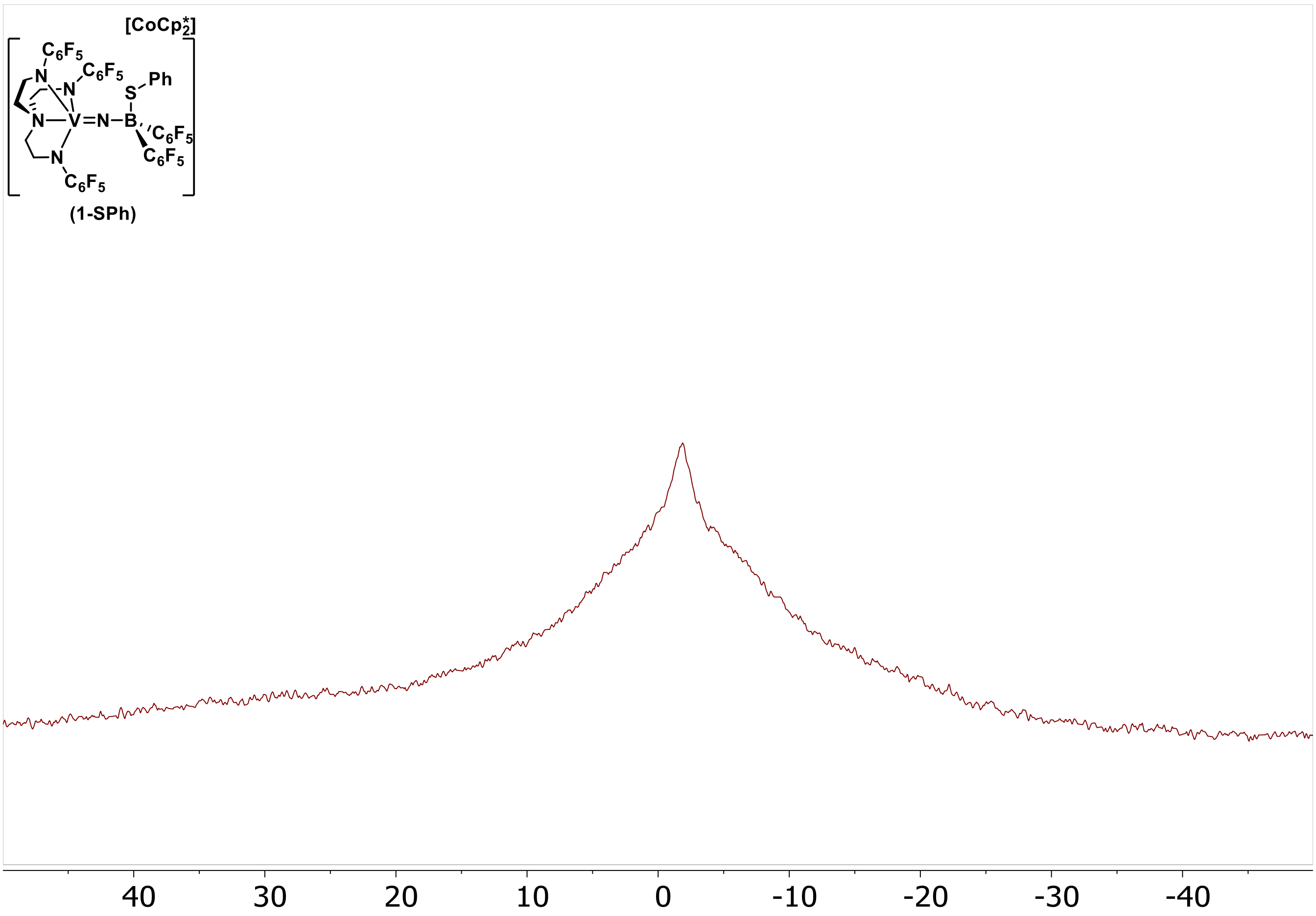

Figure S4. ^{11}B NMR spectrum of **1-SPh** (128 MHz, CD$_3$CN, 25 °C).

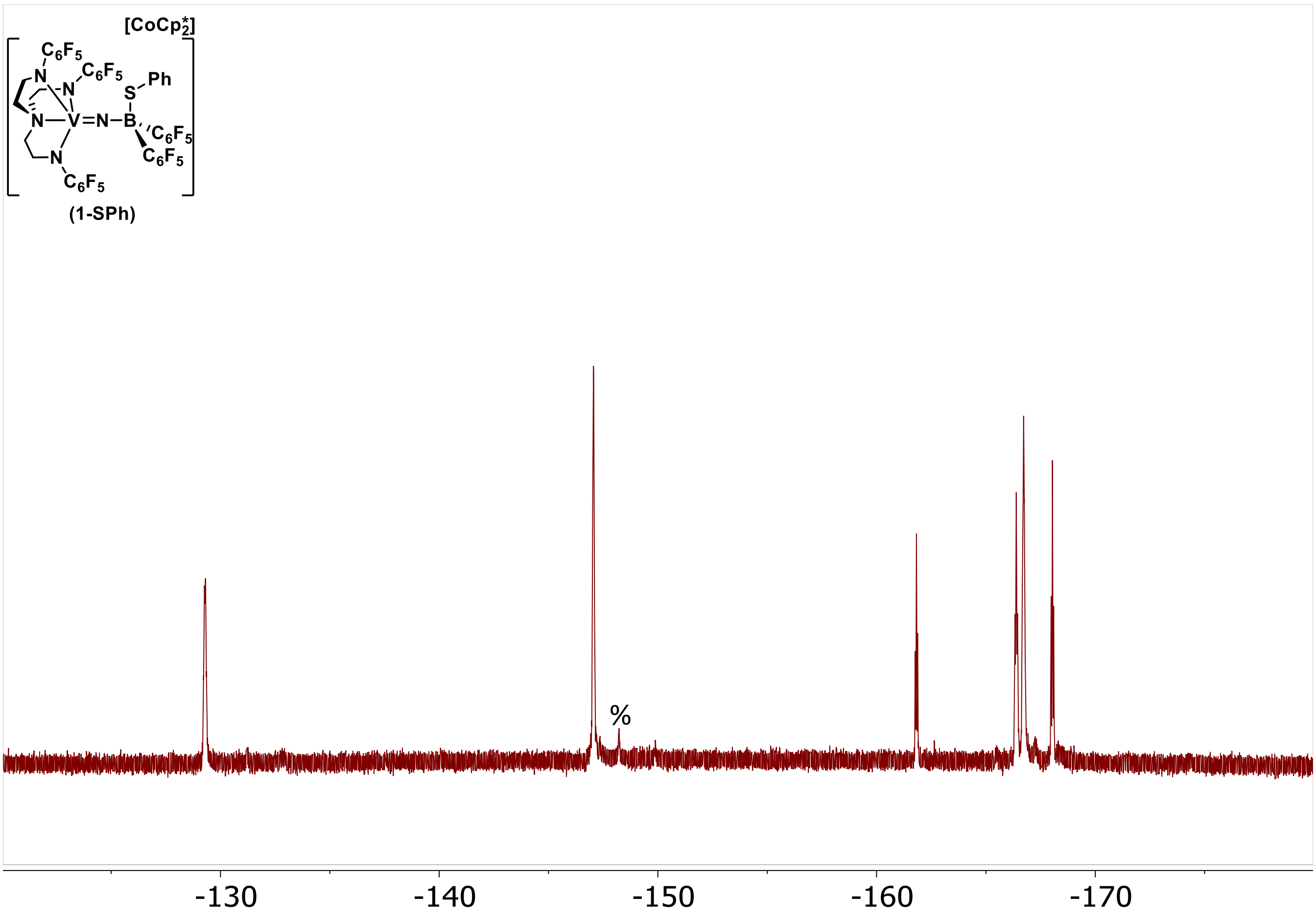

Figure S5. ^{19}F NMR spectrum of **1-SPh** (376 MHz, $CDCl_3$, 25 °C). (% = unidentified resonance)

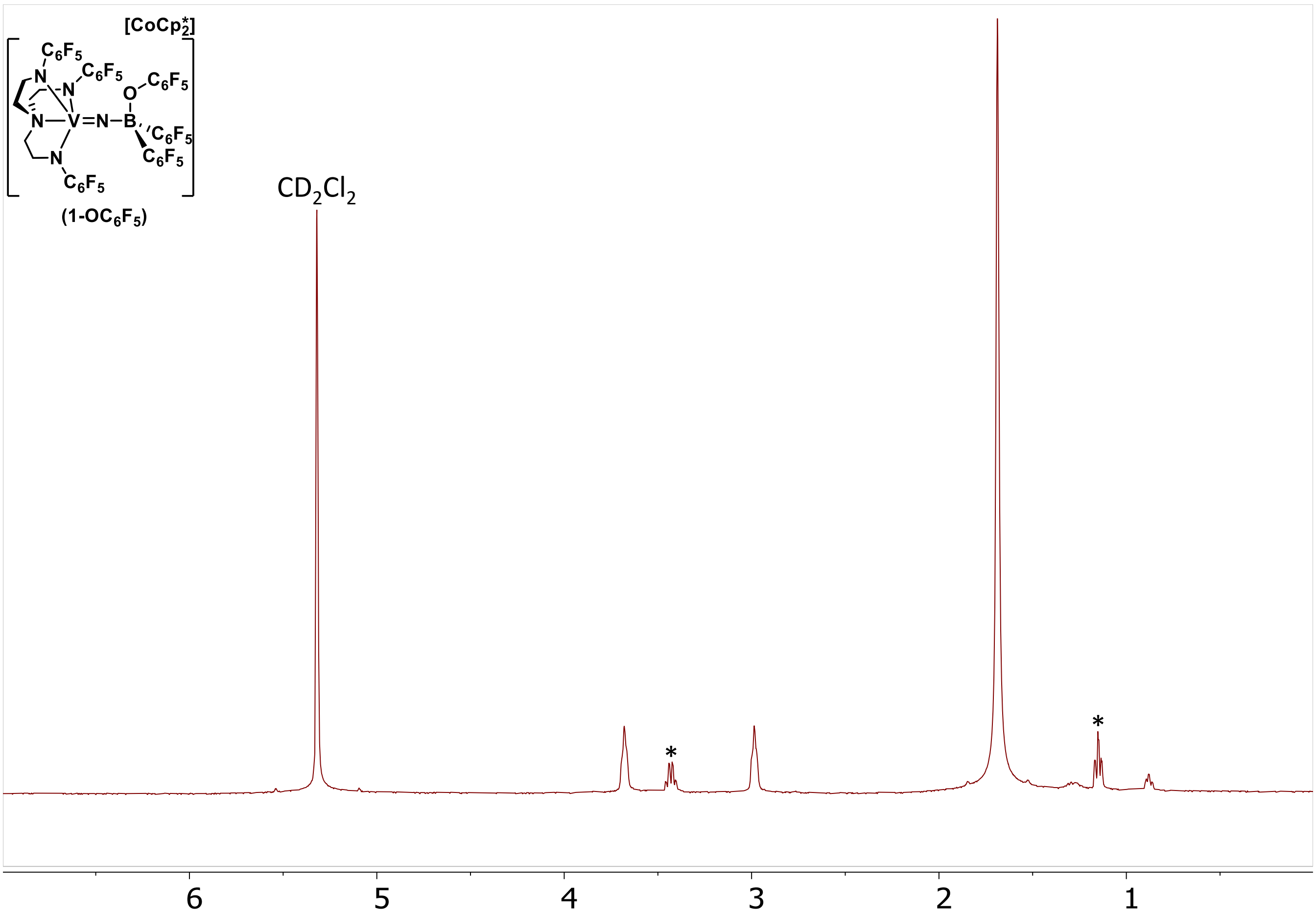

Figure S6. ^{1}H NMR spectrum of **1-OC_6F_5** (400 MHz, CD_2Cl_2, 25 °C). (* = diethyl ether)

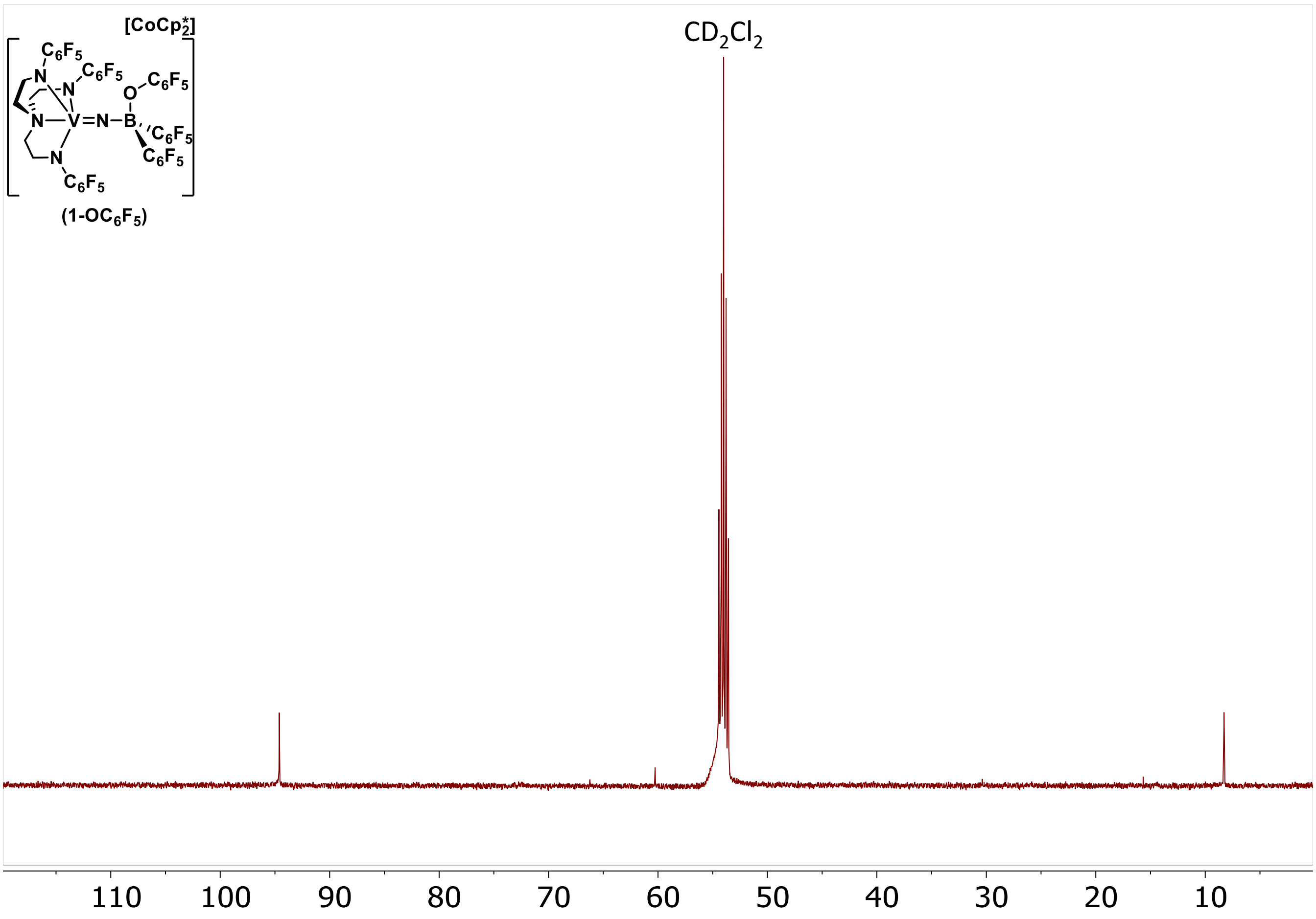

Figure S7. $^{13}C\{^1H\}$ NMR spectrum of **1-OC$_6$F$_5$** (100 MHz, CD_2Cl_2, 25 °C).

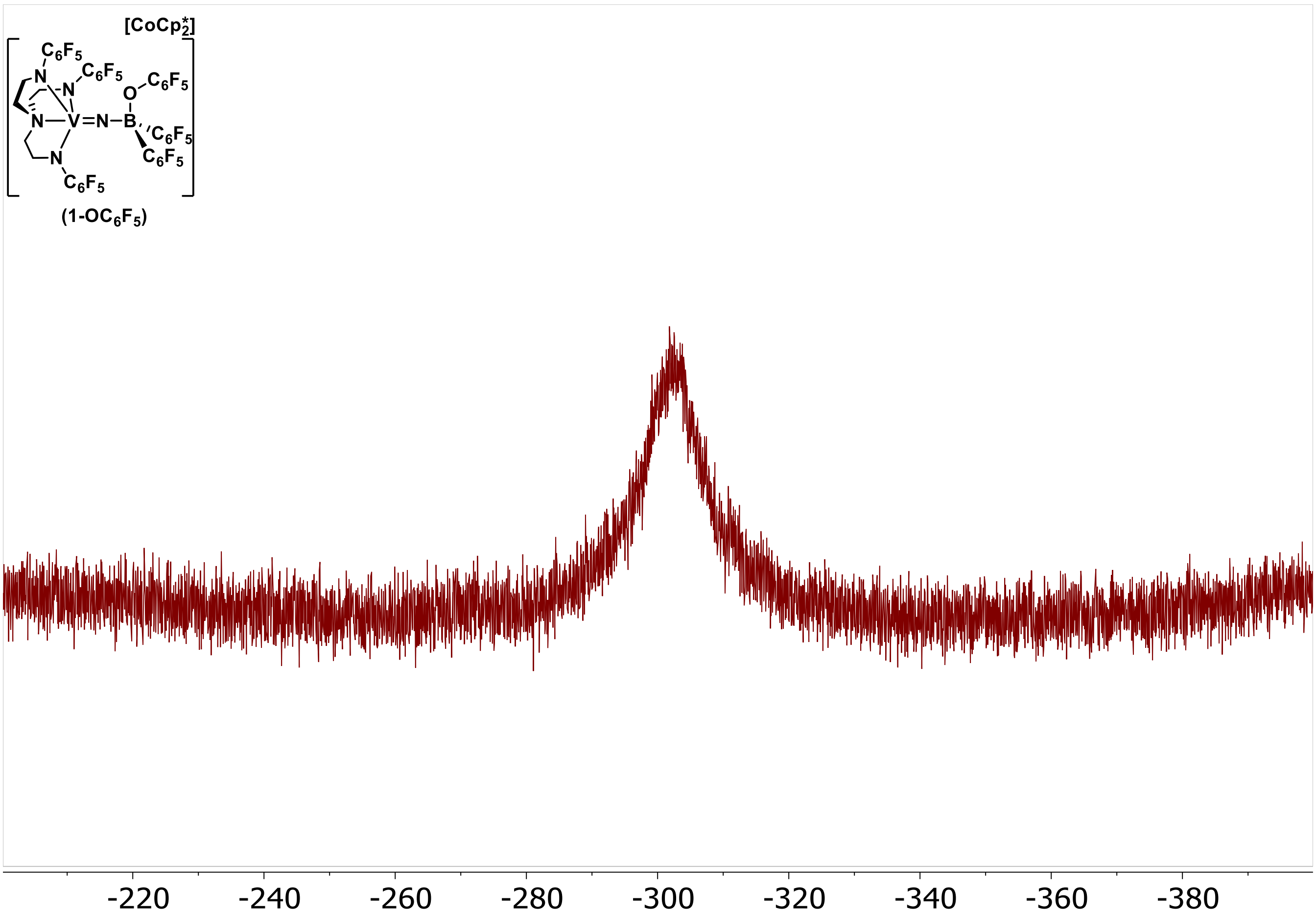

Figure S8. ^{51}V NMR spectrum of of **1-OC$_6$F$_5$** (105 MHz, CD$_2$Cl$_2$, 25 °C).

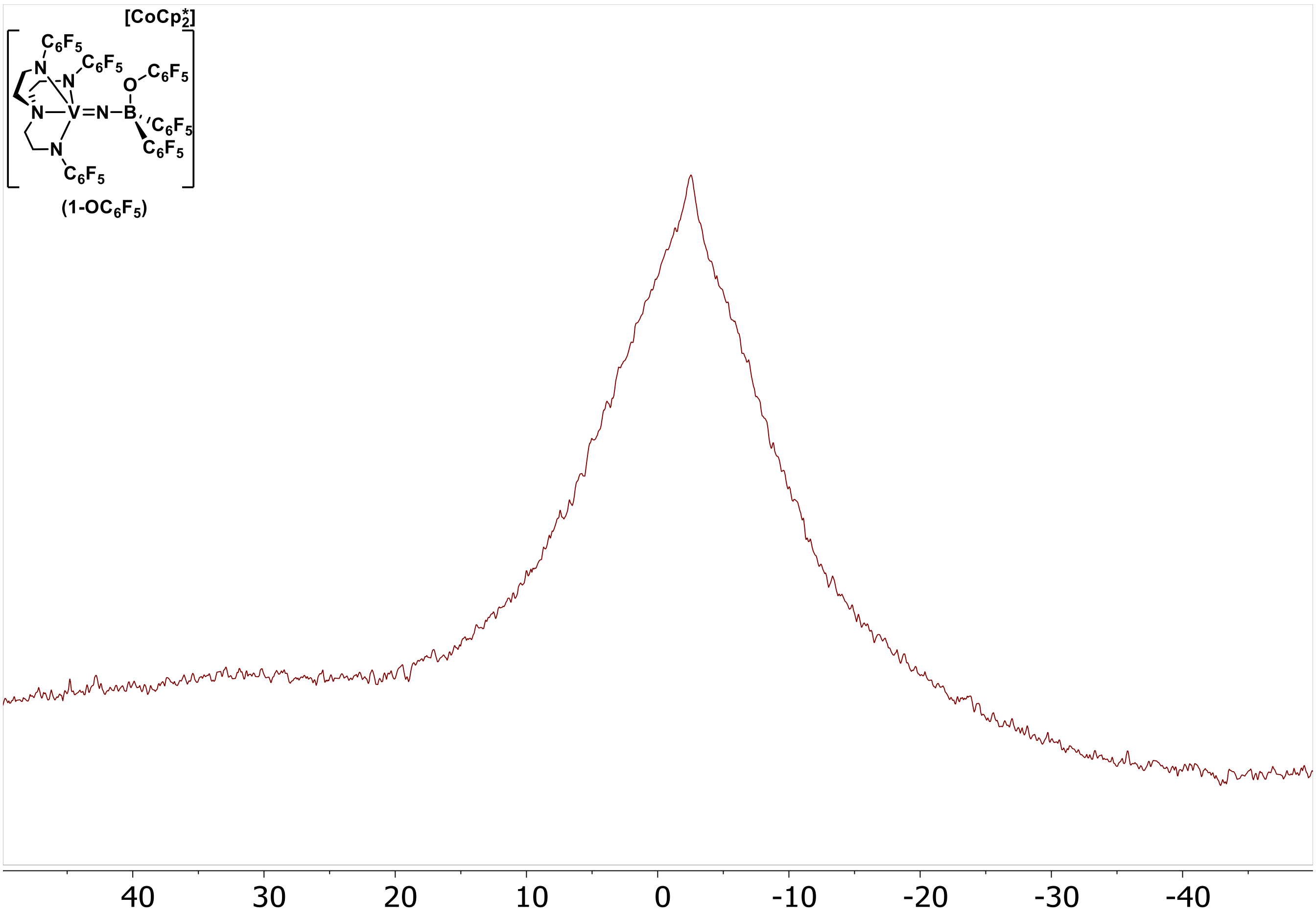

Figure S9. ^{11}B NMR spectrum of **1-OC$_6$F$_5$** (128 MHz, CD$_2$Cl$_2$, 25 ^{o}C).

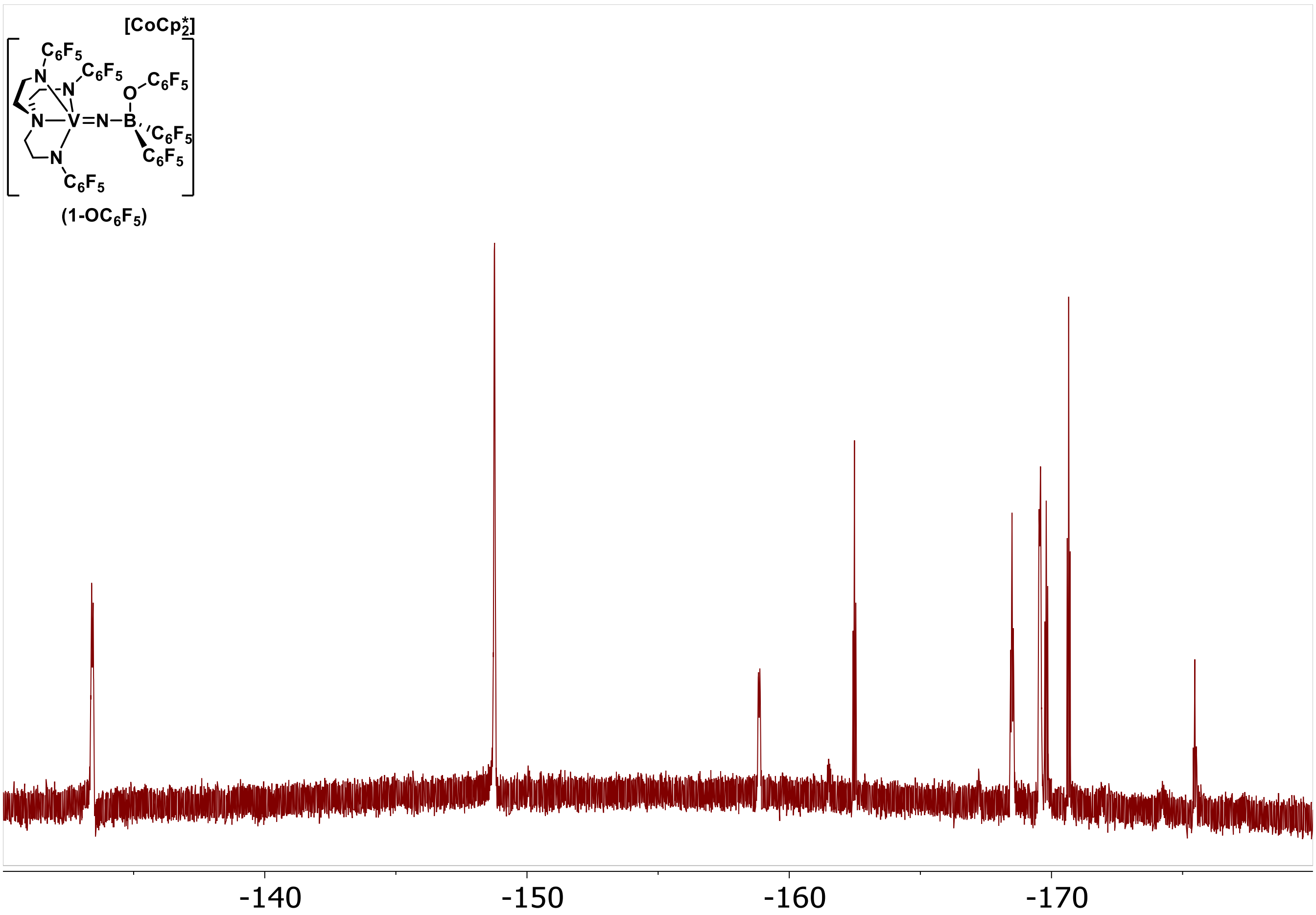

Figure S10. ^{19}F NMR spectrum of **1-OC$_6$F$_5$** (376 MHz, CD$_3$CN, 25 °C).

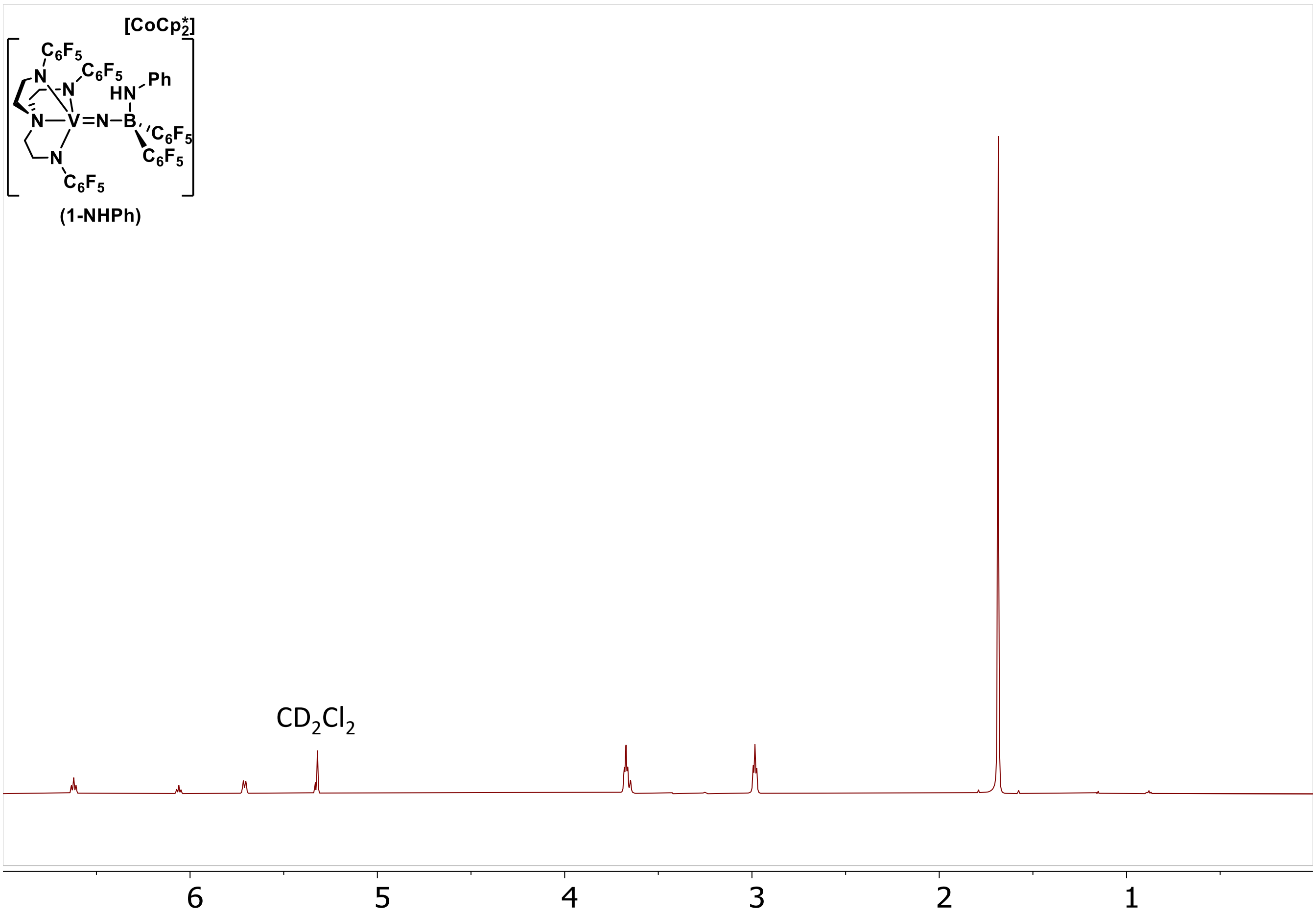

Figure S11. ^{1}H NMR spectrum of **1-NHPh** (600 MHz, CD_2Cl_2, 25 °C).

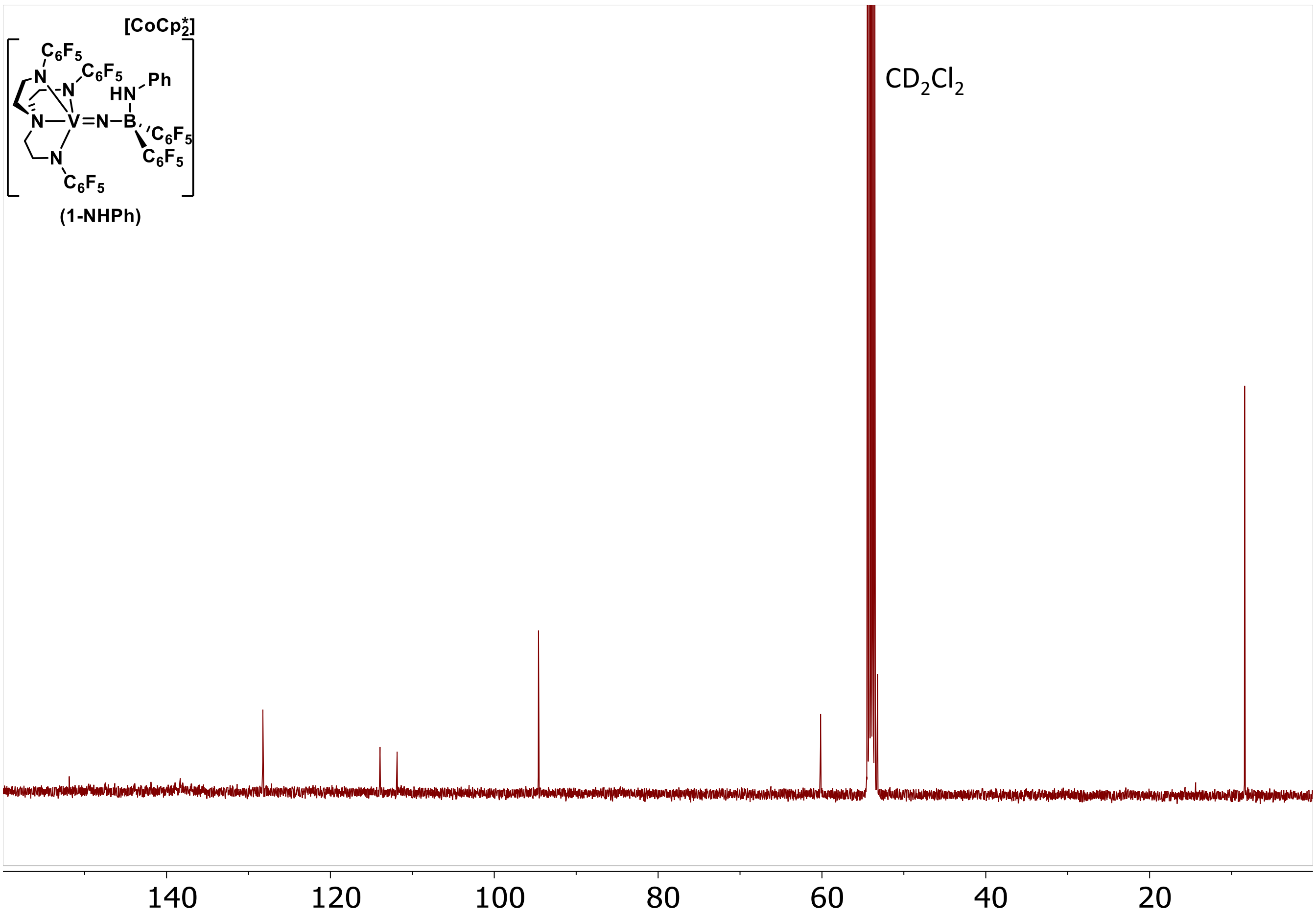

Figure S12. $^{13}C\{^1H\}$ NMR spectrum of **1-NHPh** (126 MHz, CD_2Cl_2, 25 °C).

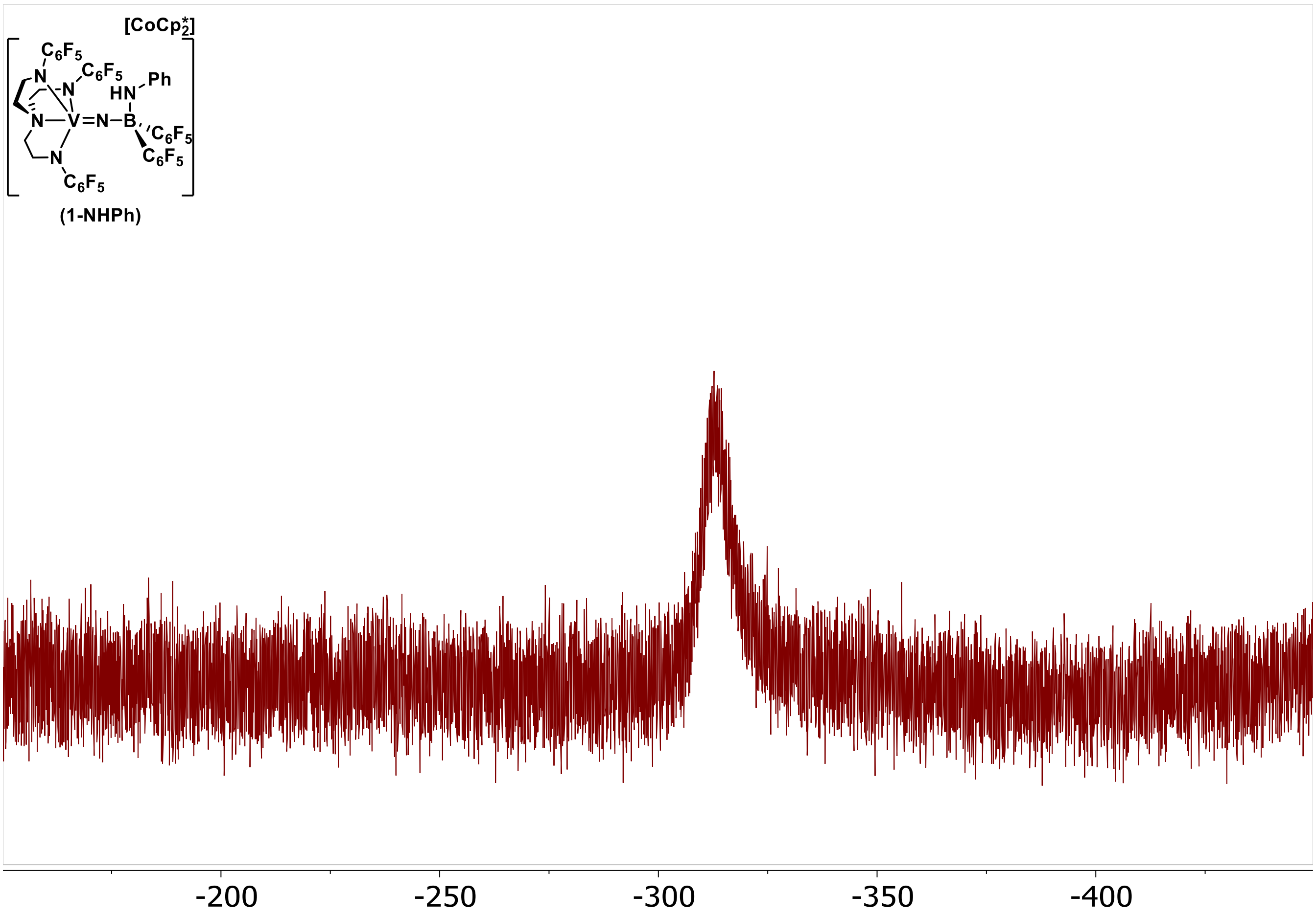

Figure S13. ^{51}V NMR spectrum of **1-NHPh** (132 MHz, CD_2Cl_2, 25 °C).

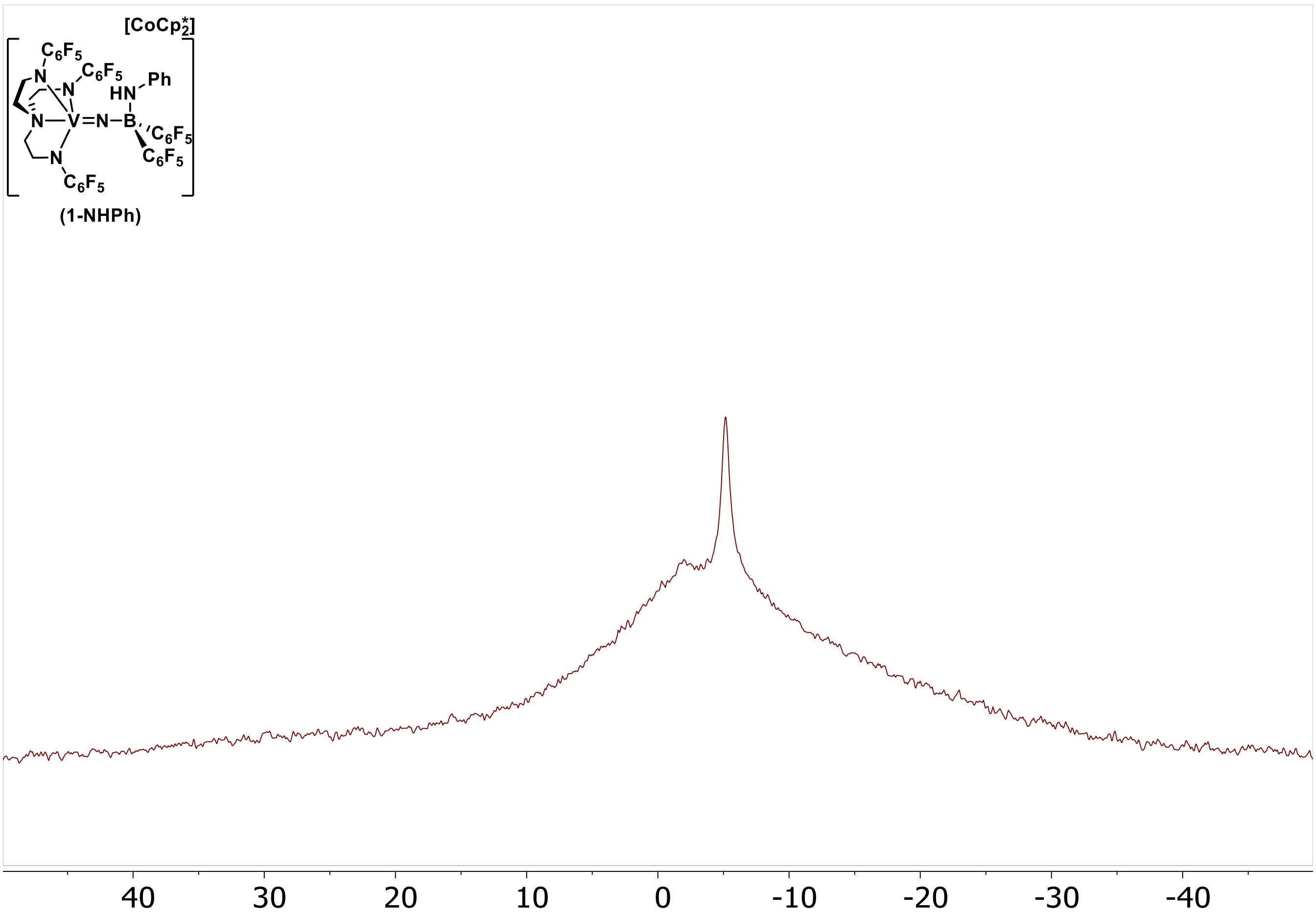

Figure S14. ^{11}B NMR spectrum of **1-NHPh** (160 MHz, CD_2Cl_2, 25 °C).

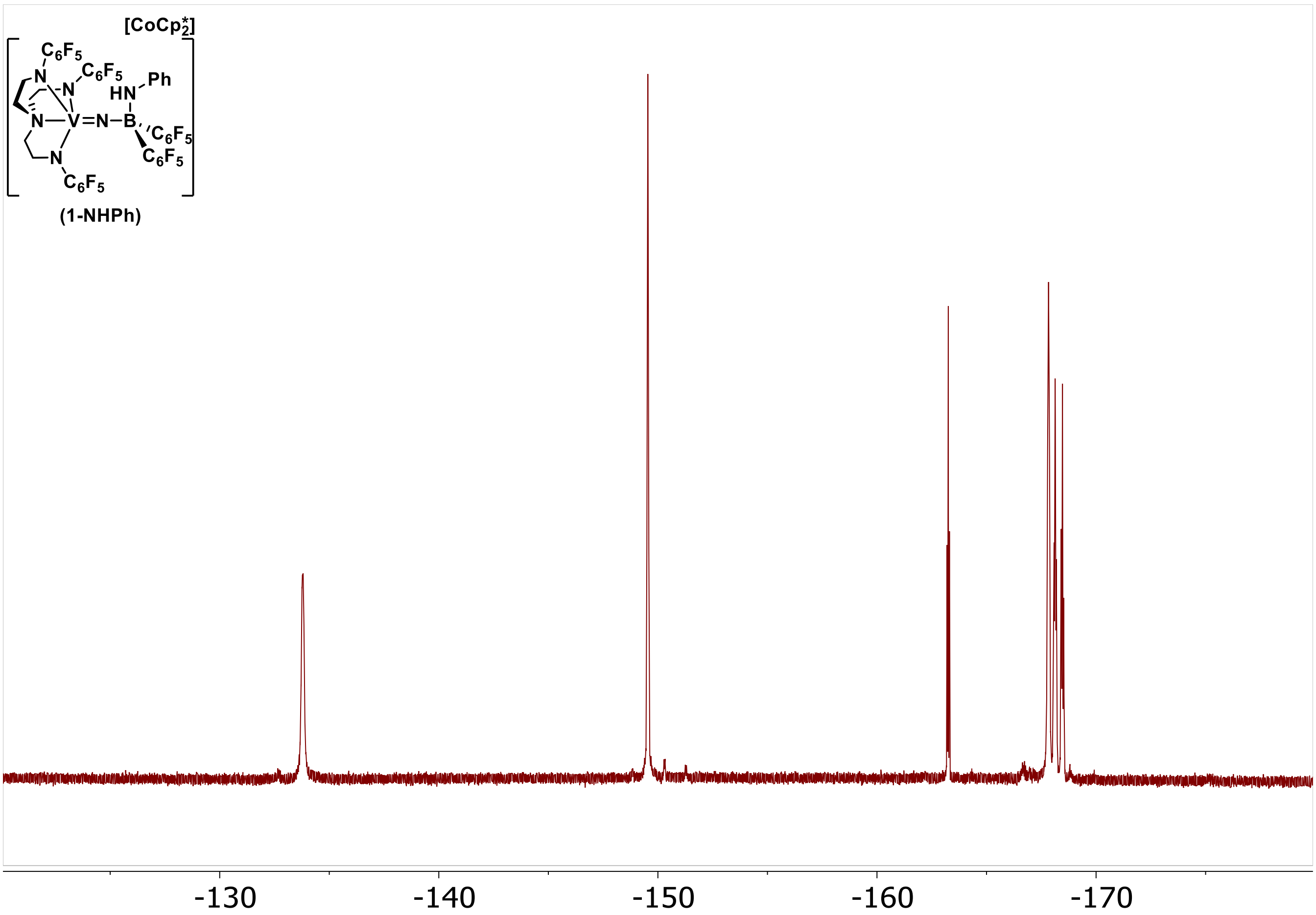

Figure S15. ^{19}F NMR spectrum of **1-NHPh** (376 MHz, CD$_2$Cl$_2$, 25 °C).

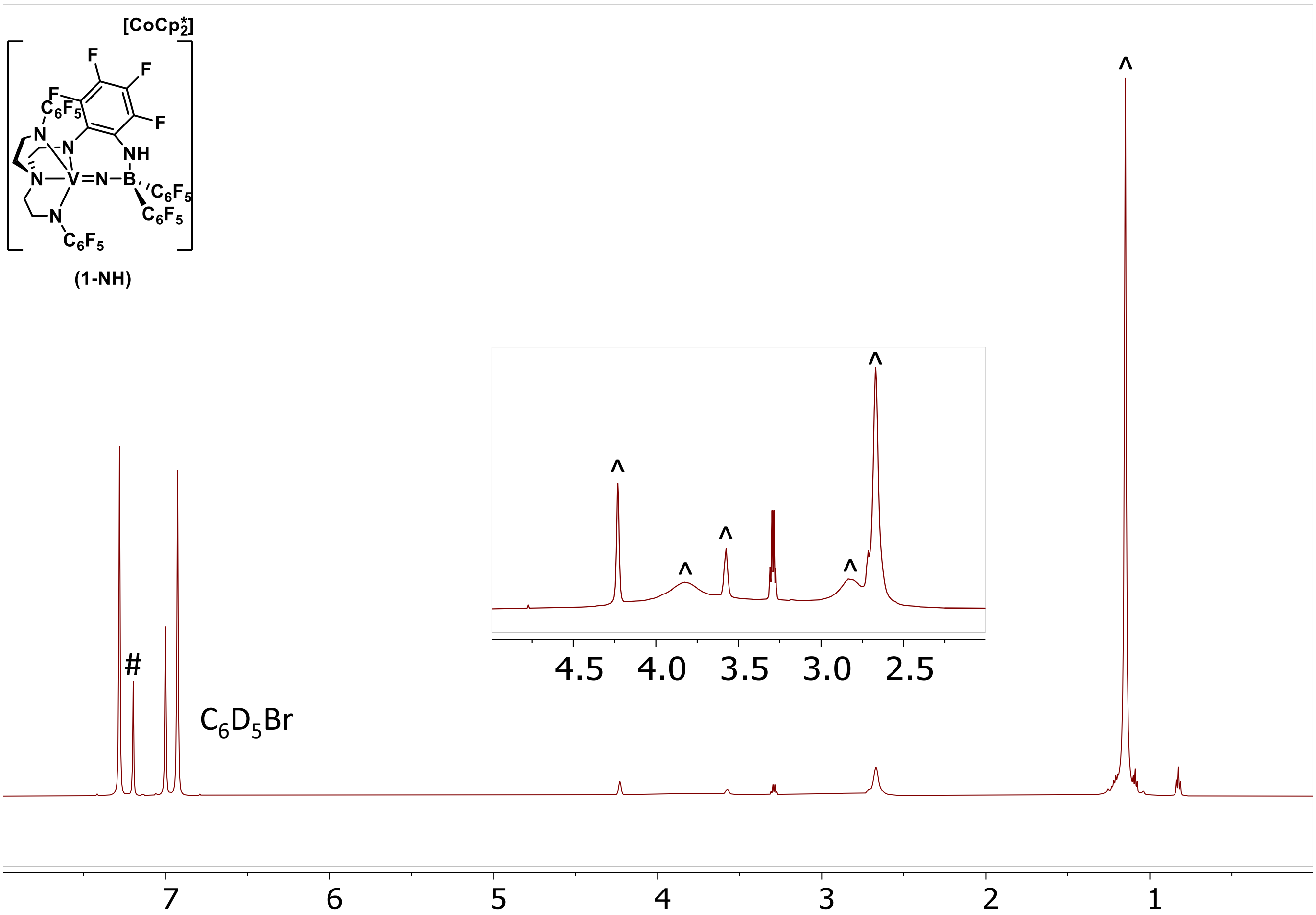

Figure S16. ^{1}H NMR spectrum of **1-NH** (^). Inset is a magnified region of the same ^{1}H NMR spectrum for clarity (bottom) (600 MHz, C_6D_5Br, 25 °C). (# = benzene)

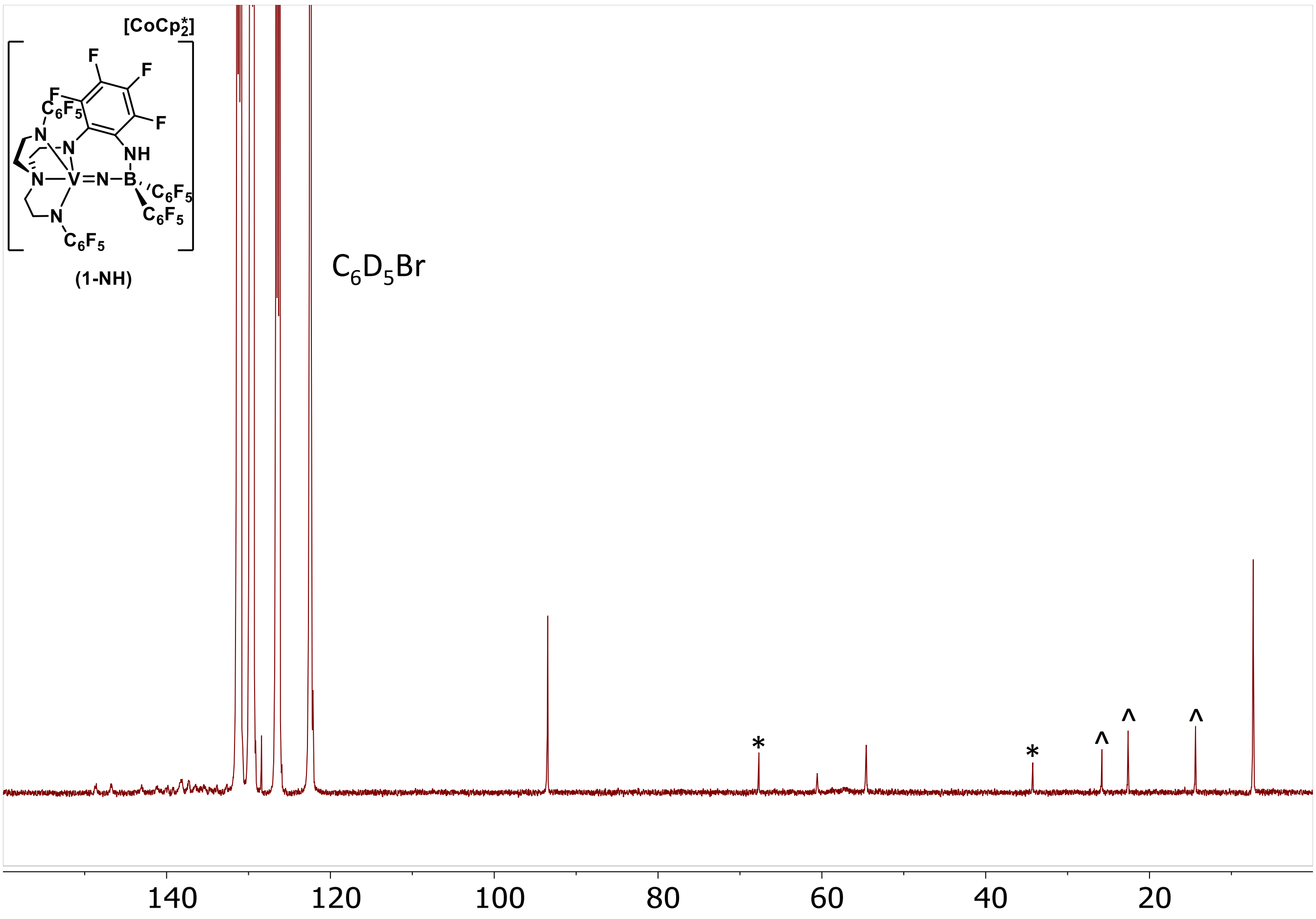

Figure S17. $^{13}C\{^{1}H\}$ NMR spectrum of **1-NH** (126 MHz, C_6D_5Br, 25 ^{o}C). (* = diethyl ether, ^ = pentane)

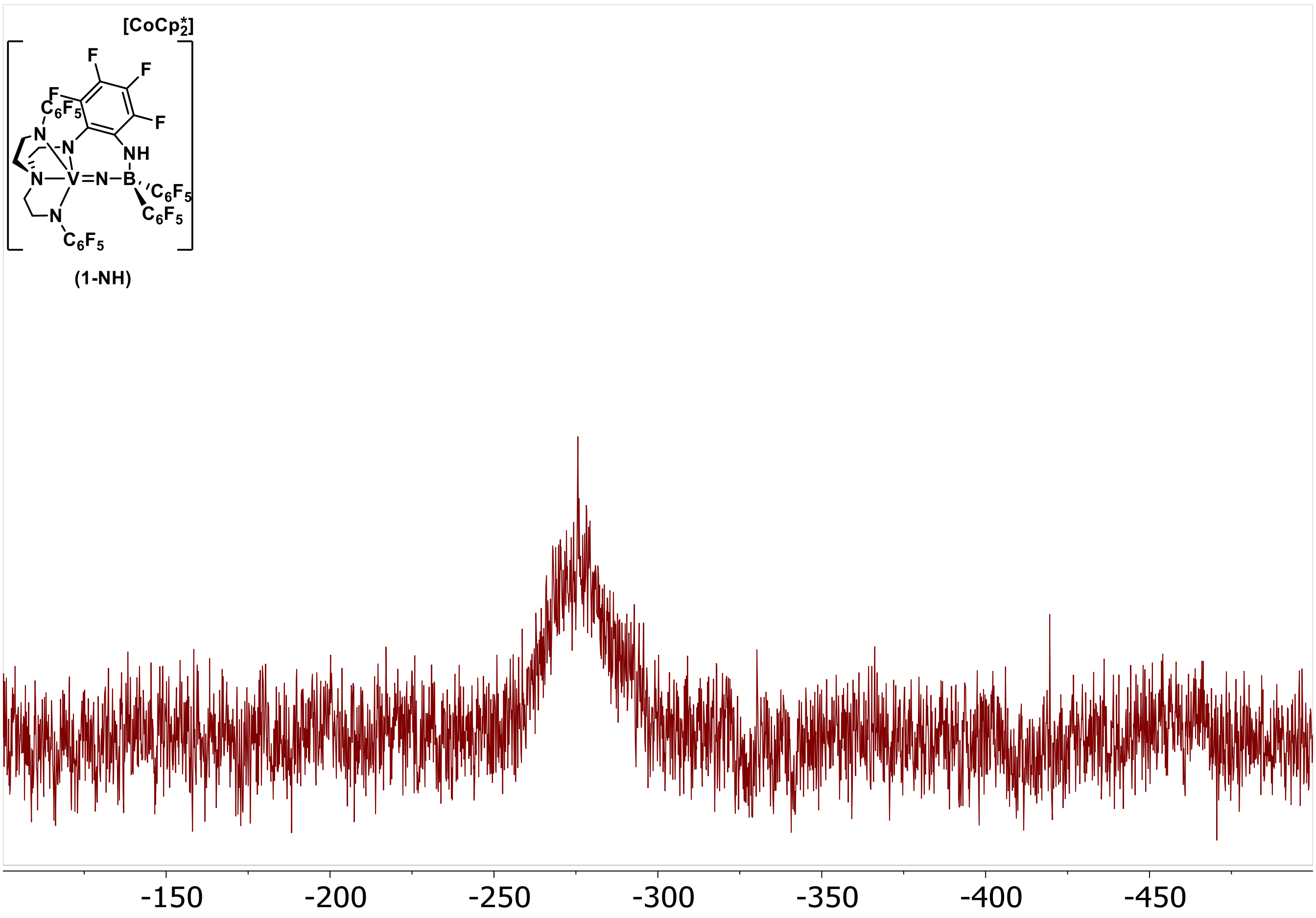

Figure S18. ^{51}V NMR spectrum of **1-NH** (105 MHz, C_6D_5Br, 25 °C).

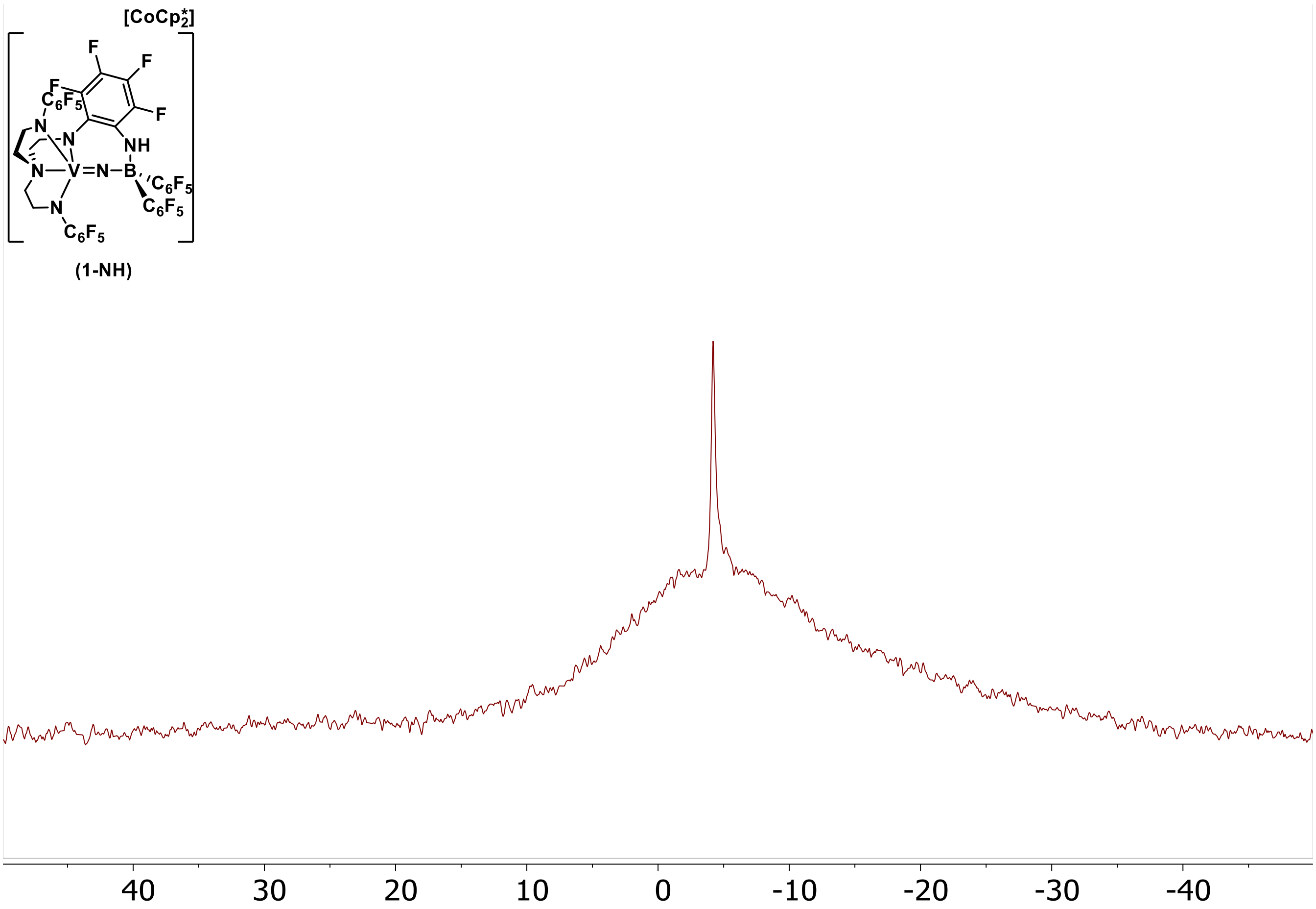

Figure S19. ^{11}B NMR spectrum of **1-NH** (128 MHz, C_6D_5Br, 25 °C).

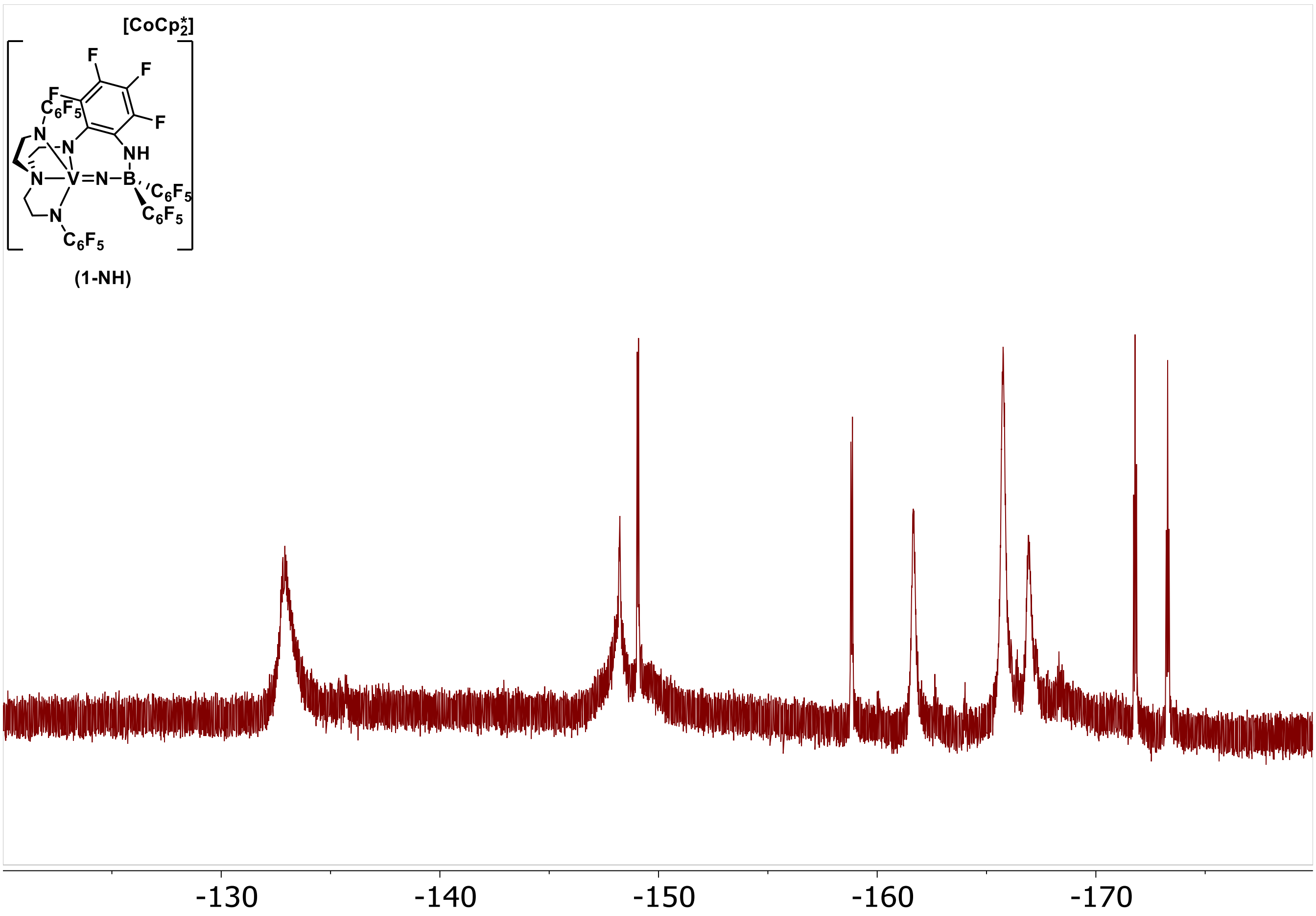

Figure S20. ^{19}F NMR spectrum of **1-NH** (376 MHz, C_6D_5Br, 25 °C).

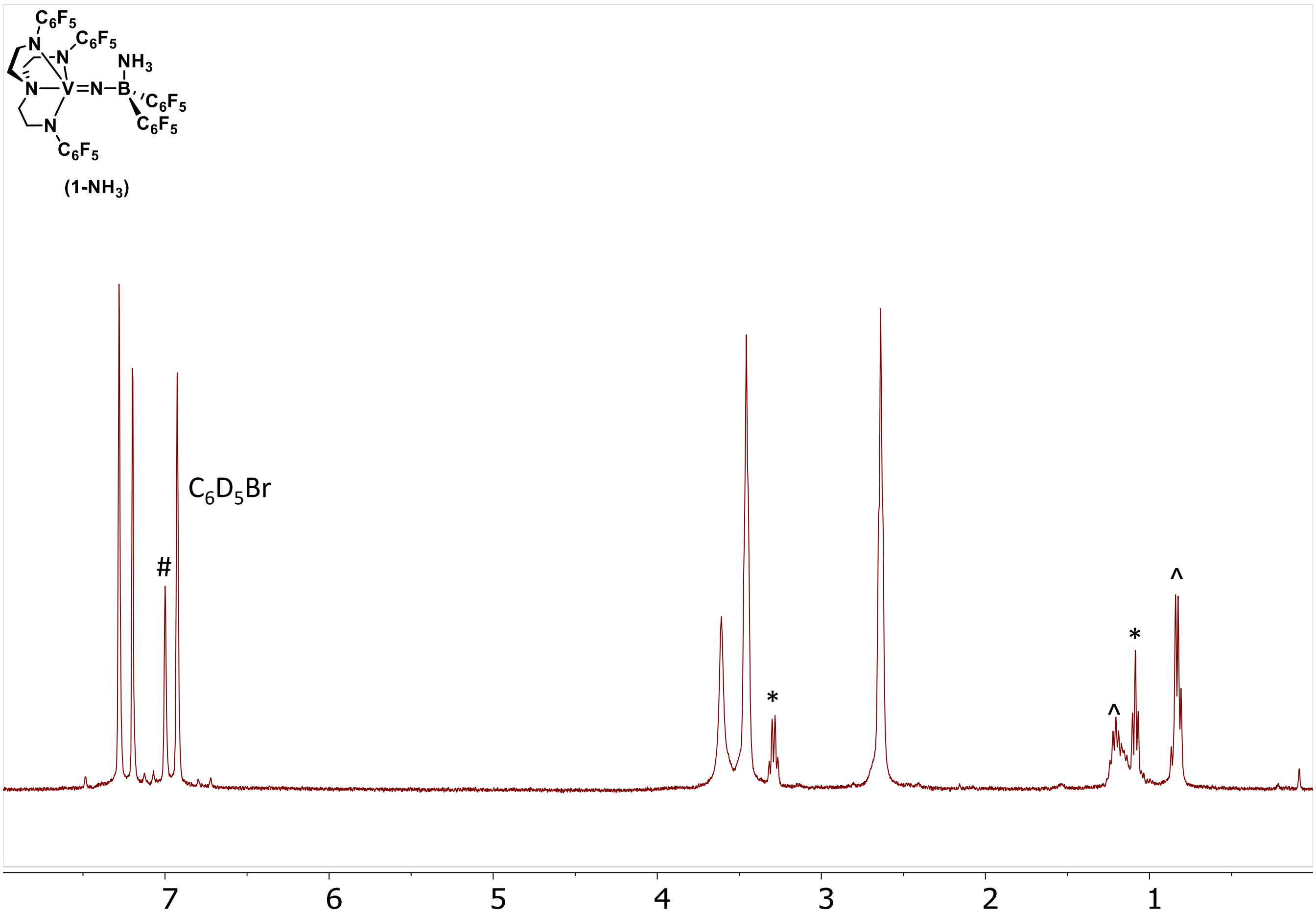

Figure S21. ^{1}H NMR of **1-NH$_3$** (400 MHz, C_6D_5Br, 25 °C). (* = diethyl ether, ^ = pentane, # = benzene)

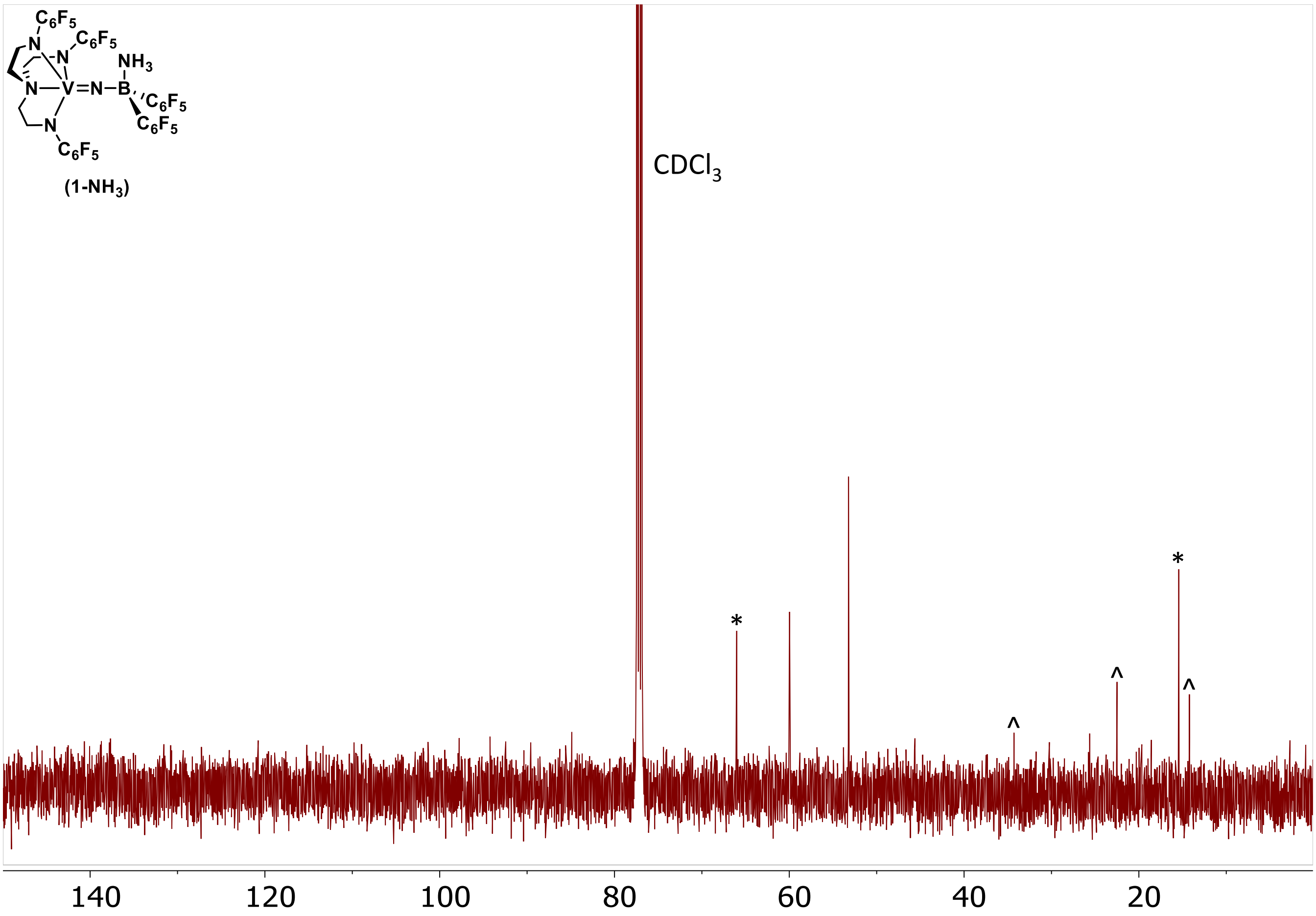

Figure S22. $^{13}C\{^1H\}$ NMR of **1-NH$_3$** (126 MHz, $CDCl_3$, 25 °C). (* = diethyl ether, ^ = pentane)

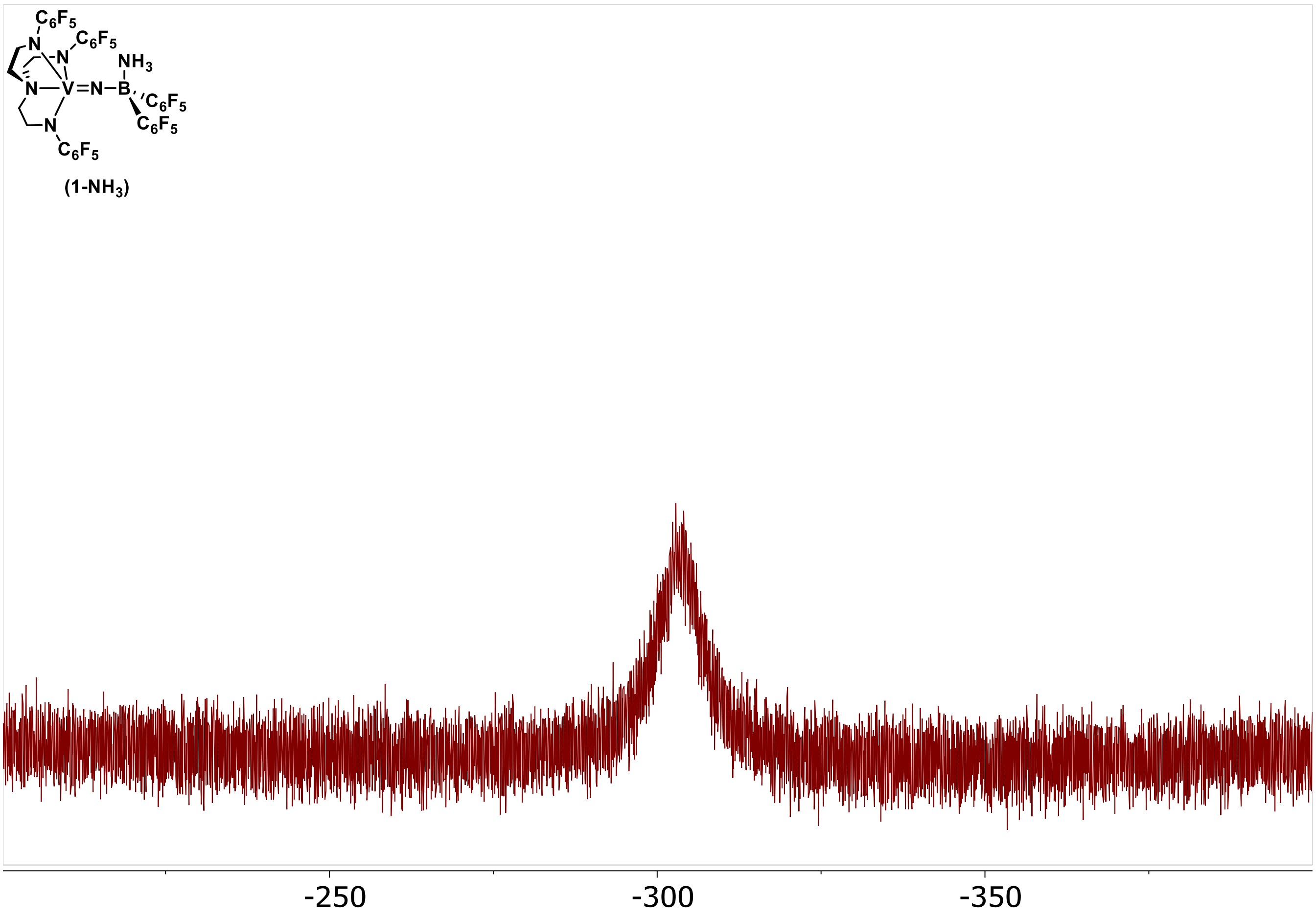

Figure S23. ^{51}V NMR of **1-NH$_3$** (105 MHz, C_6D_6, 25 °C).

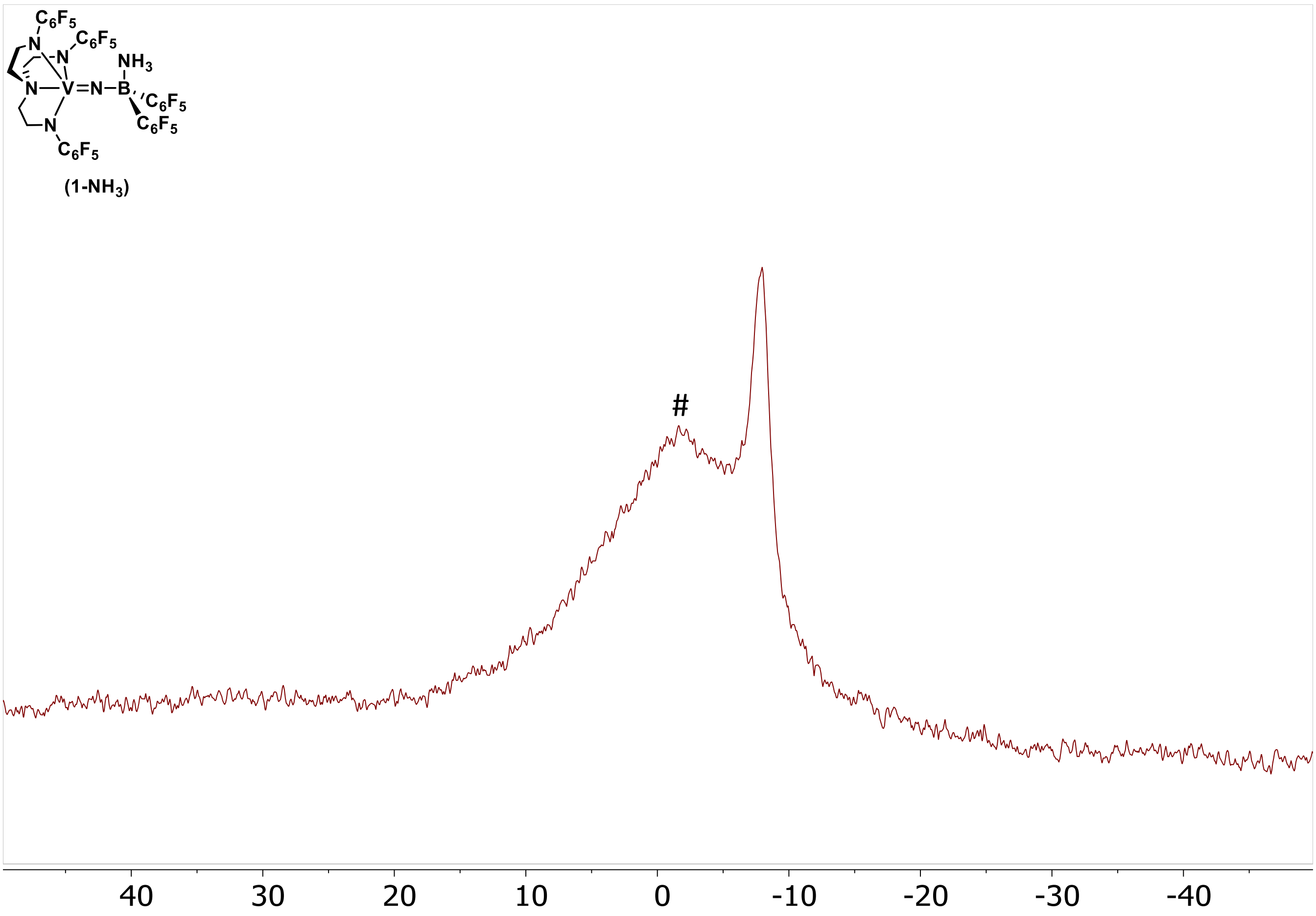

Figure S24. ^{11}B NMR of **1-NH$_3$** (128 MHz, C_6D_6, 25 °C). (# = borosilicate resonance from NMR tube)

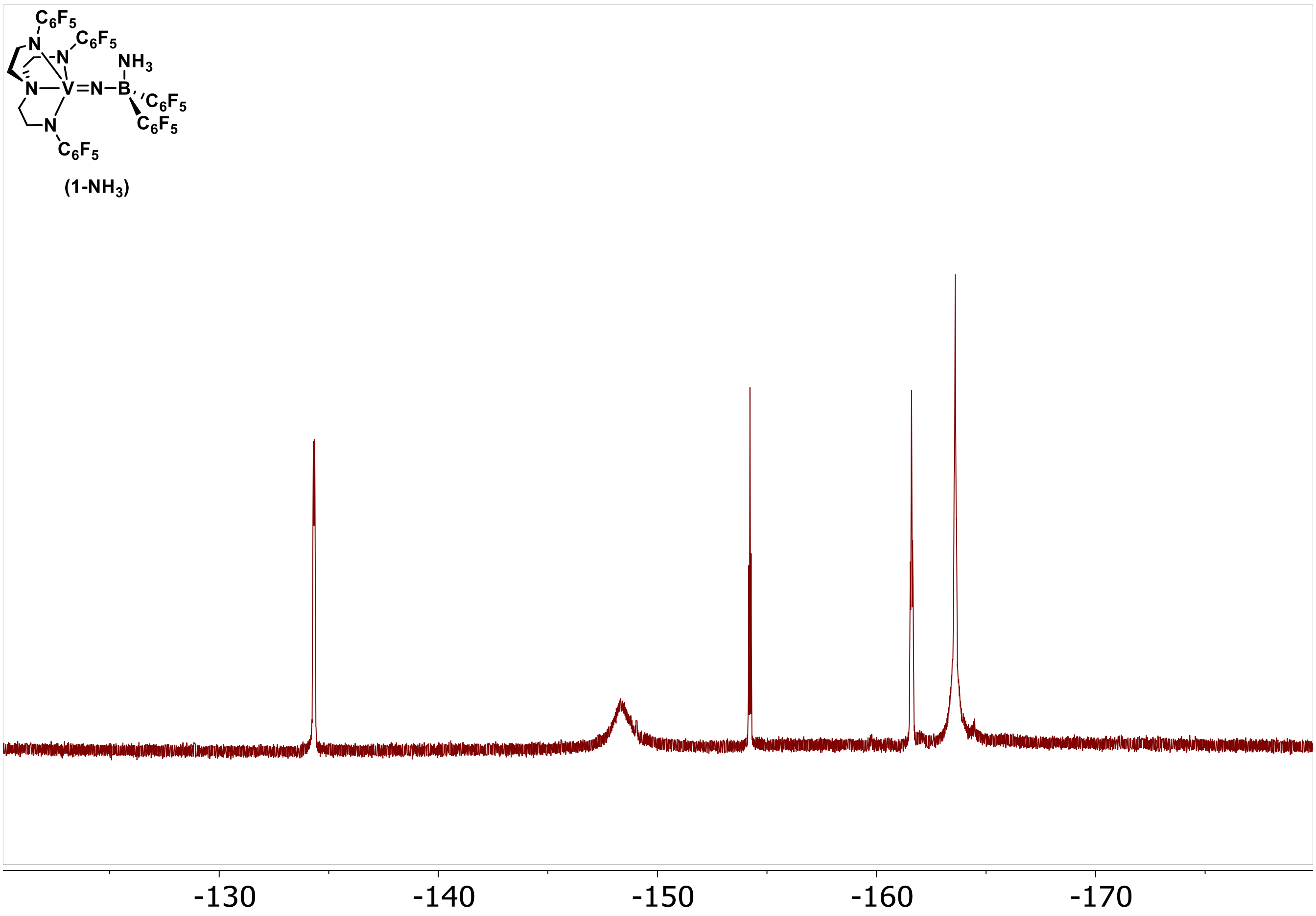

Figure S25. ^{19}F NMR of **1-NH$_3$** (376 MHz, C_6D_5Br, 25 °C).

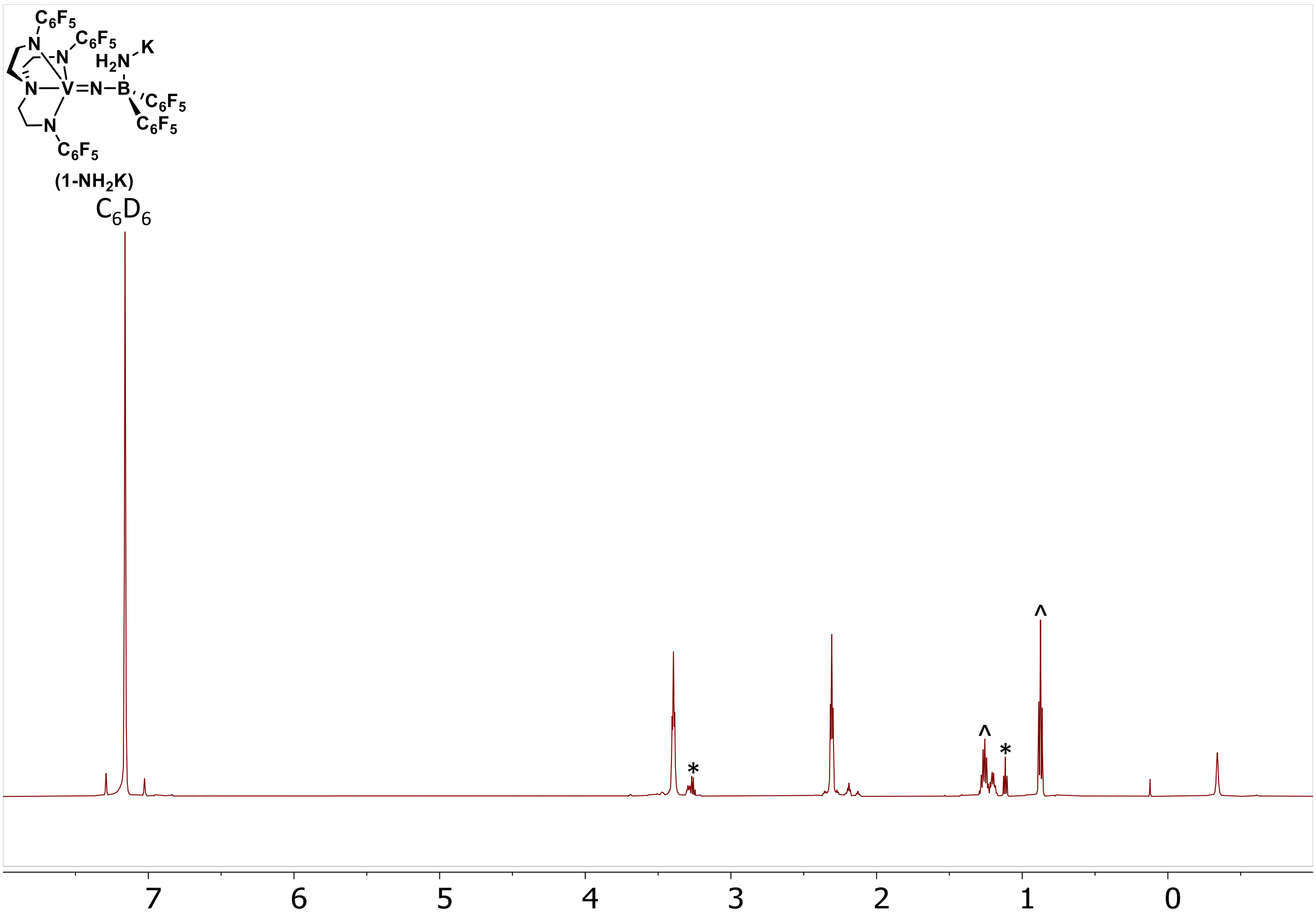

Figure S26. ^1H NMR of **1-NH$_2$K** (600 MHz, C_6D_6, 25 °C). (* = diethyl ether, ^ = pentane)

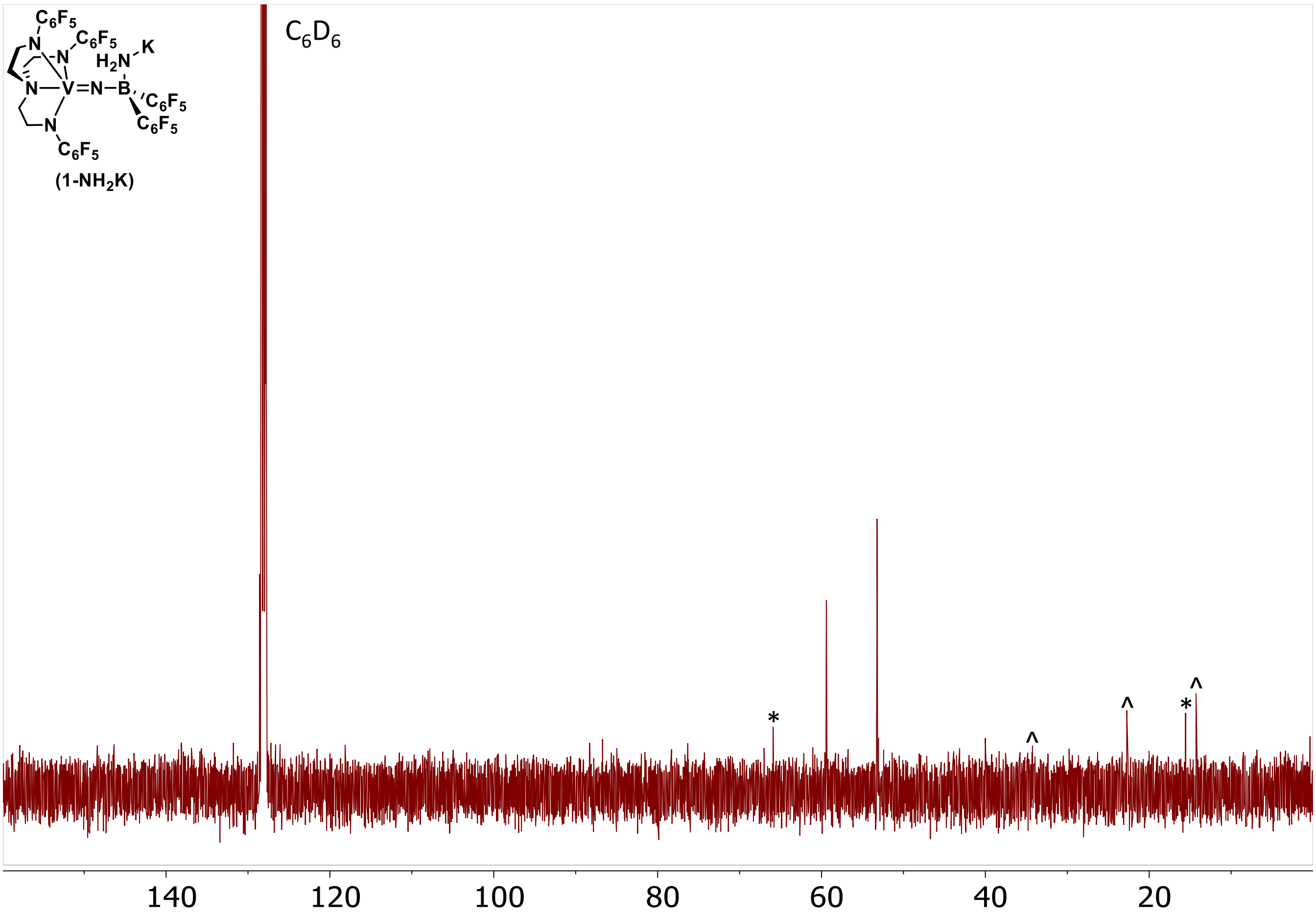

Figure S27. $^{13}C\{^1H\}$ NMR of **1-NH₂K** (100 MHz, C_6D_6, 25 °C). (* = diethyl ether, ^ = pentane)

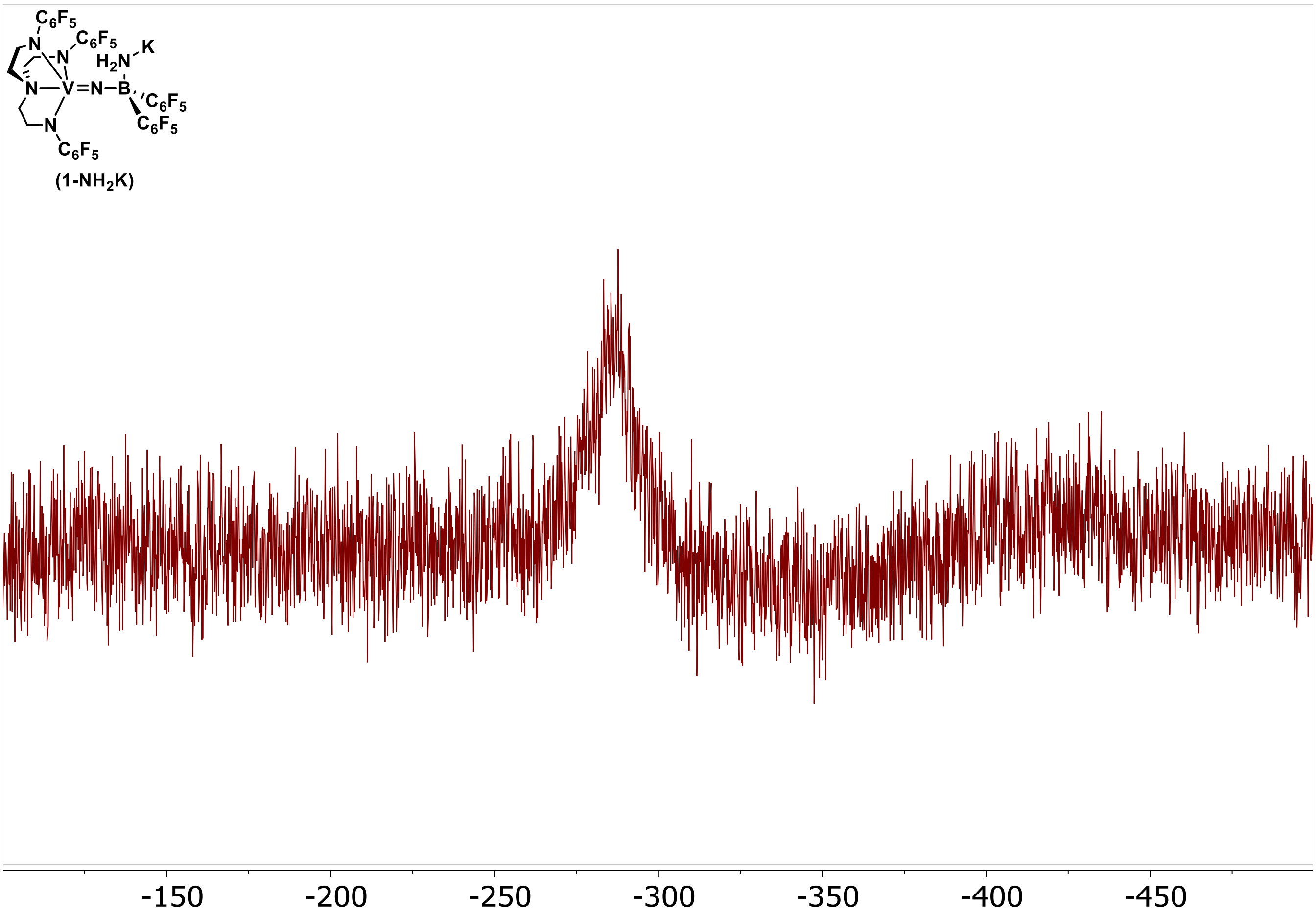

Figure S28. ^{51}V NMR of **1-NH$_2$K** (105 MHz, C_6D_6, 25 °C).

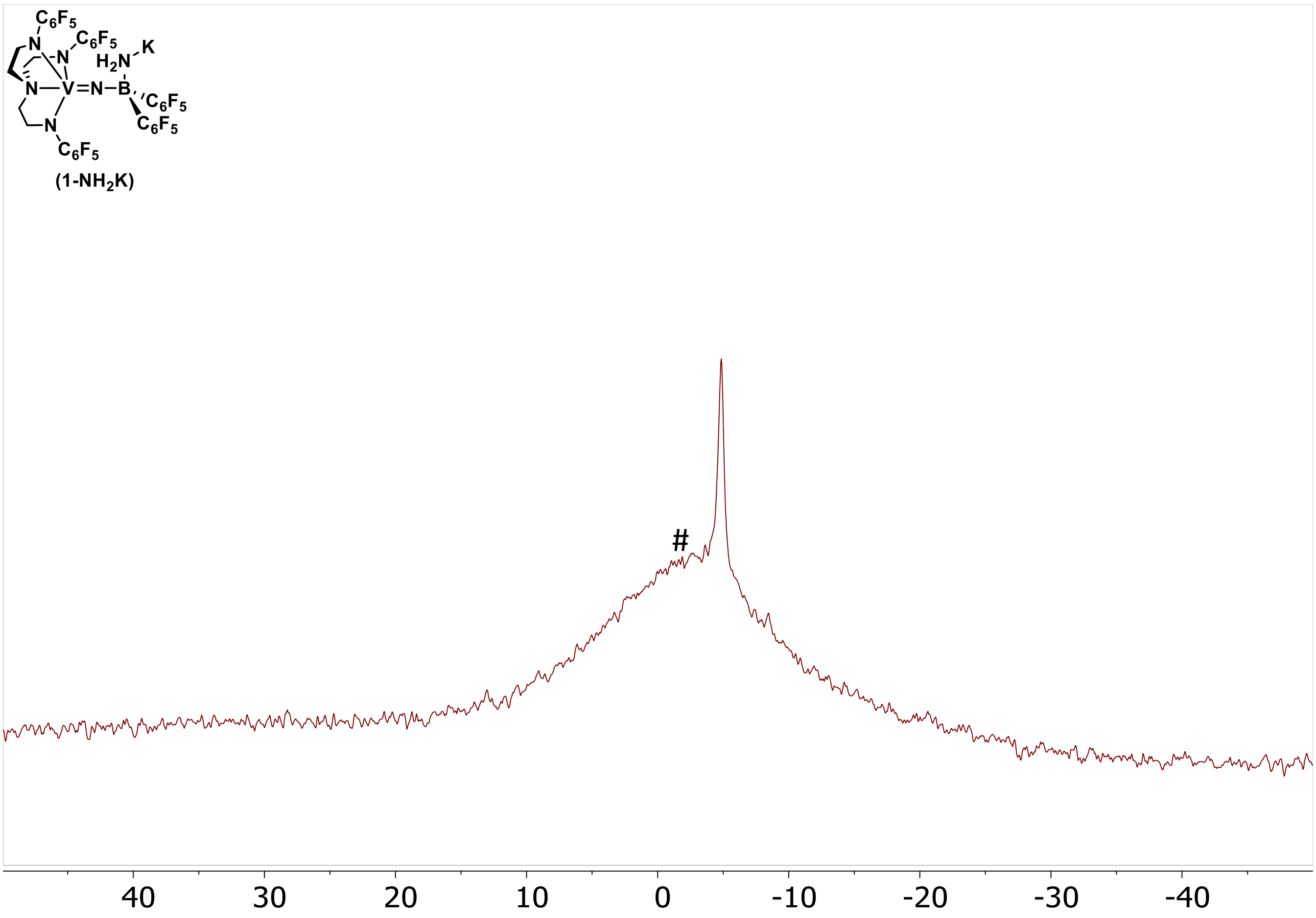

Figure S29. ^{11}B NMR of **1-NH$_2$K** (105 MHz, C_6D_6, 25 °C). (# = borosilicate resonance from NMR tube)

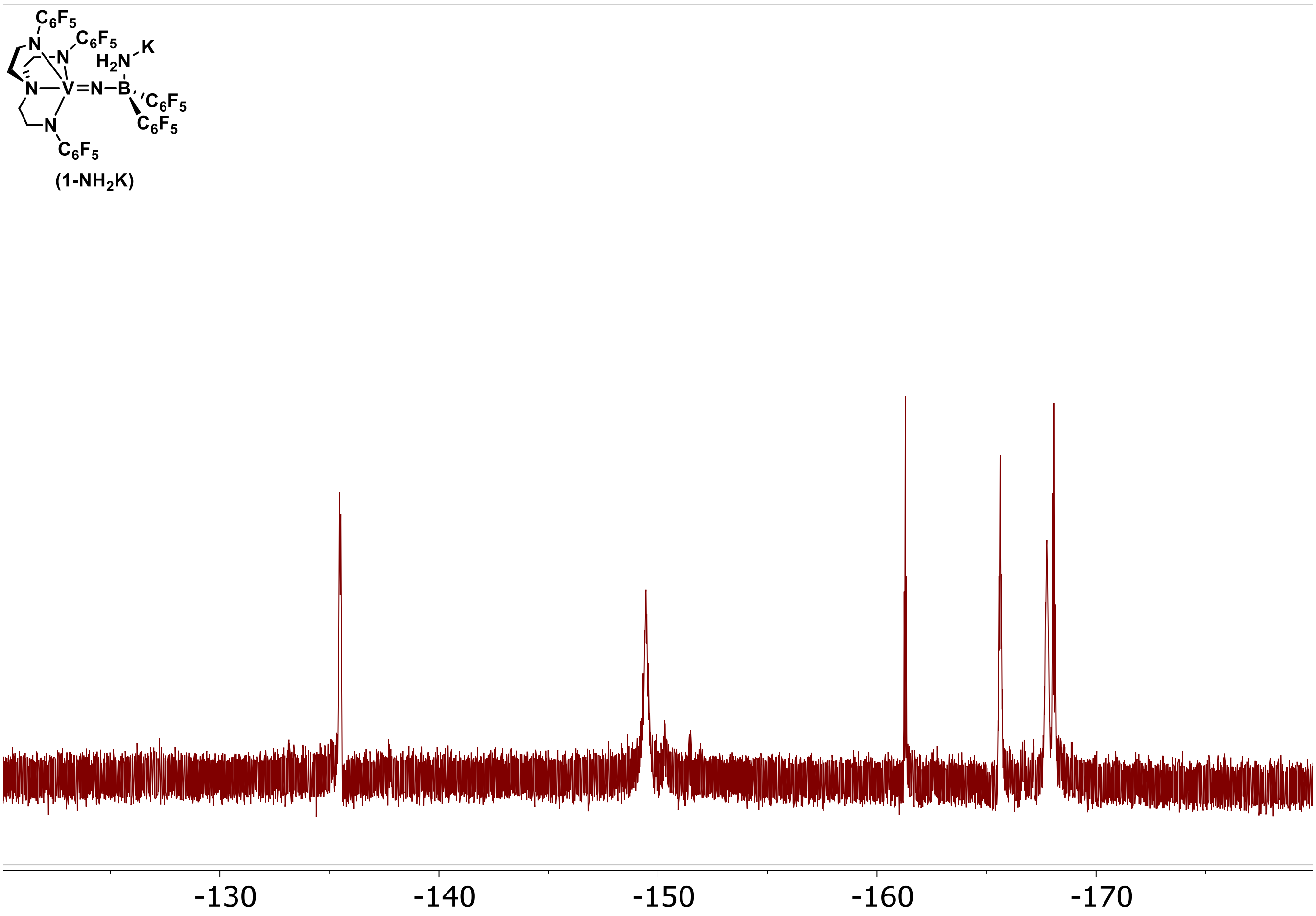

Figure S30. ^{19}F NMR of **1-NH$_2$K** (376 MHz, C_6D_6, 25 °C).

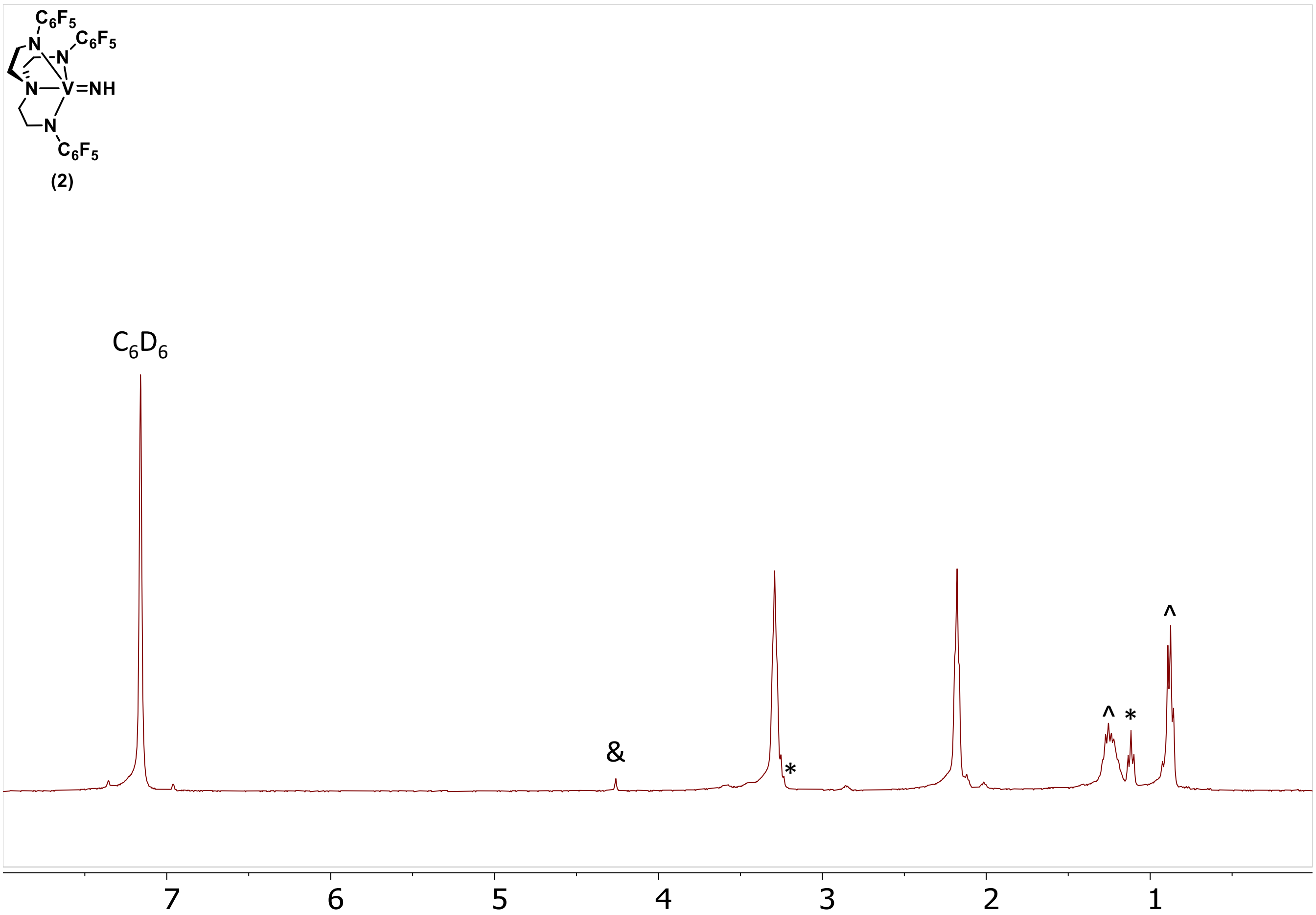

Figure S31. ^{1}H NMR of **2** (400 MHz, C_6D_6, 25 °C). (* = diethyl ether, ^ = pentane, & = DCM)

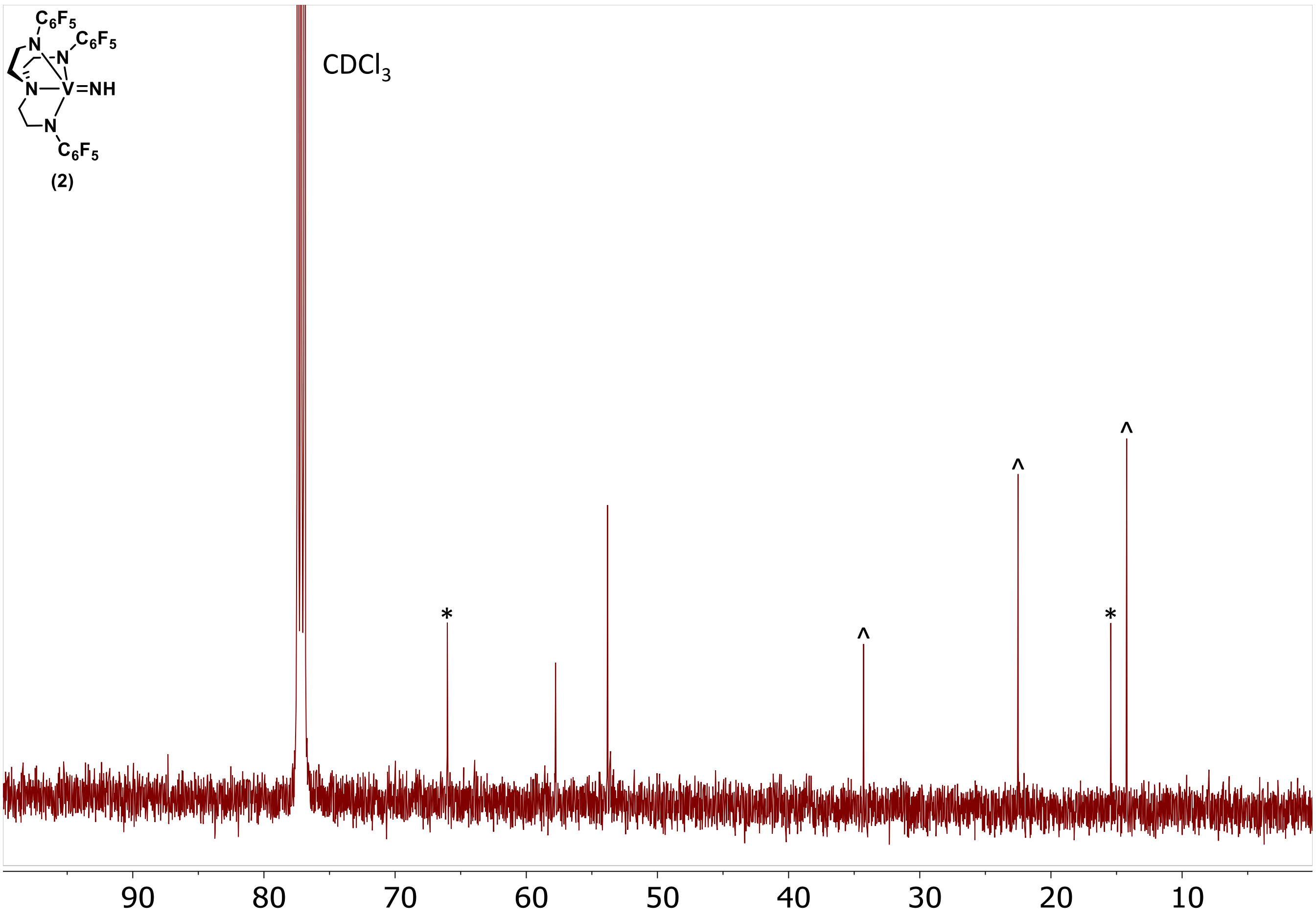

Figure S32. $^{13}C\{^1H\}$ NMR of **2** (126 MHz, $CDCl_3$, 25 °C). (* = diethyl ether, ^ = pentane)

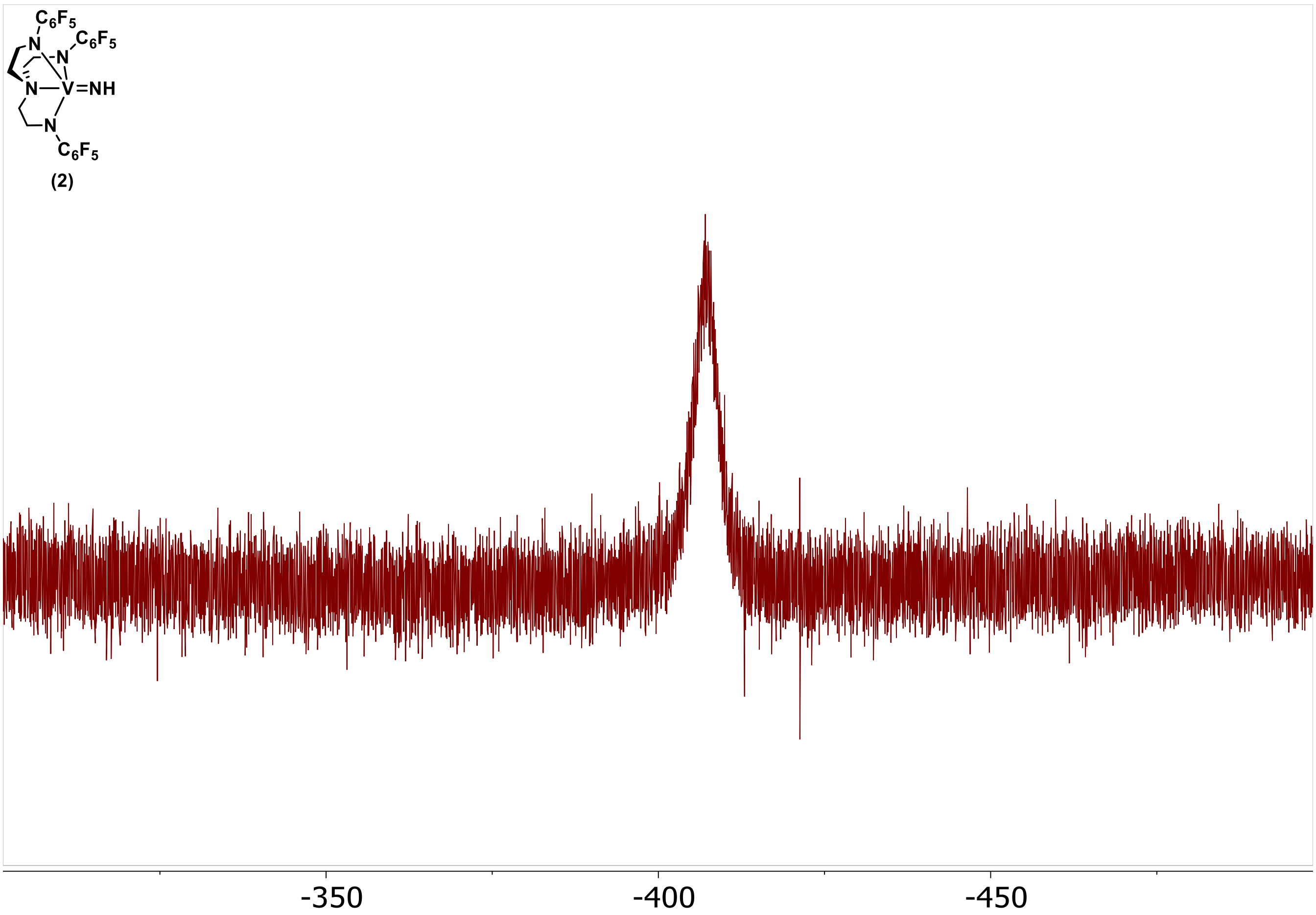

Figure S33. ^{51}V NMR of **2** (105 MHz, C_6D_6, 25 °C).

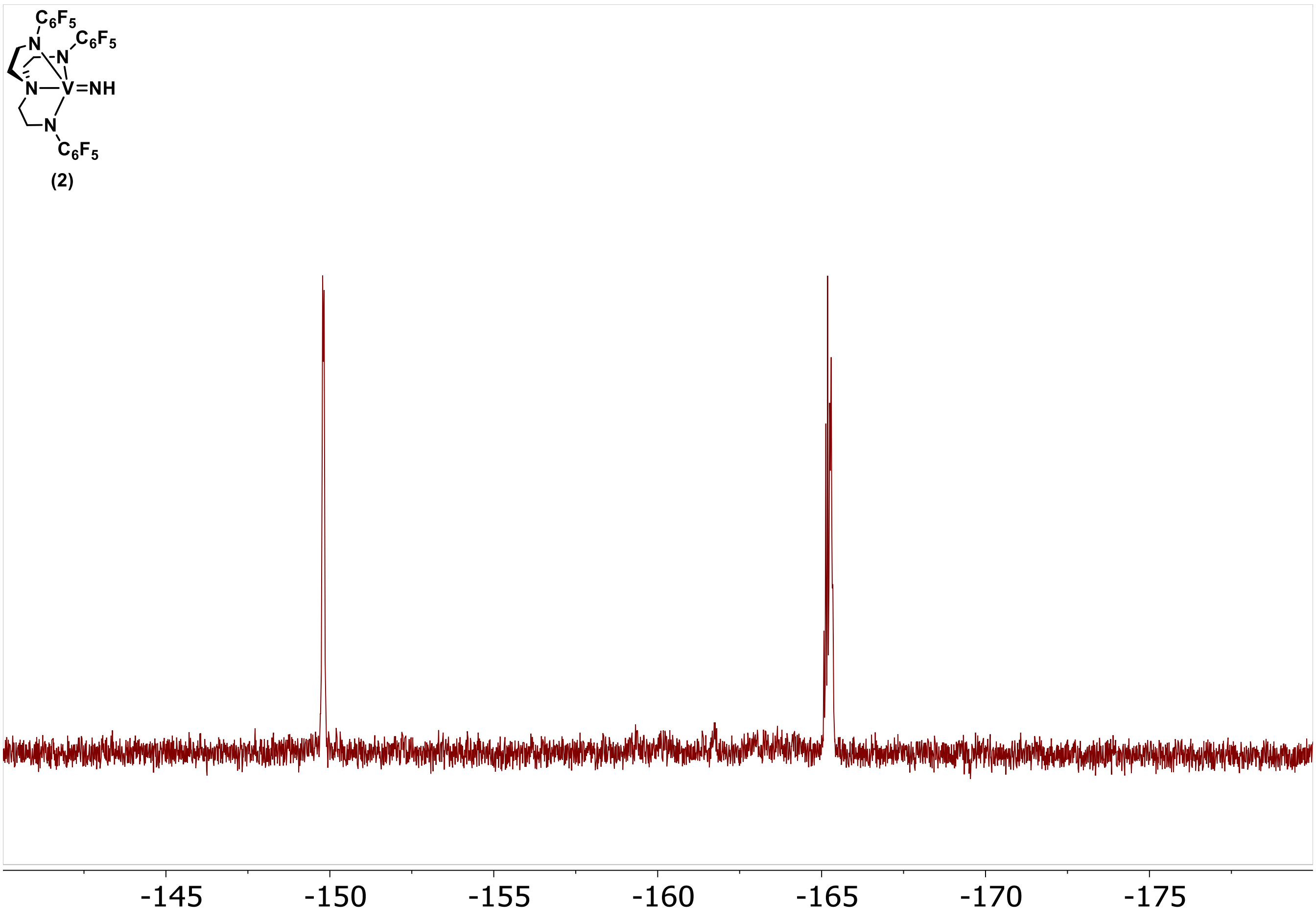

Figure S34. ^{19}F NMR of **2** (376 MHz, CDCl$_3$, 25 °C).

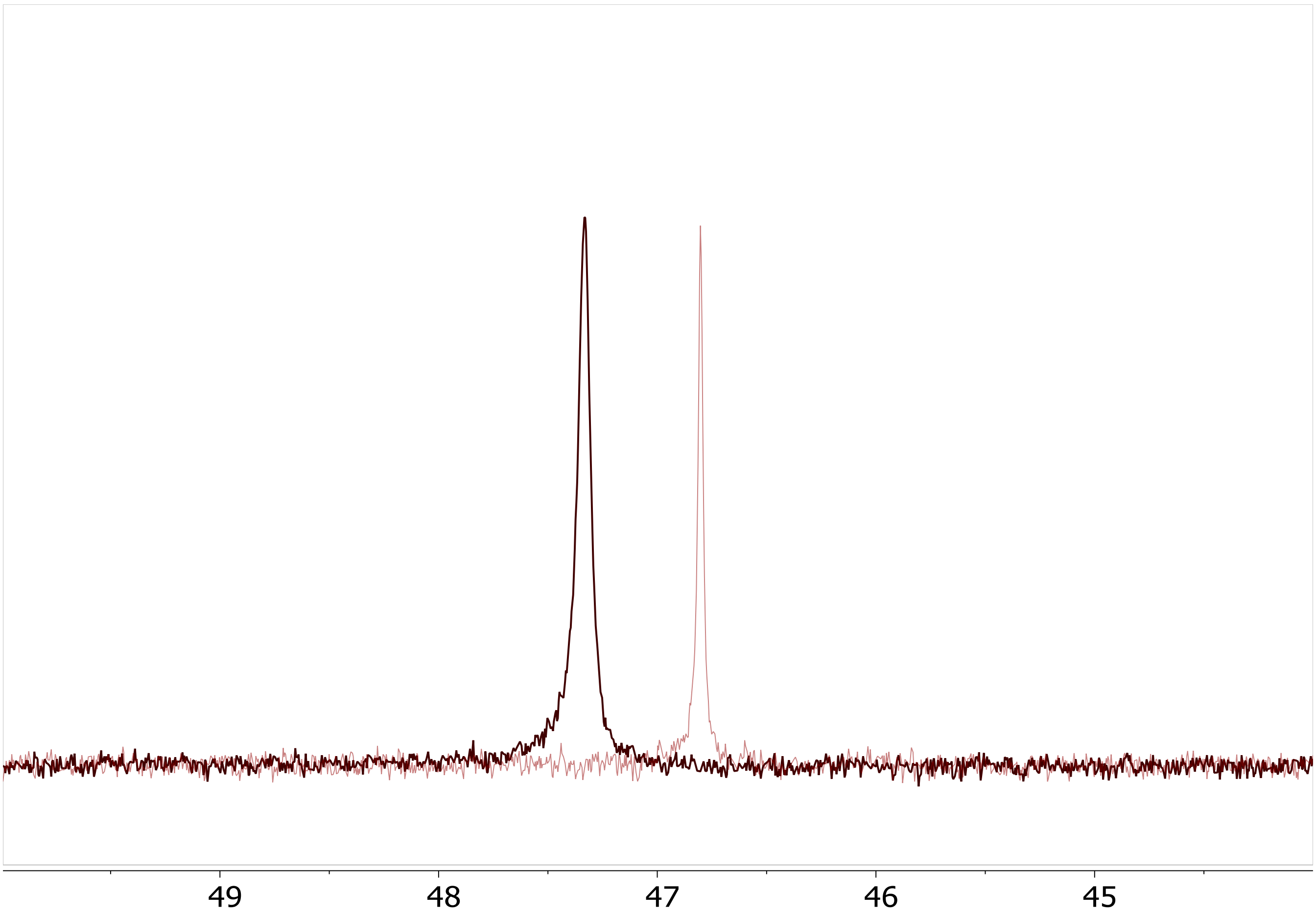

Figure S35. Overlayed ^{31}P NMR spectra (162 MHz, C_6D_5Br, 25 °C) resulting from the combination of **1**$^-$ and Et_3PO (black) and ^{31}P NMR spectrum of free Et_3PO (red). The chemical shift difference ($\Delta\delta_P$) is 0.5, leading to a calculated acceptor number (AN) value of 13.9 indicative of diminished, but non-negligible Lewis acidity of **1**$^-$ compared to **1**. We note that this assgined value is tentative given that the paramagnetic nature of **1**$^-$ may unpredictably affect the chemical shift value.

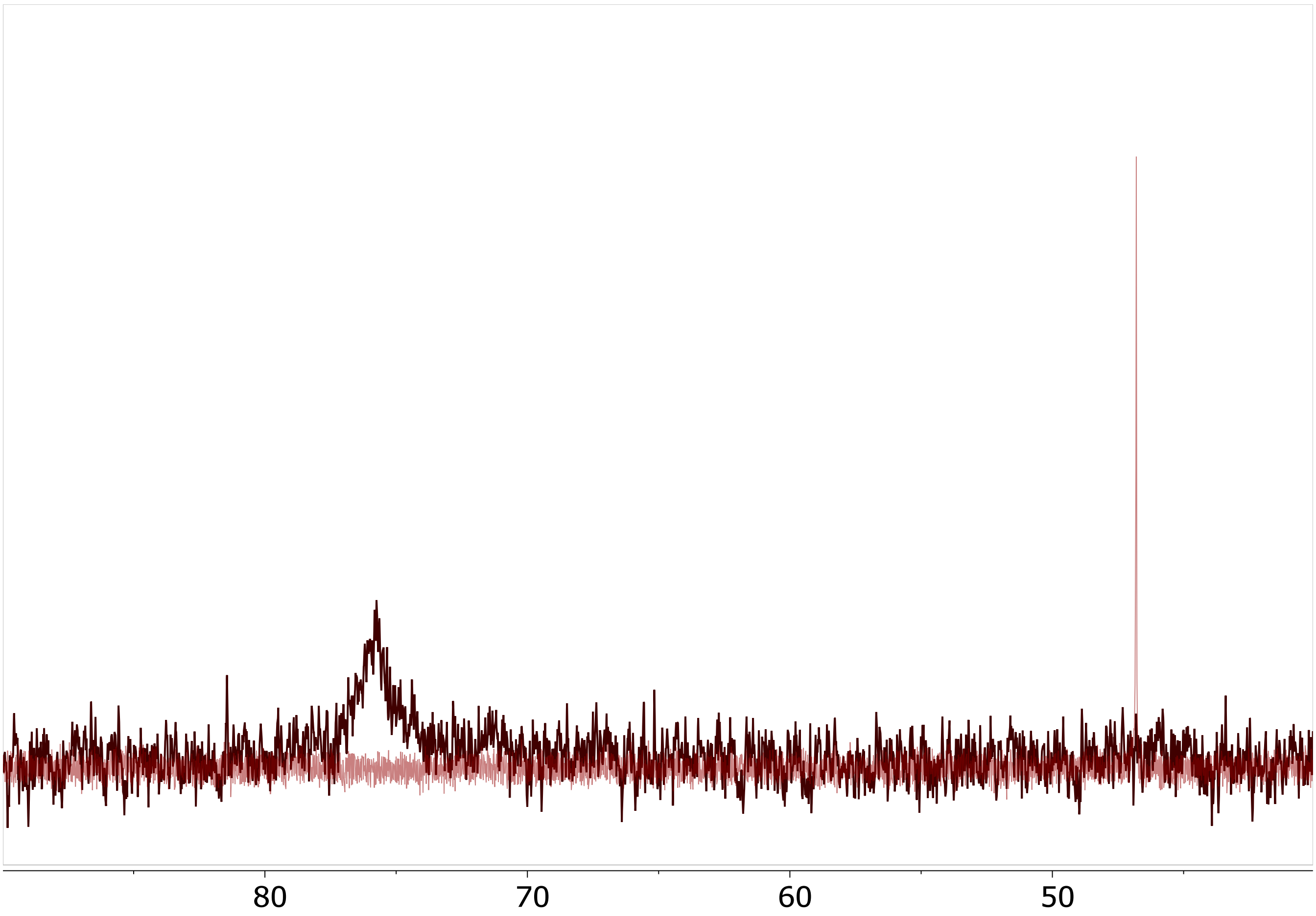

Figure S36. Overlayed ^{31}P NMR spectra (162 MHz, C_6D_6, 25 °C) resulting from the combination of **1** and Et_3PO (black) and ^{31}P NMR spectrum of free Et_3PO (red). The chemical shift difference ($\Delta\delta_P$) is 29.1, leading to a calculated acceptor number (AN) value of 77.1.

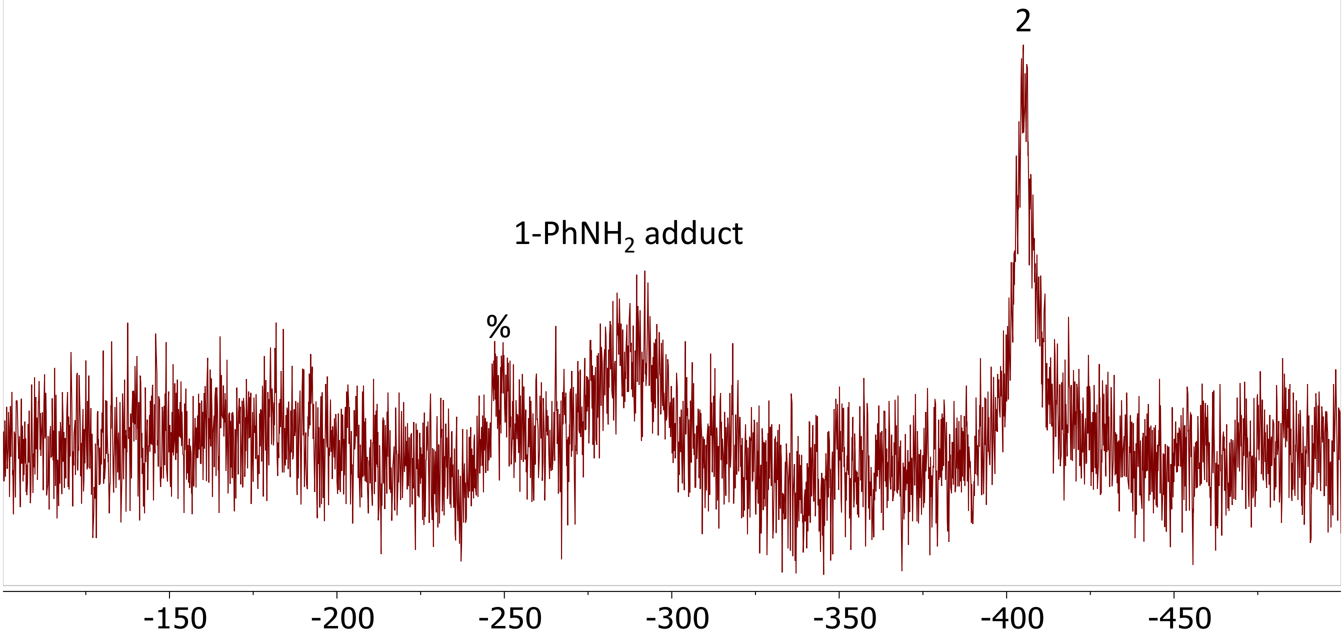

Figure S37. Crude ^{51}V NMR spectrum resulting from the reaction between **1** and PhNH$_2$ to produce a mixture of **2** (-400 ppm), the presumed unstable 1-PhNH$_2$ adduct (-289 ppm) that undergoes protonolysis to **2**, and a minor unidentified resonance at -247 ppm (105 MHz, C_6D_6, 25 °C).

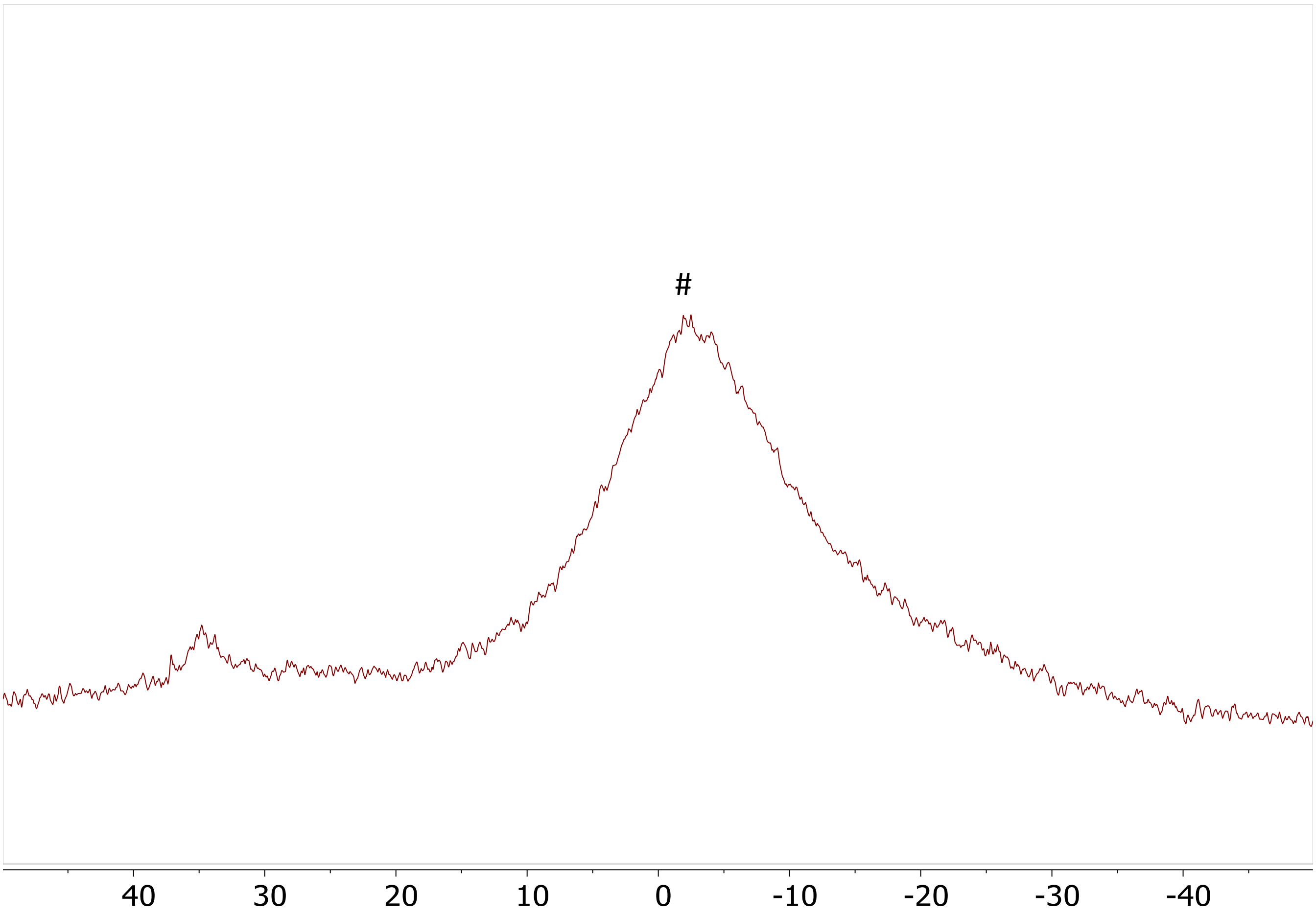

Figure S38. Crude ^{11}B NMR spectrum (128 MHz, C_6D_6, 25 °C) resulting from the reaction between **1** and $PhNH_2$ showing a broad resonance at 34.8 ppm similar to related $(C_6F_5)_2BNHR$ compounds.[5] (# = borosilicate resonance from NMR tube)

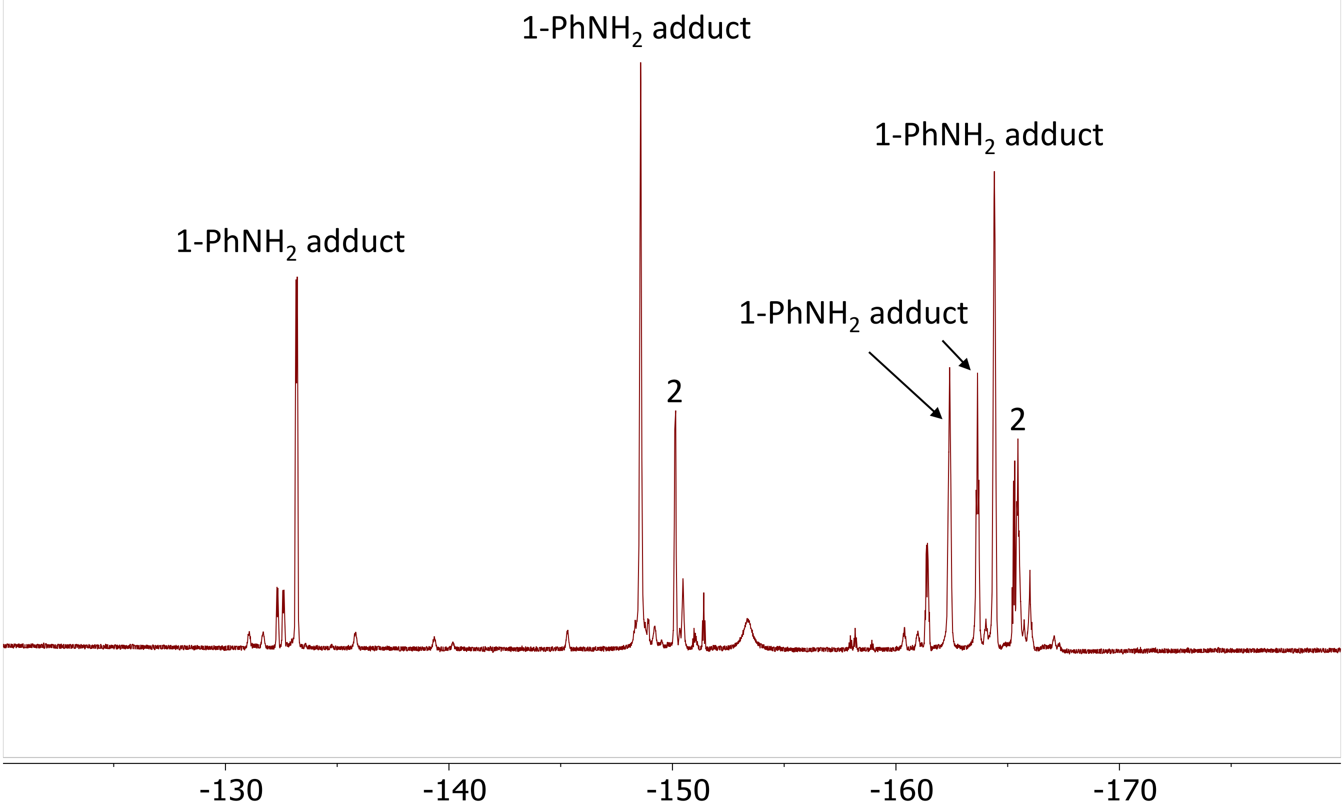

Figure S39. Crude ^{19}F NMR spectrum resulting from the reaction between **1** and $PhNH_2$ to produce a mixture of the putative 1-$PhNH_2$ adduct and **2** (376 MHz, C_6D_6, 25 °C).

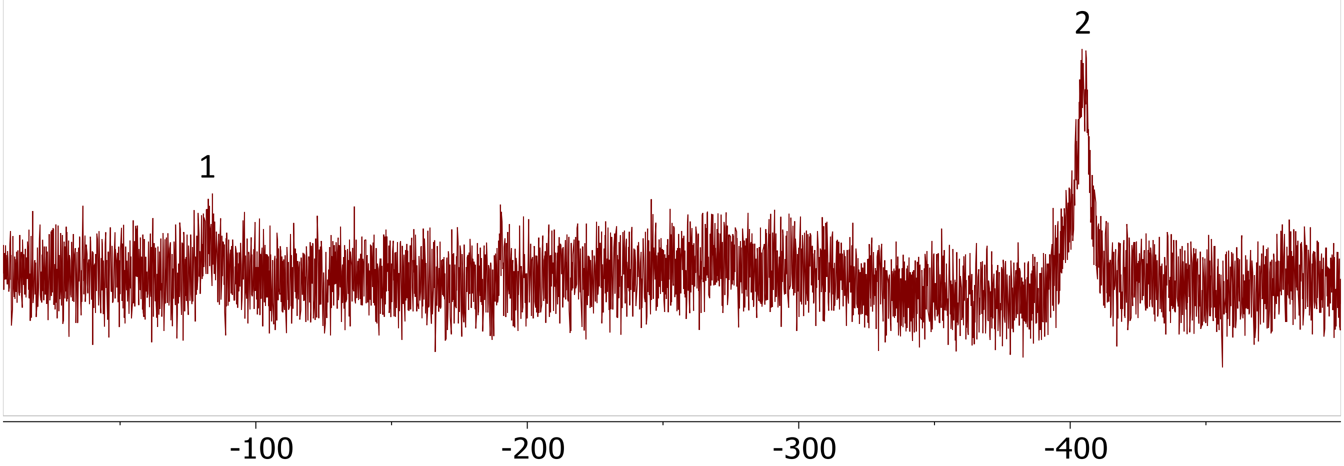

Figure S40. Crude ^{51}V NMR spectrum resulting from the reaction between **1** and C_6F_5OH revealing conversion to **2** (105 MHz, C_6D_6, 25°C).

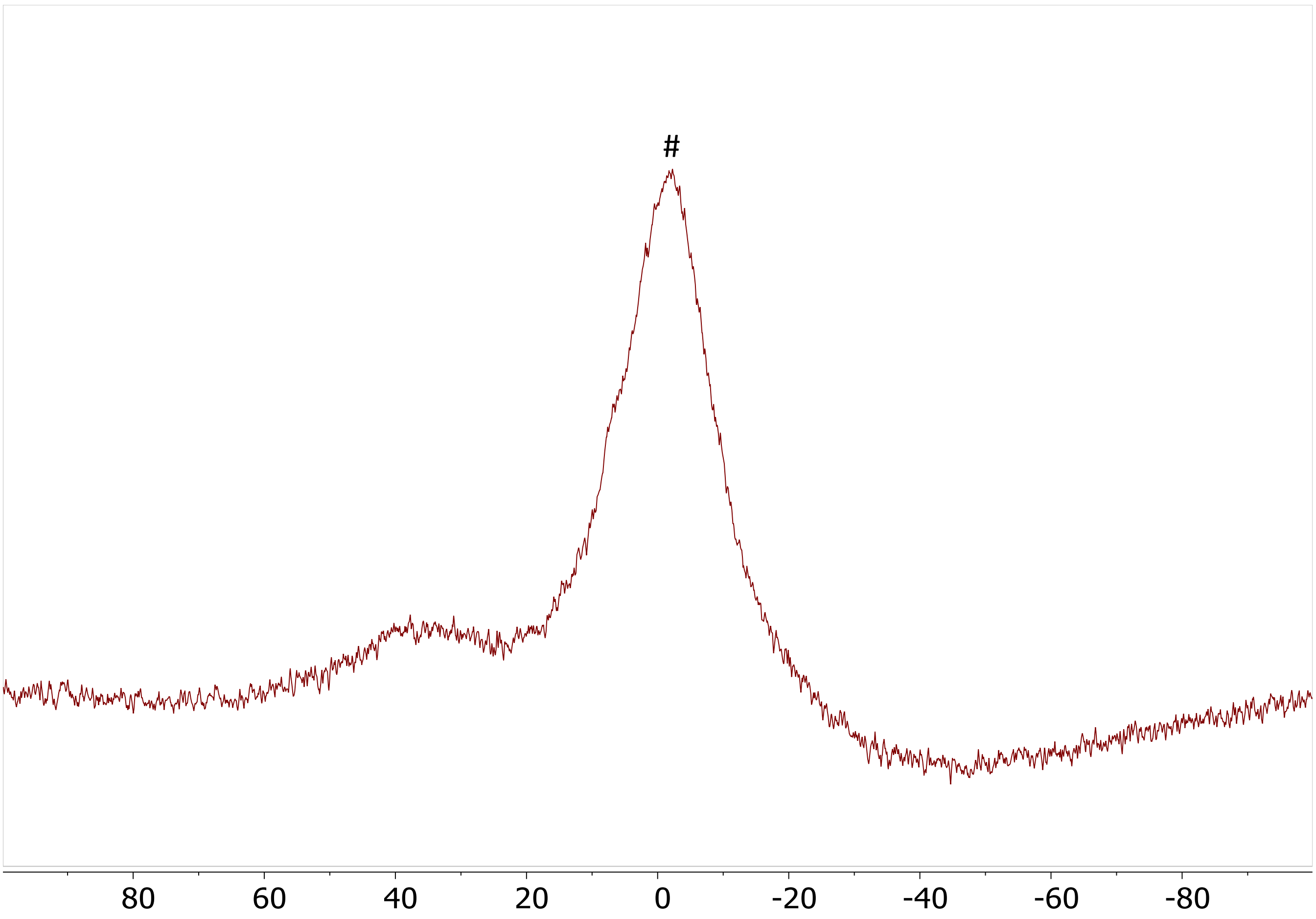

Figure S41. Crude ^{11}B NMR spectrum resulting from the reaction between **1** and C_6F_5OH revealing a broad signal ~40 ppm close to that of $(C_6F_5)_2BOC_6F_5$ (41.2 ppm) (128 MHz, C_6D_6, 25°C). (# = borosilicate resonance from NMR tube)

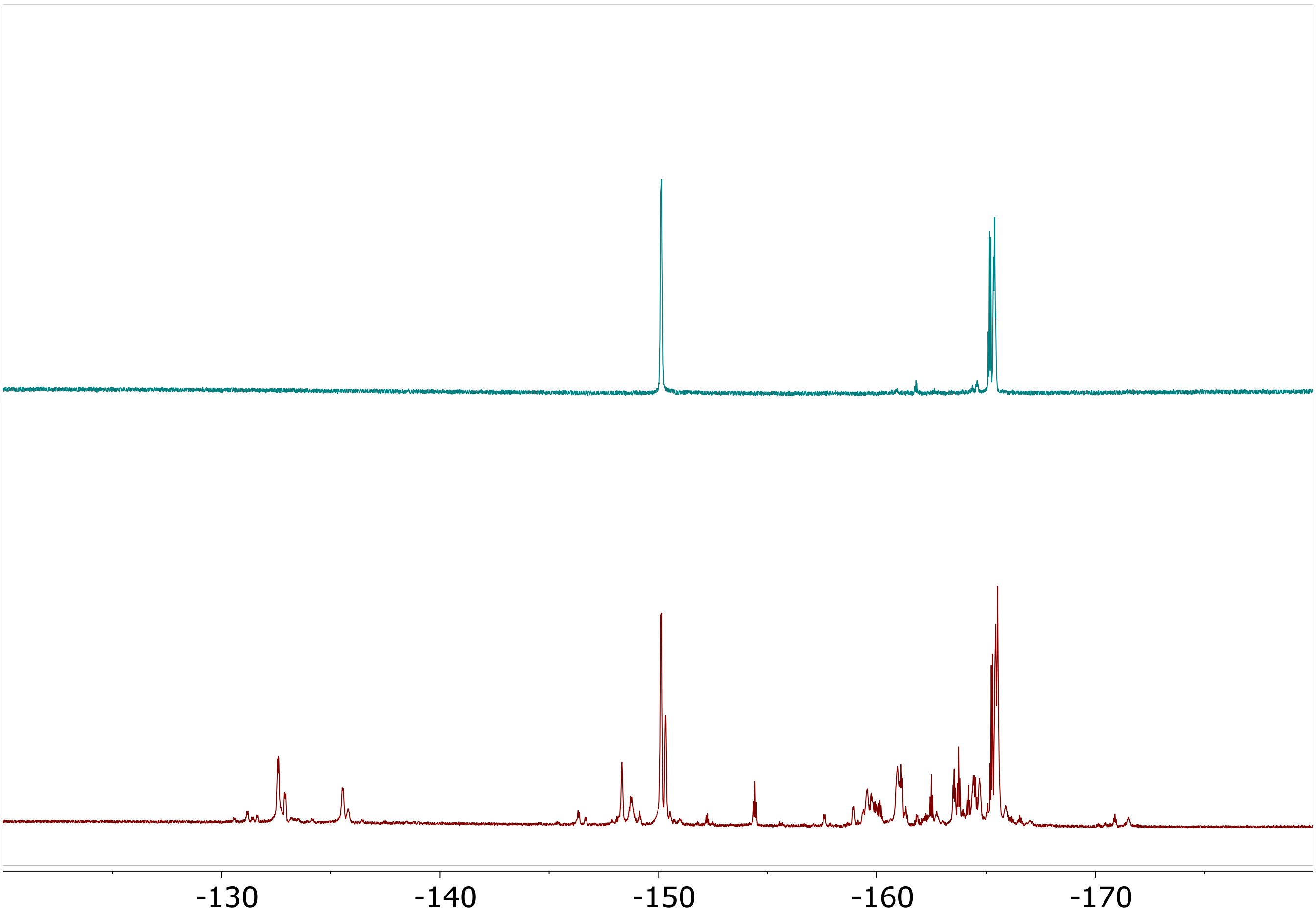

Figure S42. Crude ^{19}F NMR spectrum (376 MHz, C_6D_6, 25°C) resulting from the reaction between **1** and C_6F_5OH revealing conversion to **2** (bottom). The ^{19}F NMR spectrum of isolated **2** is provided for reference (top).

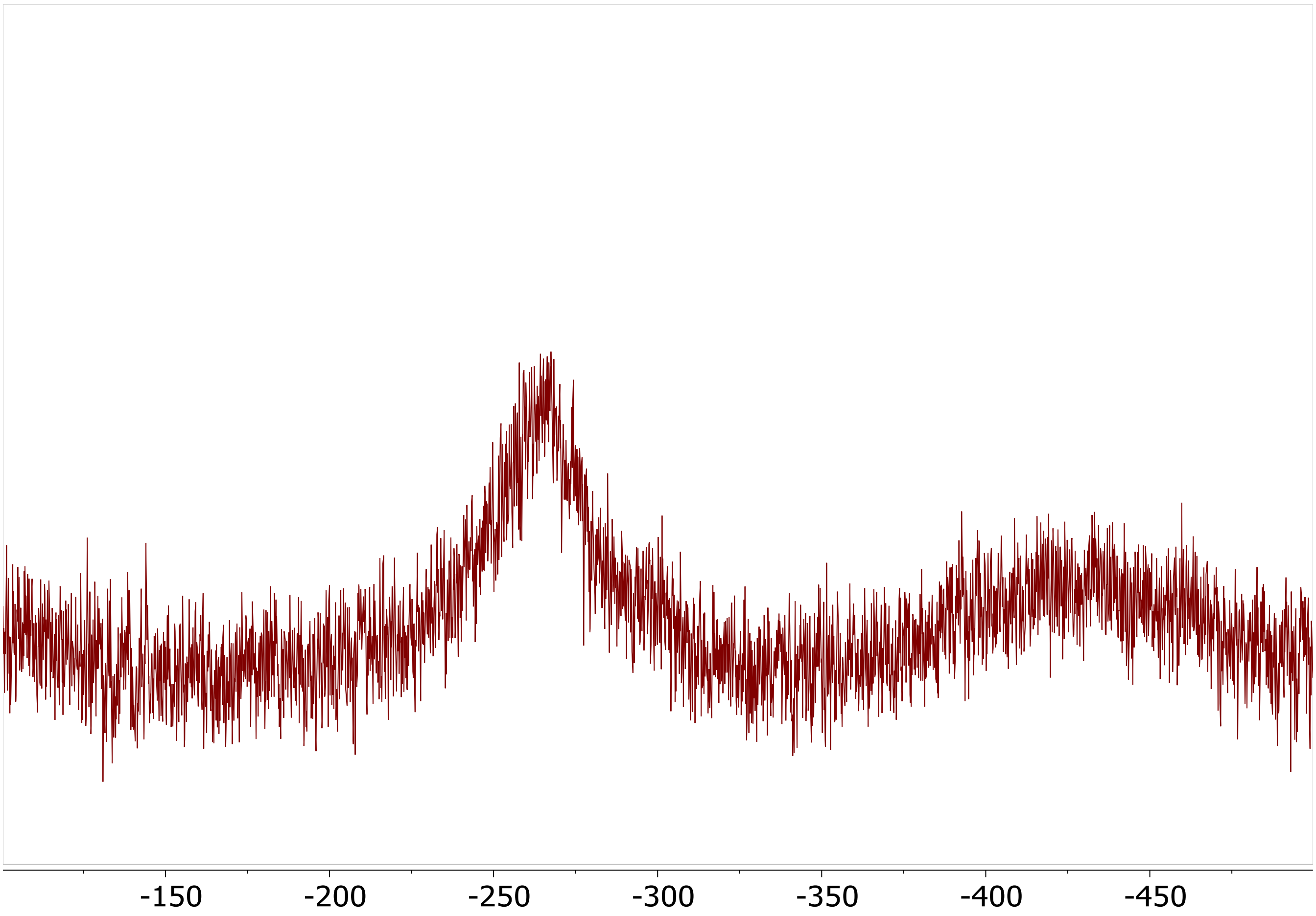

Figure S43. Crude ^{51}V NMR spectrum from the reaction between **1**$^{-}$ and PhSH revealing **1-SPh** as the sole vanadium-containing product (105 MHz, C_6D_5Br, 25°C).

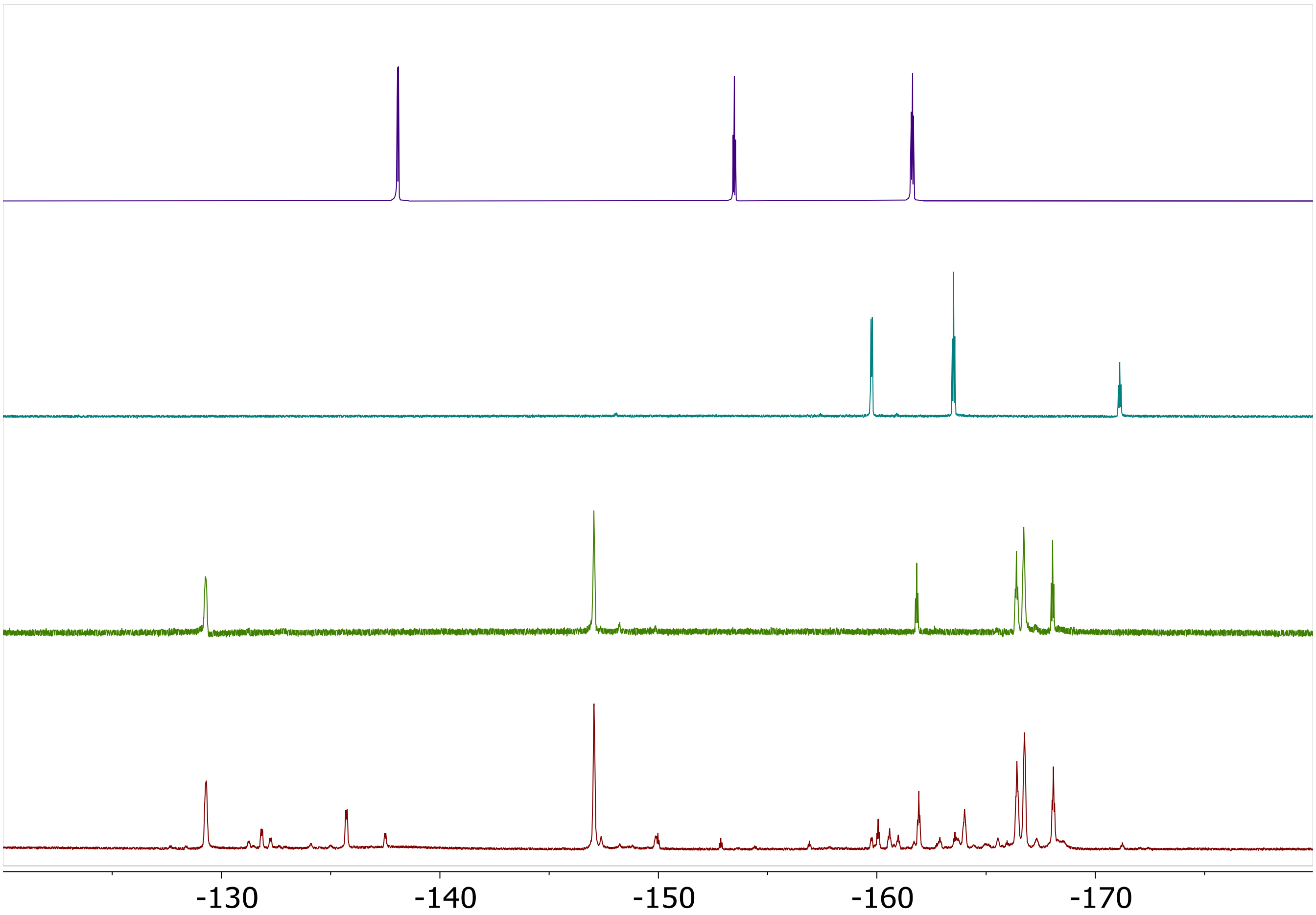

Figure S44. Crude ^{19}F NMR spectrum (376 MHz, C_6D_5Br, 25°C) of the reaction between **1**$^-$ and PhSH revealing resonances for **1-SPh**, a very small amount of free tren ligand, and no C_6F_5H (bottom). The ^{19}F NMR spectra of isolated **1-SPh** (second from bottom), free tren ligand (third from bottom), and C_6F_5H (top) are provided for reference.

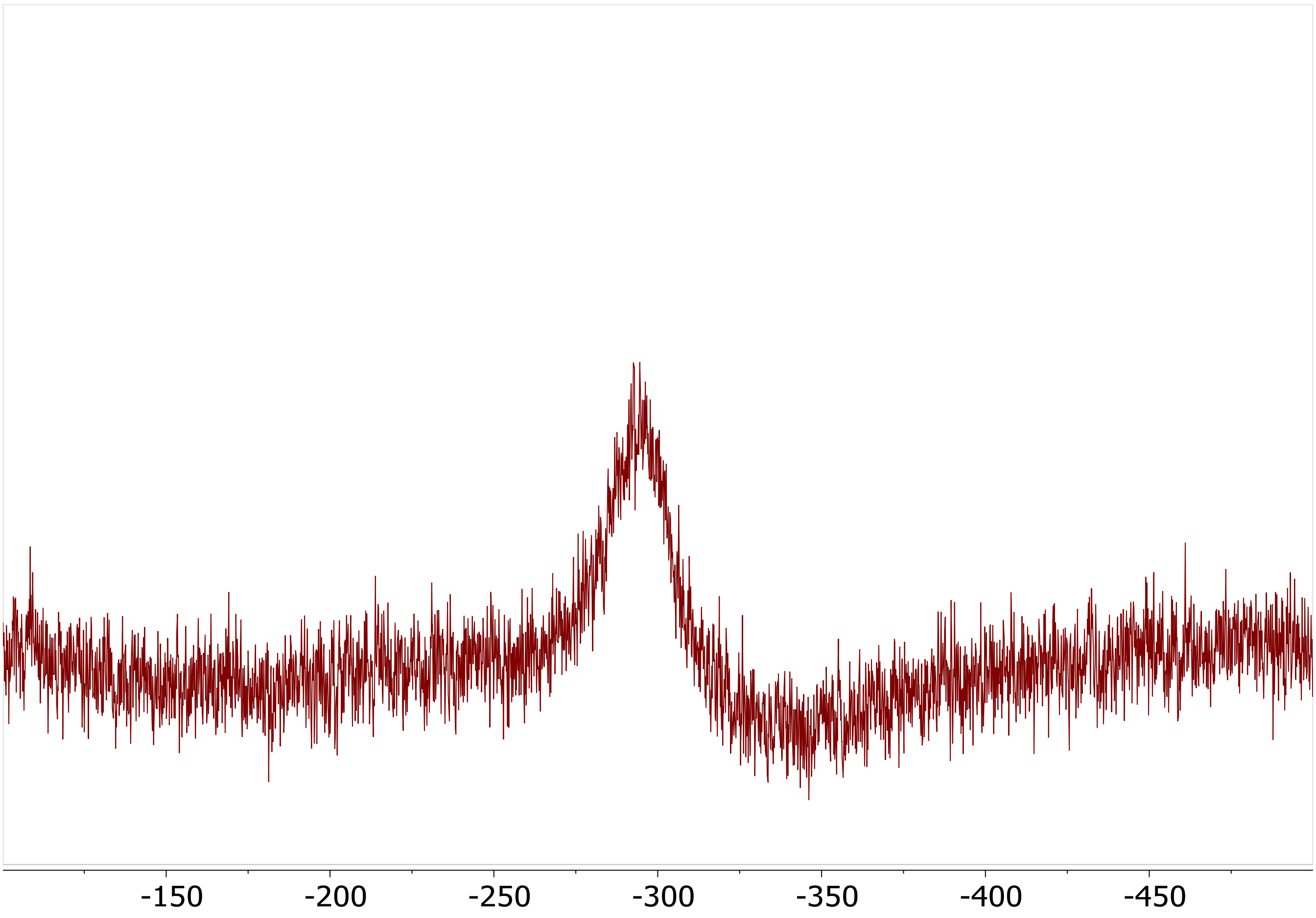

Figure S45. Crude ^{51}V NMR spectrum (105 MHz, C_6D_5Br, 25°C) resulting from the reaction between **1**$^-$ and C_6F_5OH revealing **1-OC$_6$F$_5$** as the sole V-containing product.

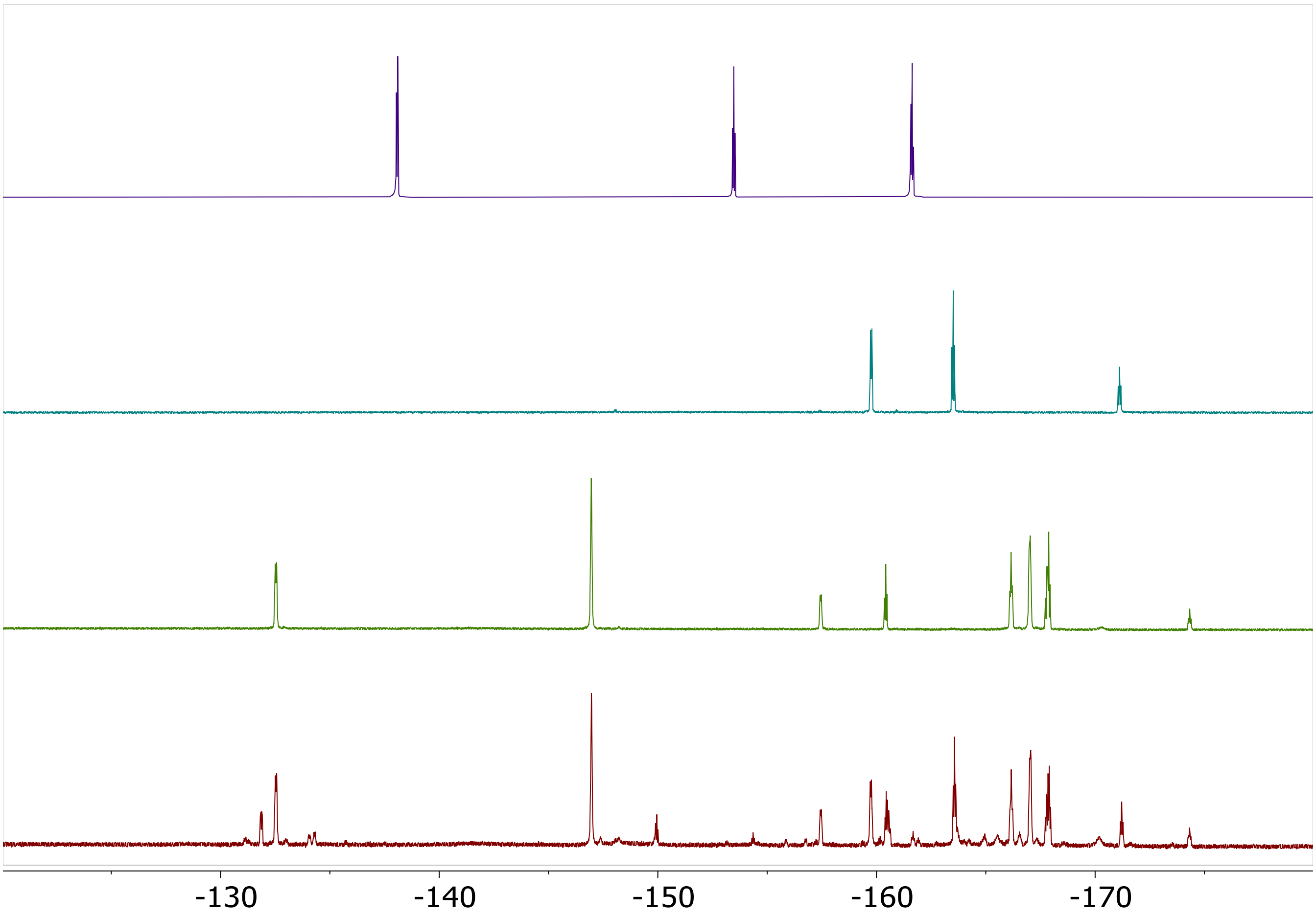

Figure S46. Crude ^{19}F NMR spectrum (376 MHz, C_6D_5Br, 25°C) resulting from the reaction between **1**$^{-}$ and C_6F_5OH revealing a mixture of **1-OC$_6$F$_5$** and free tren ligand (bottom). The ^{19}F NMR spectra of isolated **1-OC$_6$F$_5$** (second from bottom), free tren ligand (third from bottom), and C_6F_5H (top) are provided for reference.

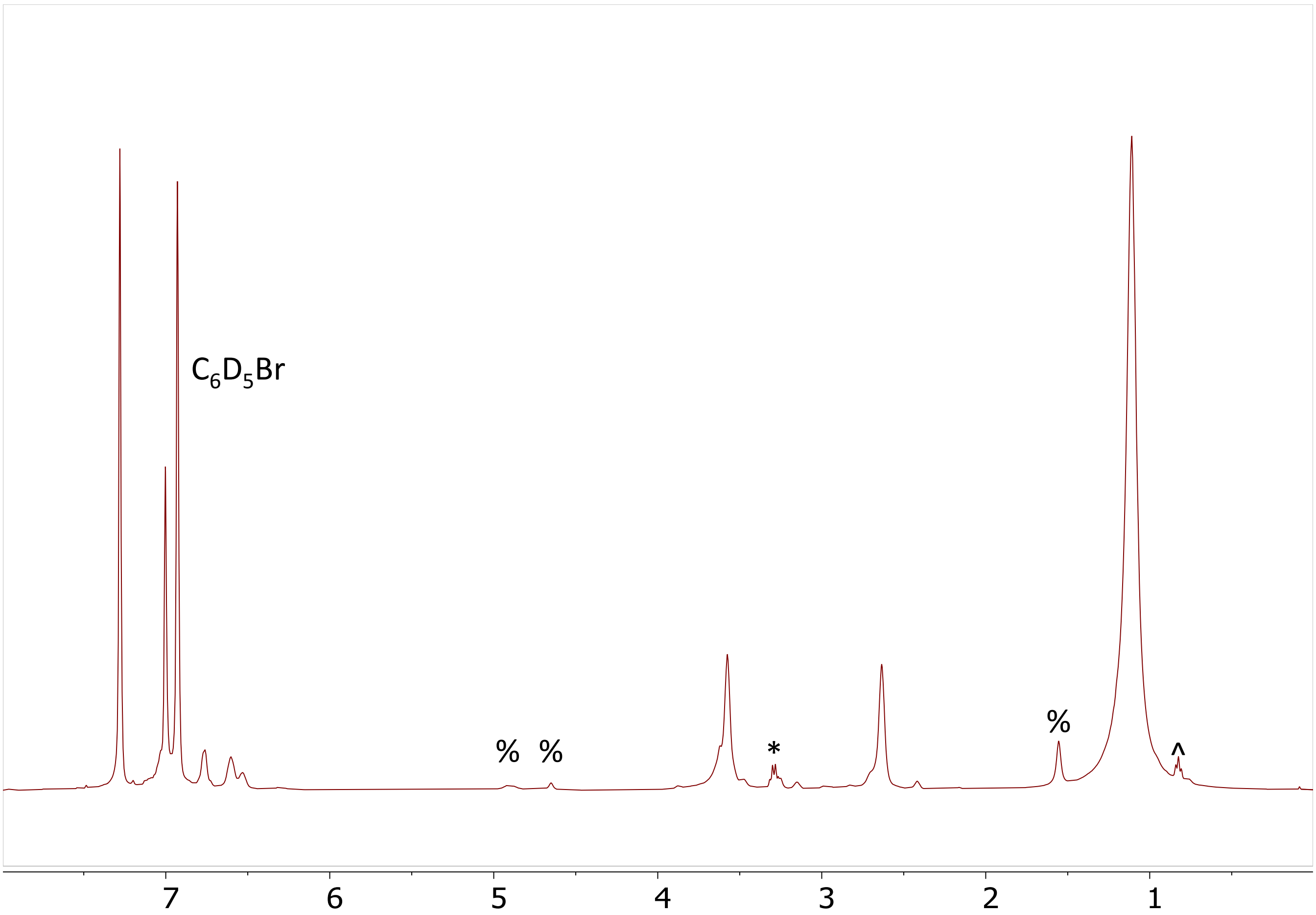

Figure S47. Crude ^{1}H NMR spectrum (400 MHz, C_6D_5Br, 25°C) resulting from the reaction between **1**$^-$ and PhSH revealing **1-SPh**. The fate of the putative H• in this transformation remains unclear. (* = diethyl ether, ^ = pentane, % = unidentified resonances)

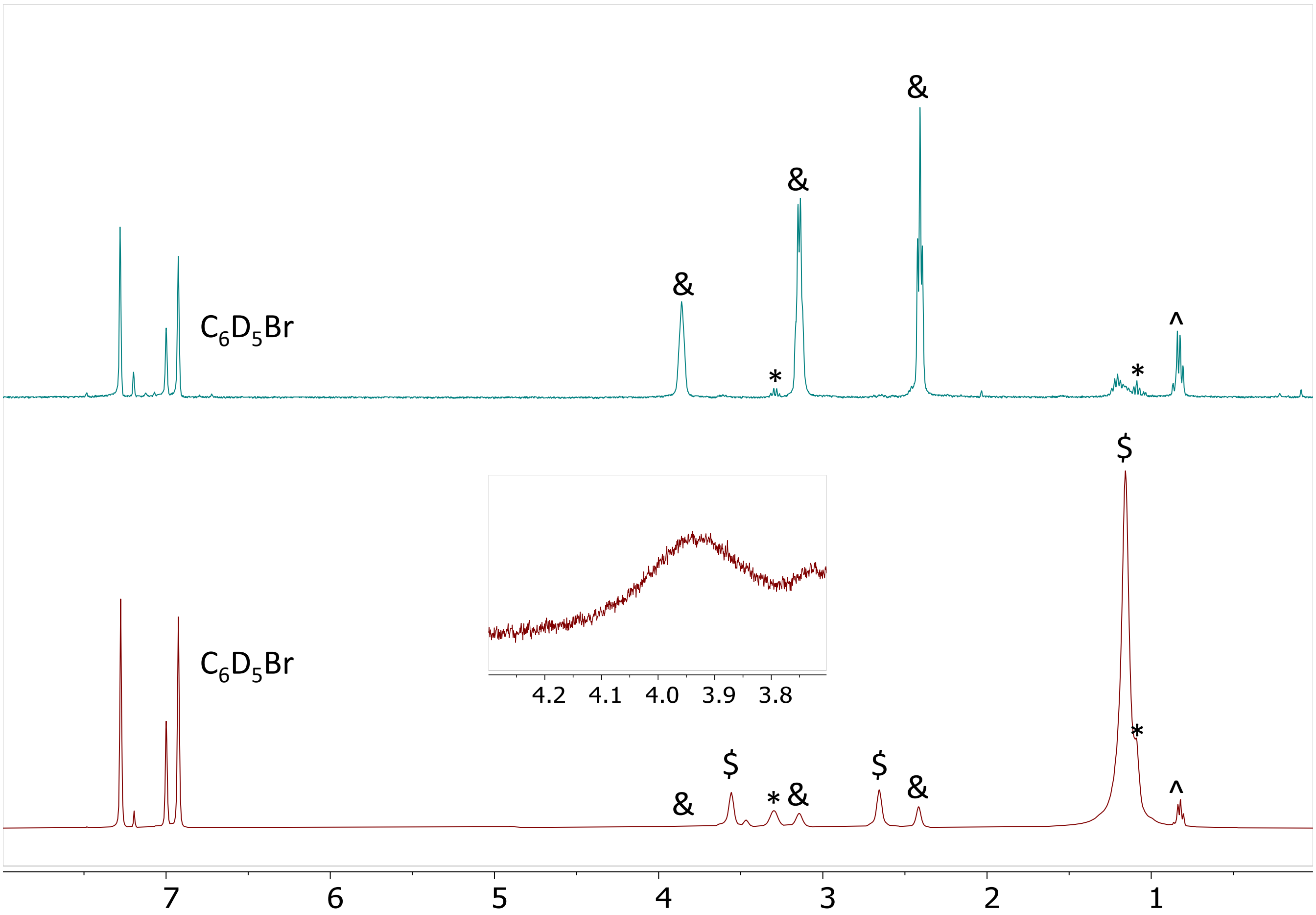

Figure S48. Crude ^{1}H NMR spectrum resulting from the reaction between **1**$^{-}$ and C_6F_5OH revealing resonances for **1-OC$_6$F$_5$** ($) and free tren ligand (&). Inset is a magnified region of the same ^{1}H NMR spectrum revealing a broad peak consistent with the NH resonance for free tren ligand (bottom). The ^{1}H NMR spectrum of free tren ligand (top) is provided for reference (400 MHz, C_6D_5Br, 25°C). (* = diethyl ether, ^ = pentane)

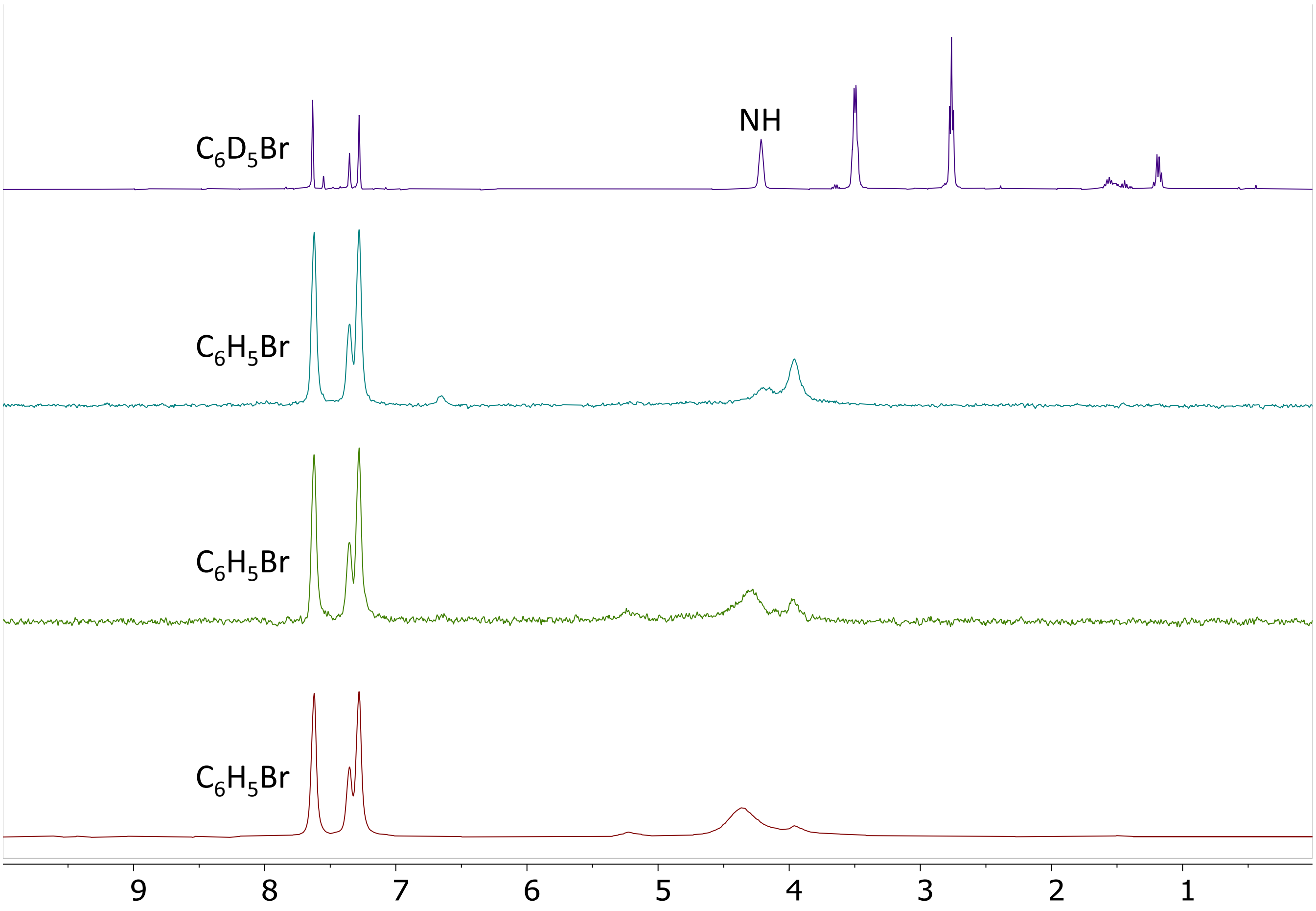

Figure S49. ^{2}H NMR spectrum (77 MHz, C_6H_5Br, 25°C) resulting from the reaction between **1**$^-$ and the C_6F_5OD isotopologue immediately after addition (bottom), after four hours (second from bottom), and after 24 hours (third from bottom). The broad resonance at ~4 ppm in conjunction with the ^{19}F NMR suggests the formation of free tren ligand. The ^{1}H NMR spectrum of free tren ligand (top) is provided for reference.

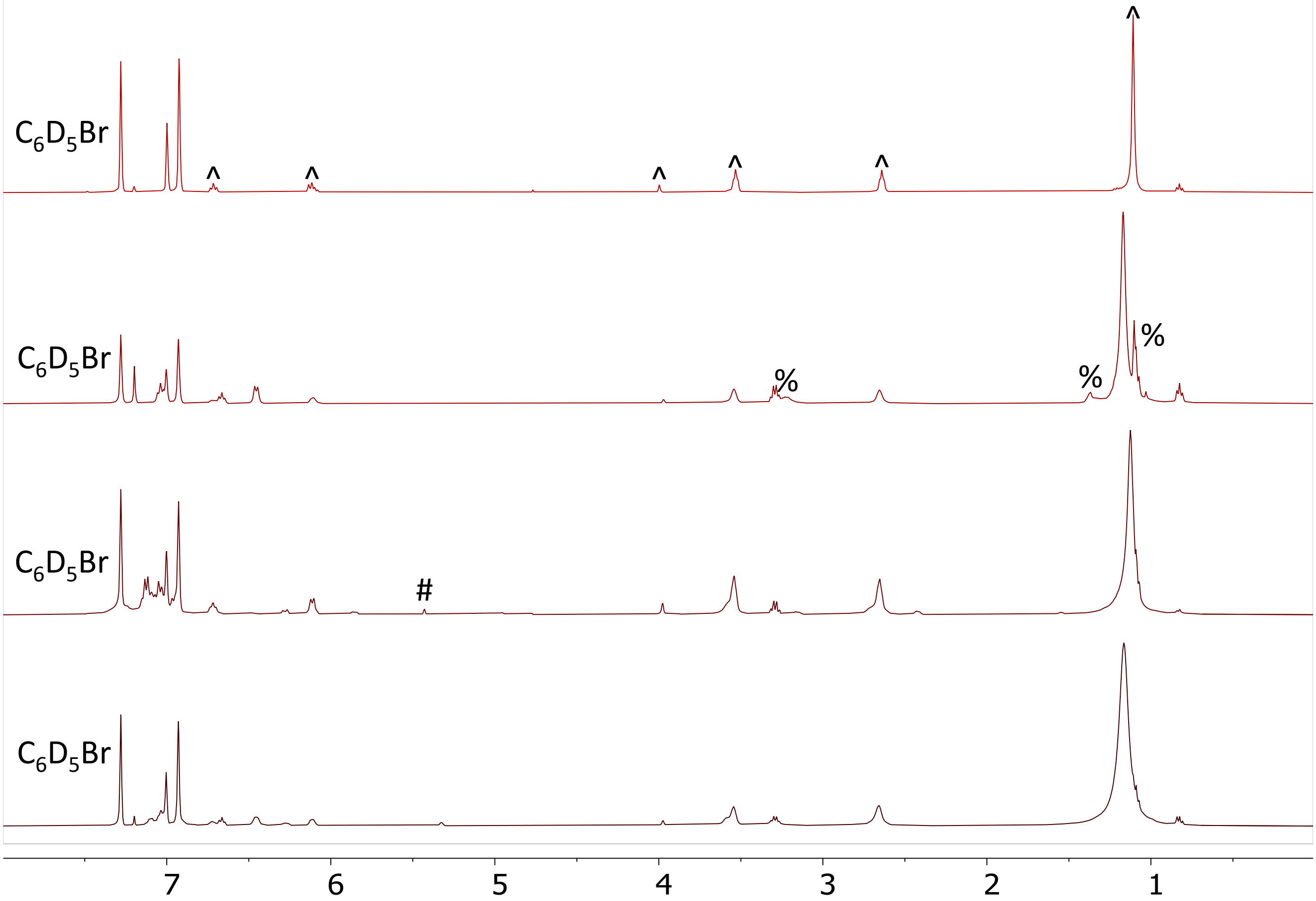

Figure S50. Crude ^{1}H NMR spectra (400 MHz, C_6D_5Br, 25°C) resulting from the reaction between **1**$^-$ and $PhNH_2$ in the absence of HAA agent (bottom), with half an equivalent of Gomberg's dimer (second from bottom), with one equivalent of TEMPO (third from bottom) revealing common resonances attributed to **1-NHPh** and the $Ph_3C–H$ (#) and TEMPO–H (%) byproducts expected from HAA. The ^{1}H NMR spectrum of isolated **1-NHPh** (^) (top) is provided for reference.

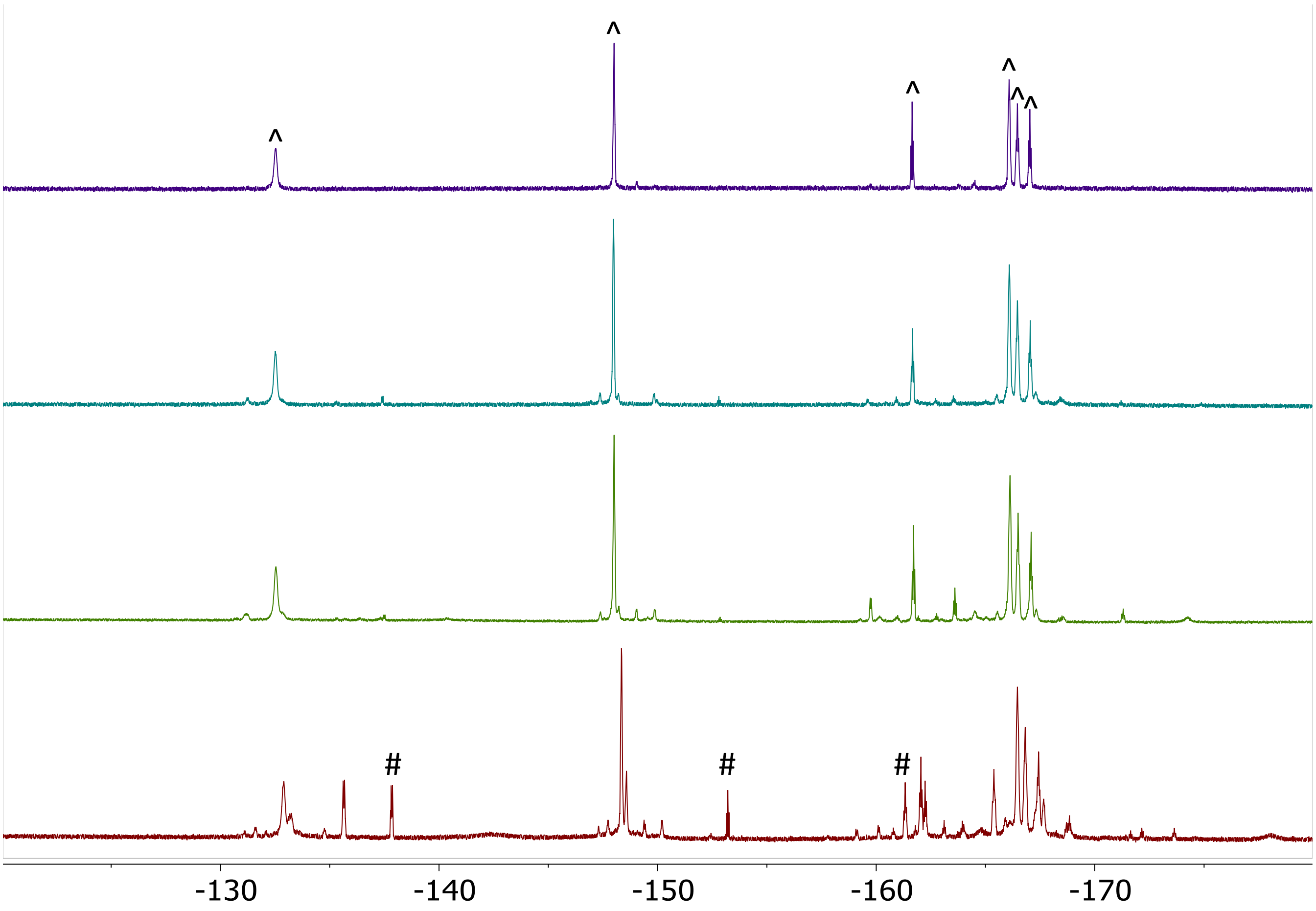

Figure S51. Crude ^{19}F NMR spectra (376 MHz, C_6D_5Br, 25°C) resulting from the reaction between **1**$^{-}$ and $PhNH_2$ in the absence of HAA (bottom), with half an equivalent of Gomberg's dimer (second from bottom), and with one equivalent of TEMPO (third from bottom) revealing six common resonances attributed to **1-NHPh**. A substantial amount of C_6F_5H (#) is observed in the bottom spectrum while the addition of either HAA agent results in cleaner, faster reactions (second and third from bottom). The ^{1}H NMR spectrum of isolated **1-NHPh** (^) (top) is provided for reference.

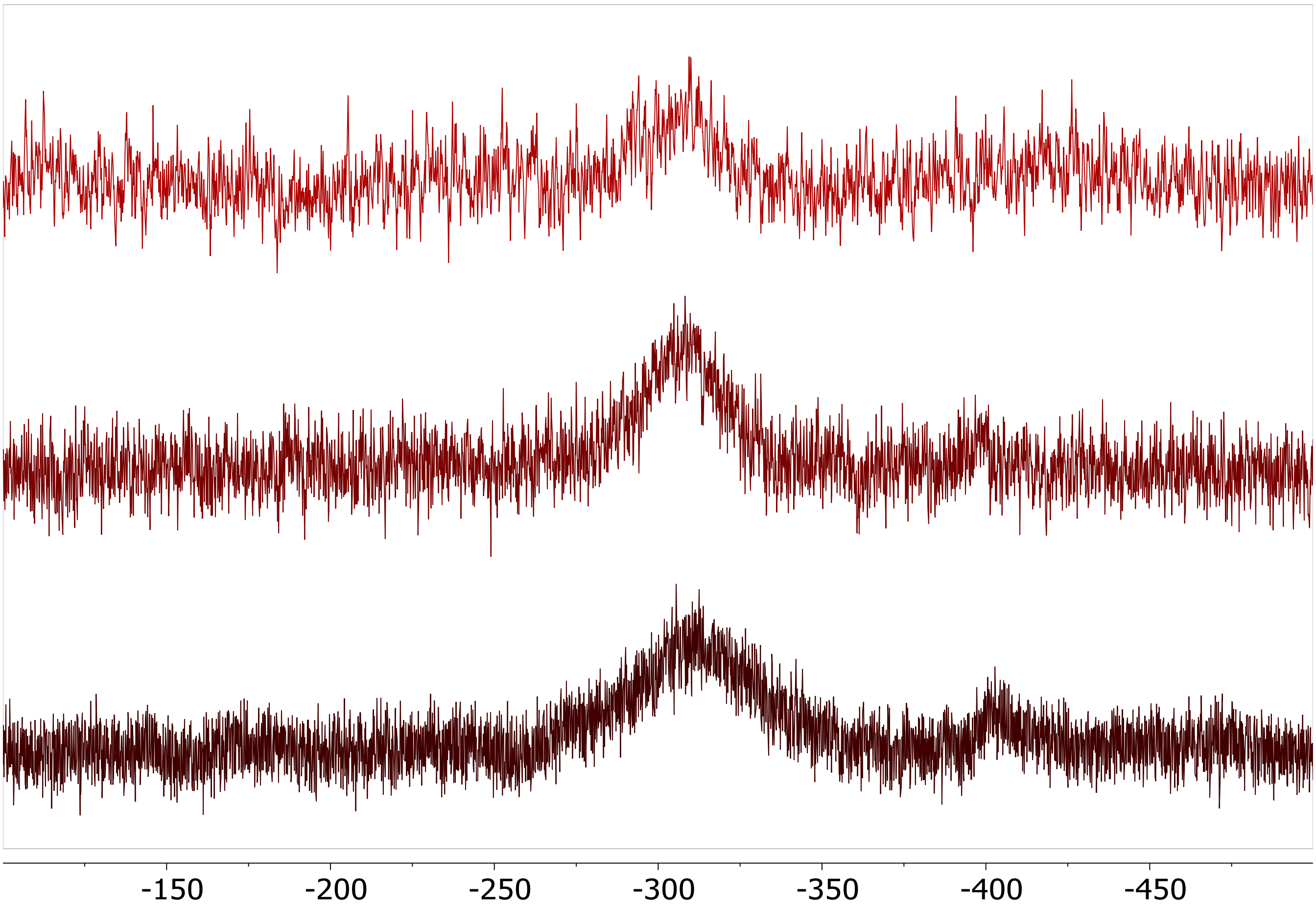

Figure S52. Crude ^{51}V NMR spectra (105 MHz, C_6D_5Br, 25°C) resulting from the reaction between **1**$^-$ and $PhNH_2$ in the absence of HAA (bottom), with half an equivalent of Gomberg's dimer (middle), and with one equivalent of TEMPO (top) revealing a common broad resonance at -312 ppm (**1-NHPh**) and minor amounts of **2** (-400 ppm).

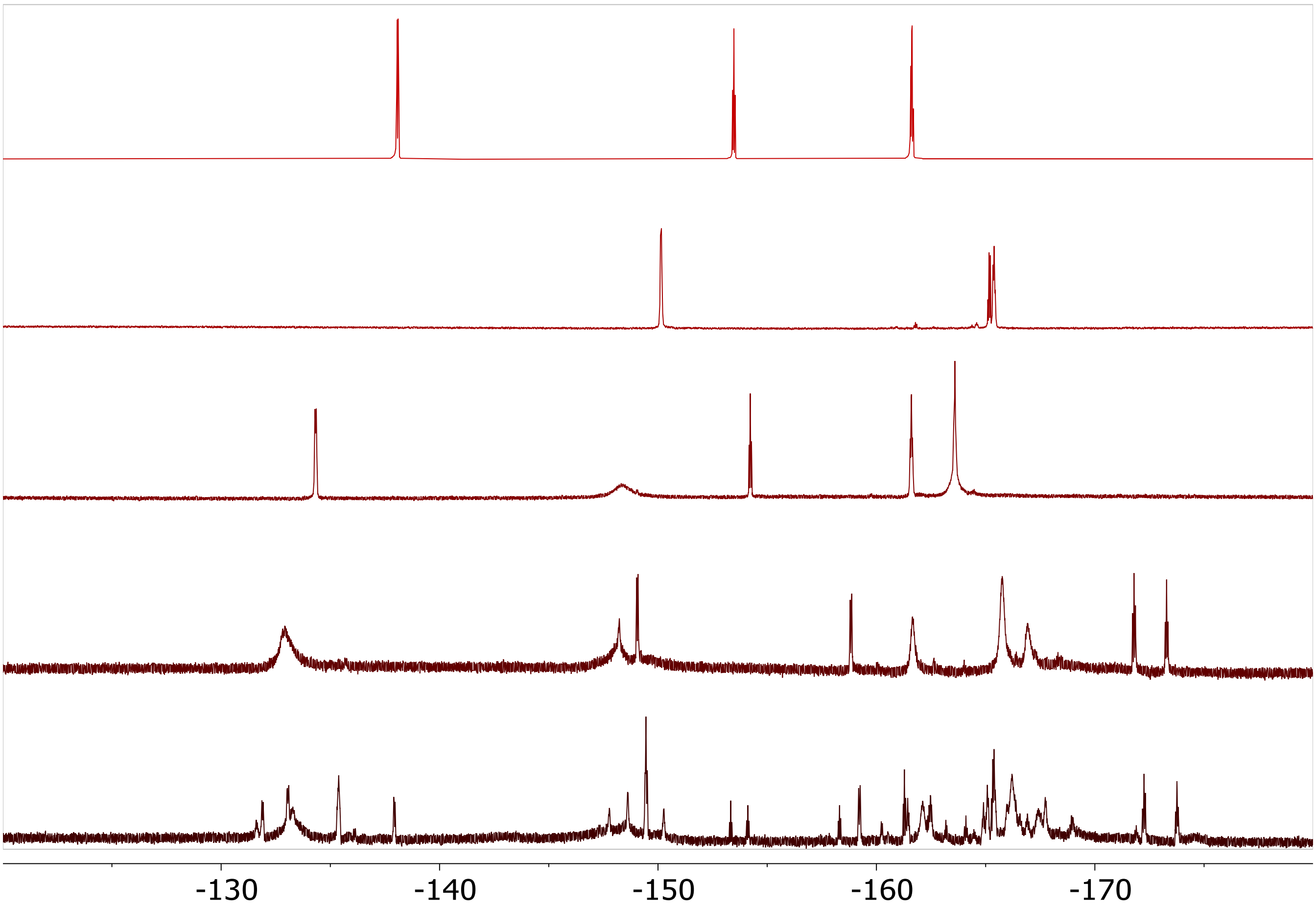

Figure S53. Crude ^{19}F NMR spectrum resulting from the reaction between **1**$^{-}$ and NH_3 (0.4 M in THF) in the absence of HAA (bottom), ^{19}F NMR spectrum of isolated **1-NH** (second from bottom), ^{19}F NMR spectrum of isolated **1-NH$_3$** (third from bottom), ^{19}F NMR spectrum of isolated **2** (fourth from bottom), and ^{19}F NMR spectrum of C_6F_5H (top). The crude reaction contains a mixture of **1-NH**, **2**, C_6F_5H, but no **1-NH$_3$** (376 MHz, C_6D_5Br, 25°C).

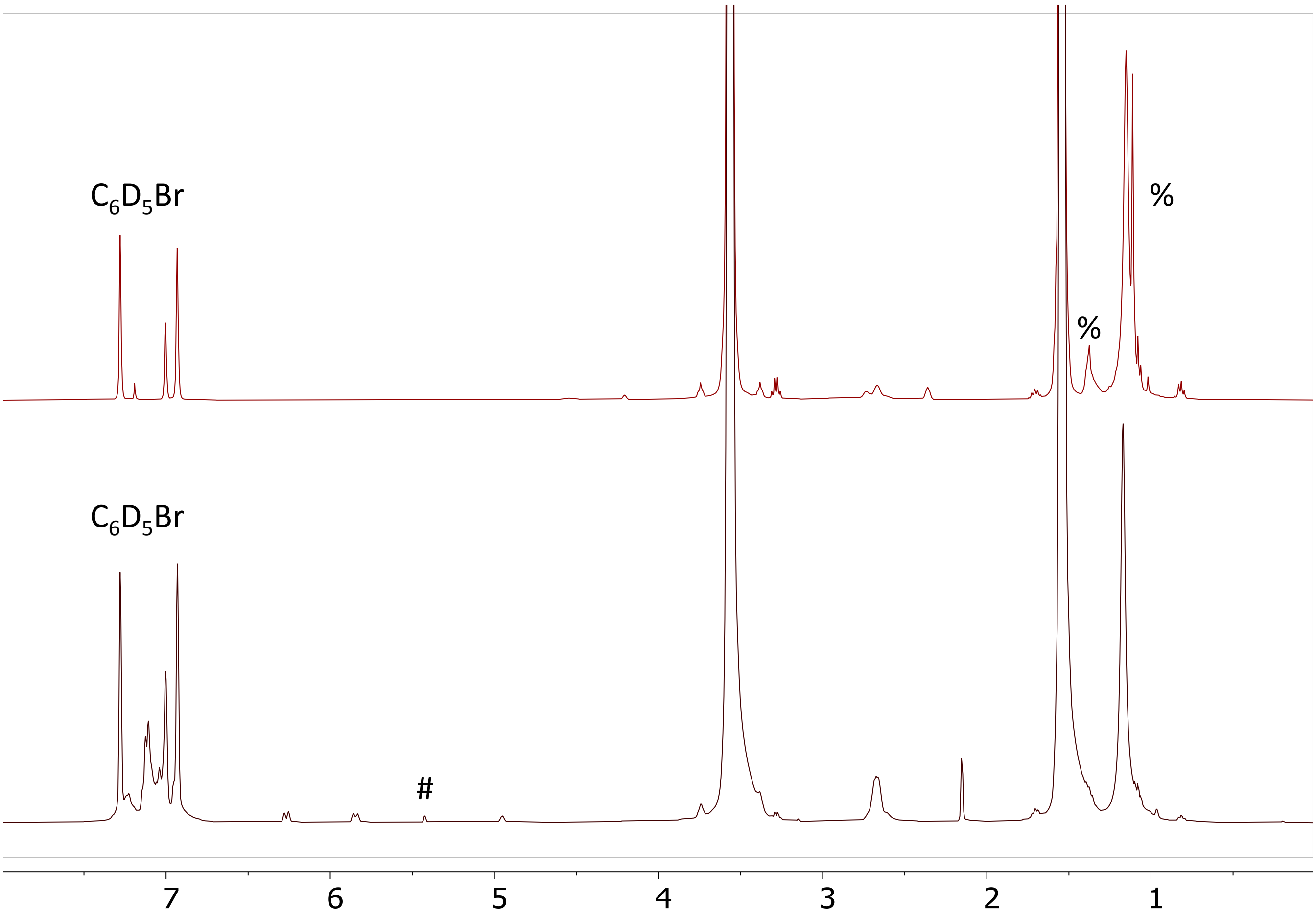

Figure S54. Crude ^{1}H NMR spectra (400 MHz, C_6D_5Br, 25°C) resulting from the reaction between **1**$^-$, HAA agent (Ph_3C• (bottom) or TEMPO (top)), and NH_3 (0.4 M in THF). The byproducts of HAA, Ph_3C–H (bottom, #) and TEMPO–H (top, %) are observed along with diamagnetic tren-based resonances indicative of an HAA process.

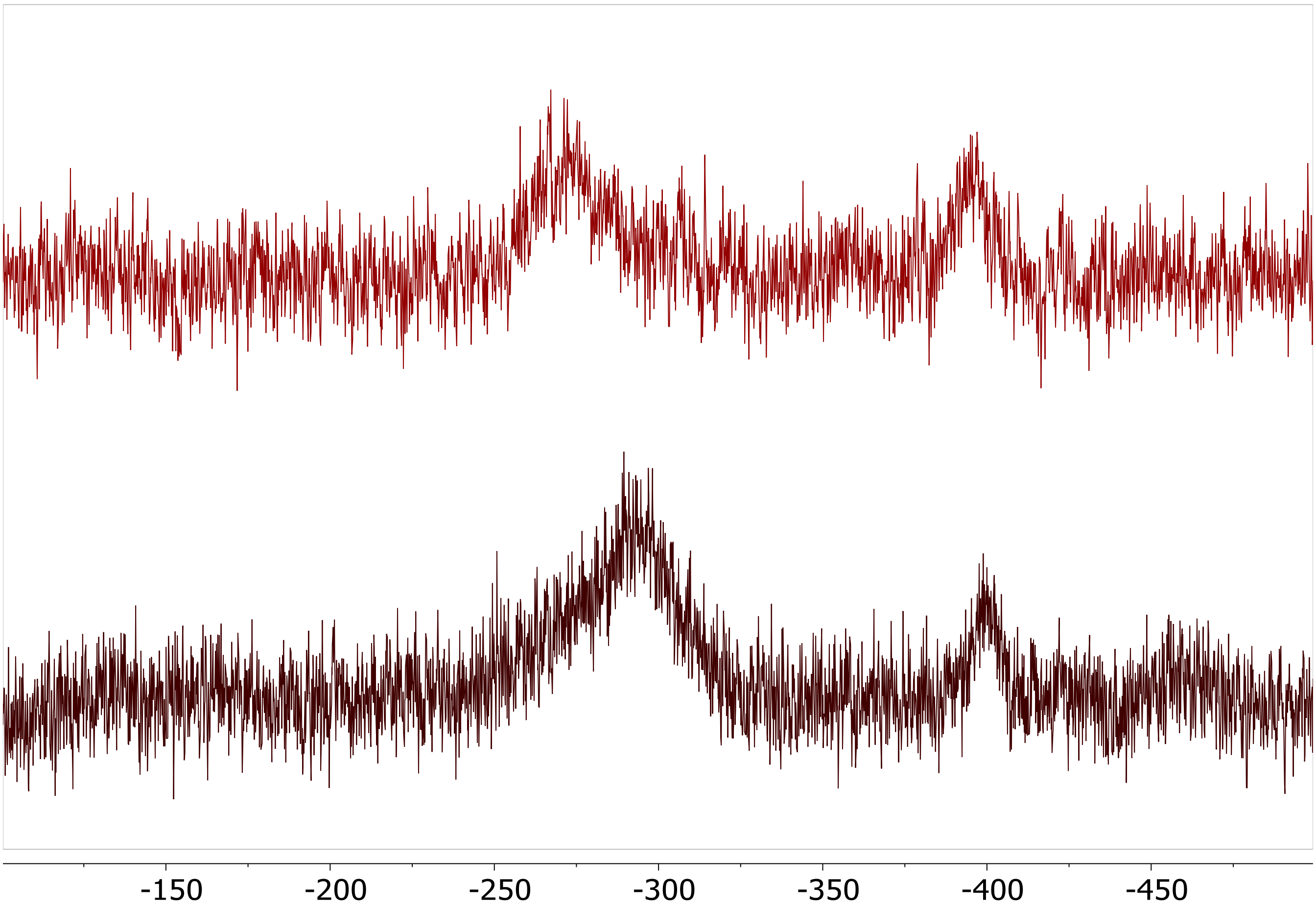

Figure S55. Crude ^{51}V NMR spectra (105 MHz, C_6D_5Br, 25°C) resulting from the reaction between **1**$^-$, HAA (Ph_3C• (bottom) or TEMPO (top)), and NH_3 (0.4 M in THF). Both spectra reveal a broad resonance similar to the **1-NH** product and minor amounts of **2** (-400 ppm), which may be formed from *in situ* generated HF.

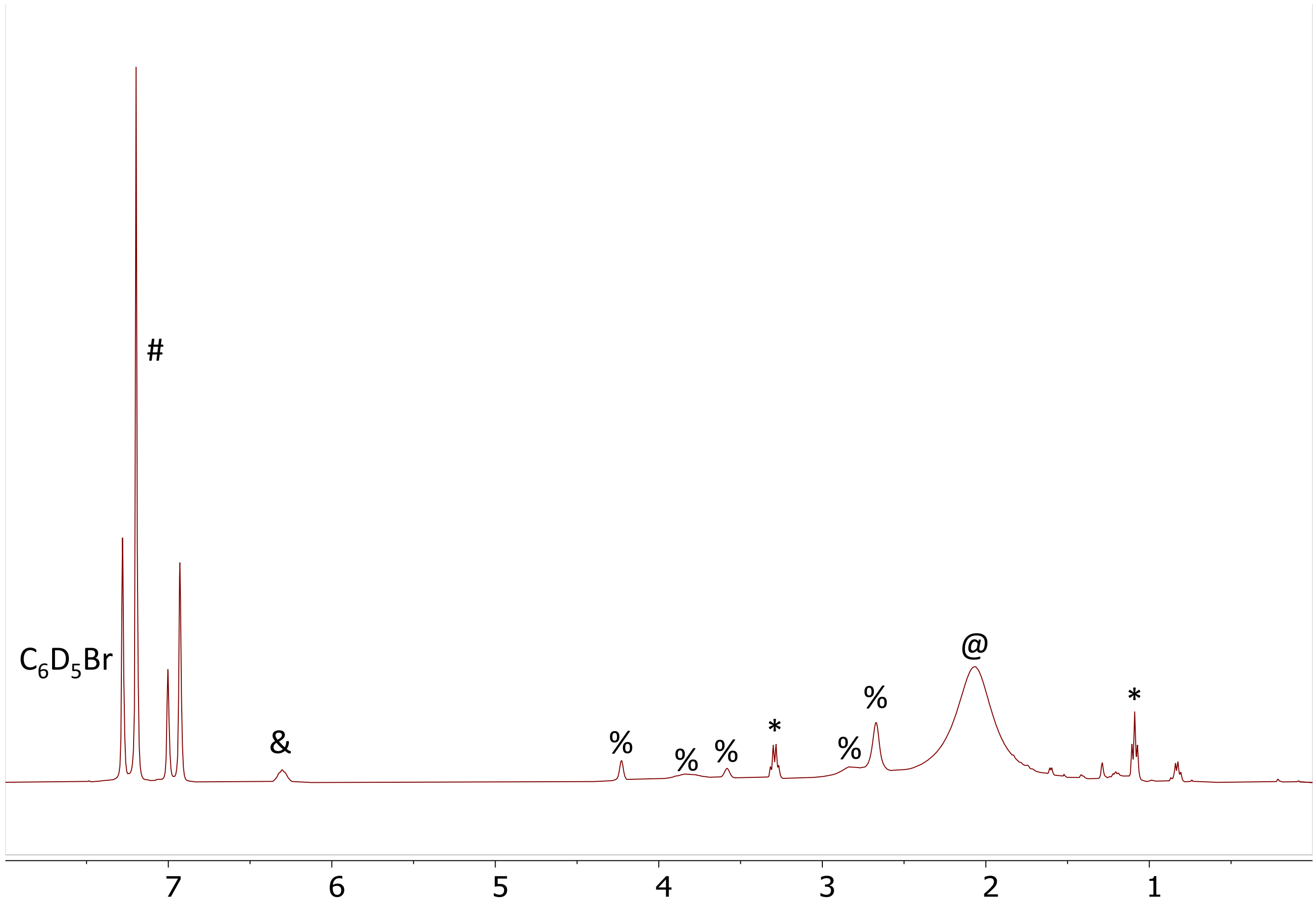

Figure S56. Crude ^{1}H NMR spectrum (400 MHz, C_6D_5Br, 25°C) resulting from the reaction between **1-NH$_3$** and decamethylcobaltocene revealing resonances ascribed to the **1-NH** product (%) and C_6F_5H (&). The broad decamethylcobaltocenium resonance (@) may be due to the presence of residual decamethylcobaltocene in solution. (* = diethyl ether, # = benzene)

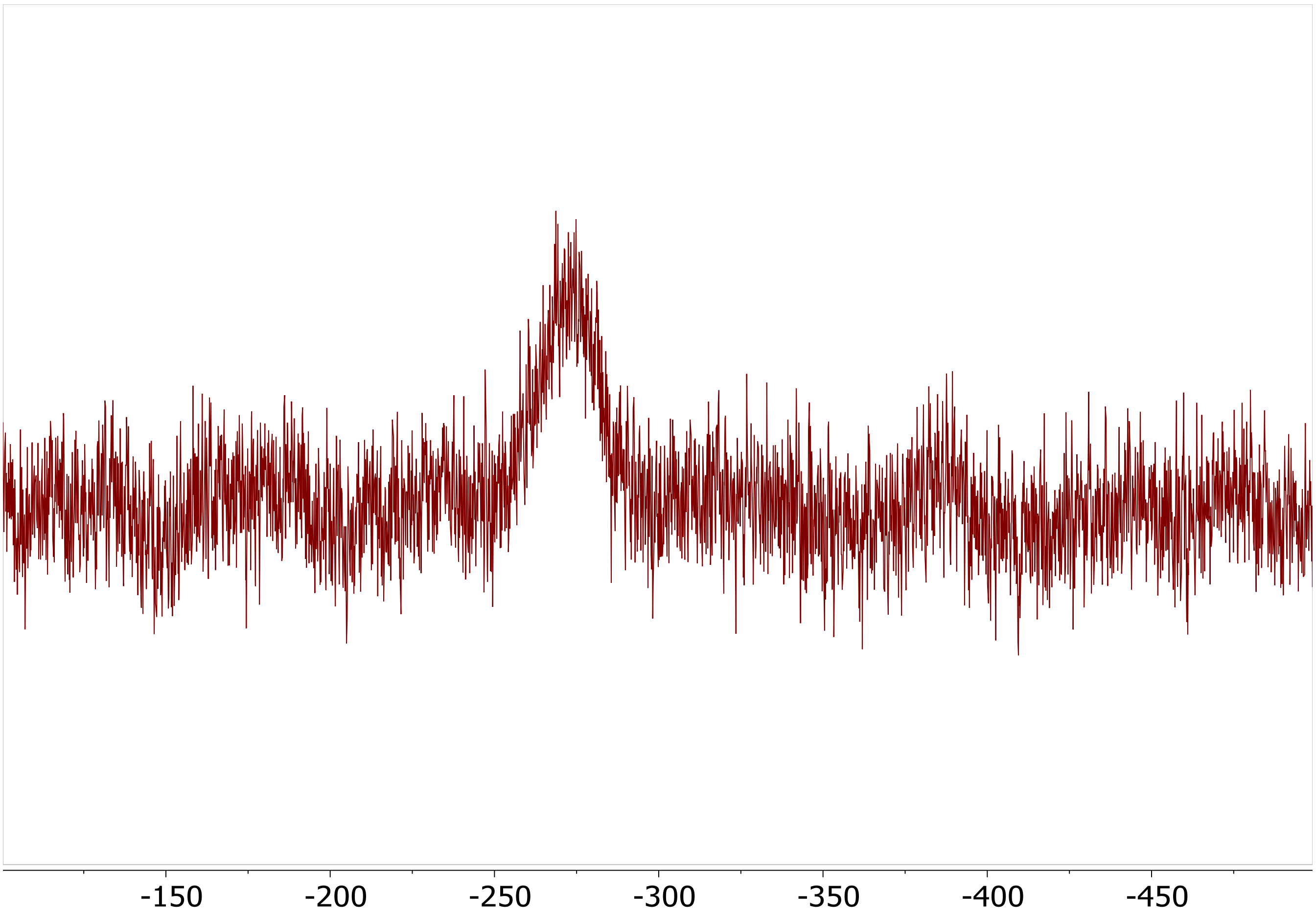

Figure S57. Crude ^{51}V NMR spectrum (105 MHz, C_6D_5Br, 25°C) resulting from the reaction bteween **1-NH$_3$** and decamethylcobaltocene revealing **1-NH** as the sole vanadium-containing product.

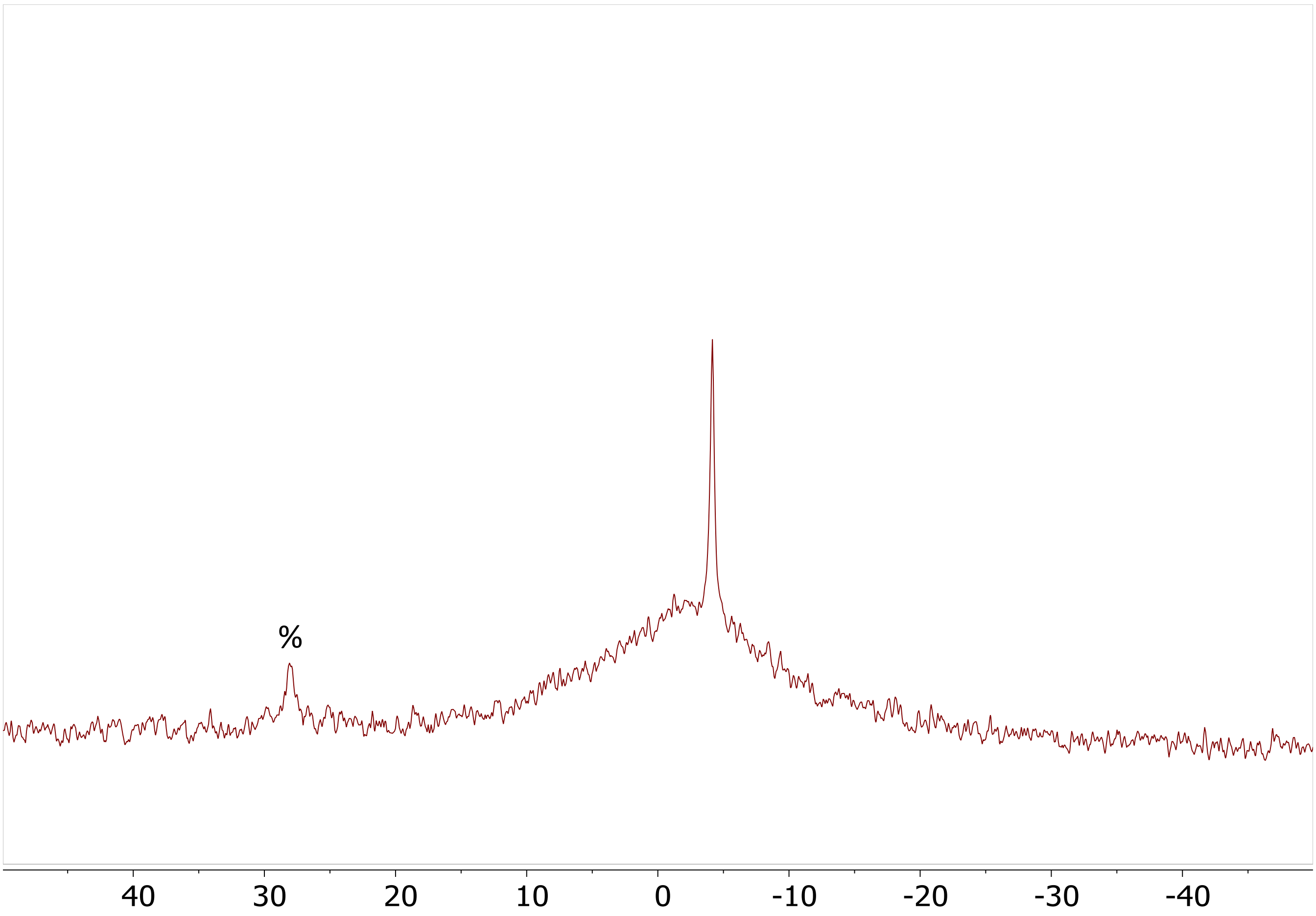

Figure S58. Crude ^{11}B NMR spectrum (128 MHz, C_6D_5Br, 25°C) resulting from the reaction between **1-NH$_3$** and decamethylcobaltocene revealing a sharp resonance at -4.2 ppm (**1-NH**). (% = unidentified boron-containing product)

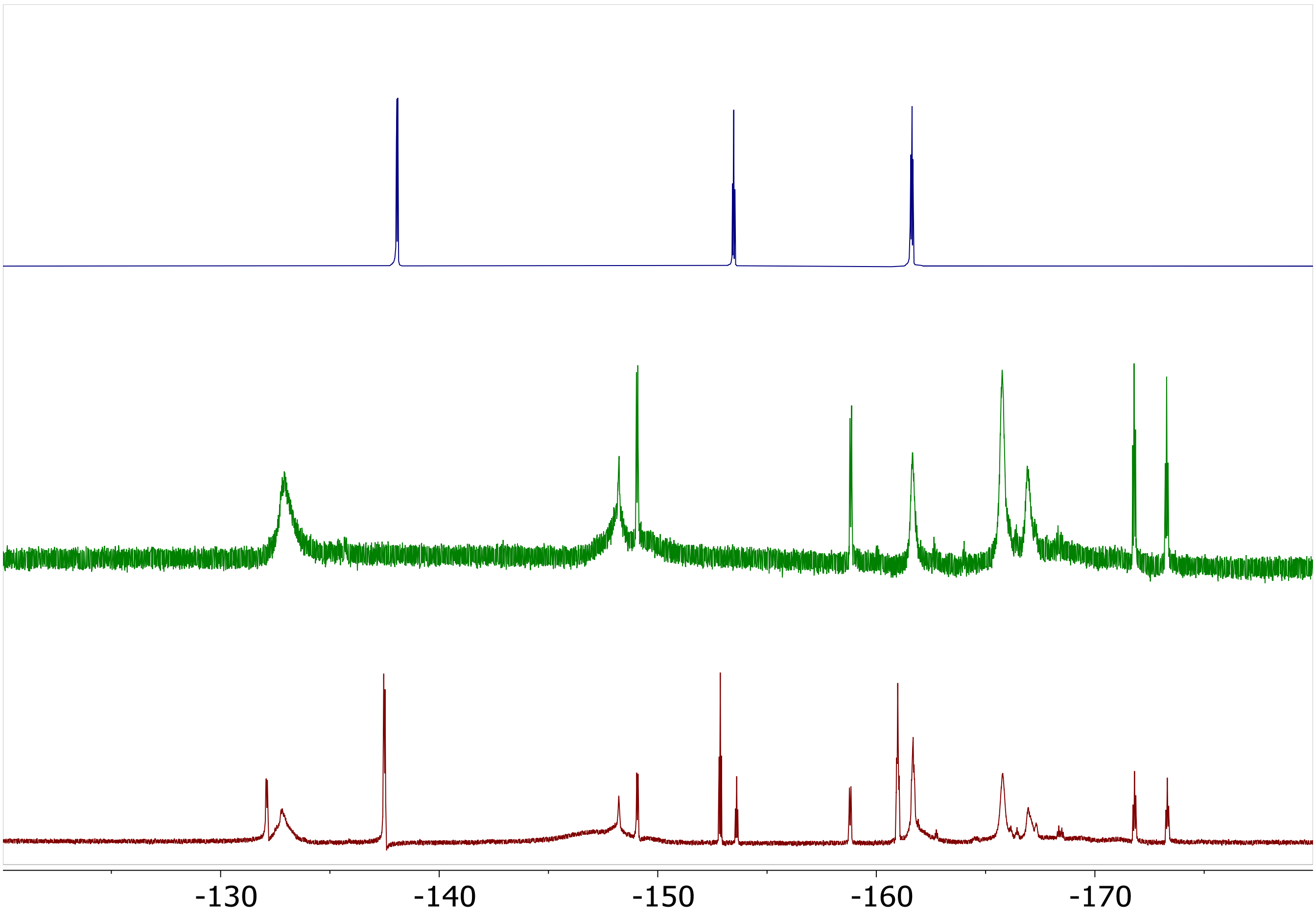

Figure S59. Crude ^{19}F NMR spectrum resulting from the reaction between **1-NH$_3$** and decamethylcobaltocene revealing multiple resonances attributed to **1-NH** and C_6F_5H (bottom). ^{19}F NMR spectra of isolated **1-NH** (middle) and C_6F_5H (top) are provided for reference (376 MHz, C_6D_5Br, 25°C). Note that resonances for C_6F_5H in the bottom spectrum are slightly shifted relative to the top spectrum likely due to residual paramagnetism in the former.

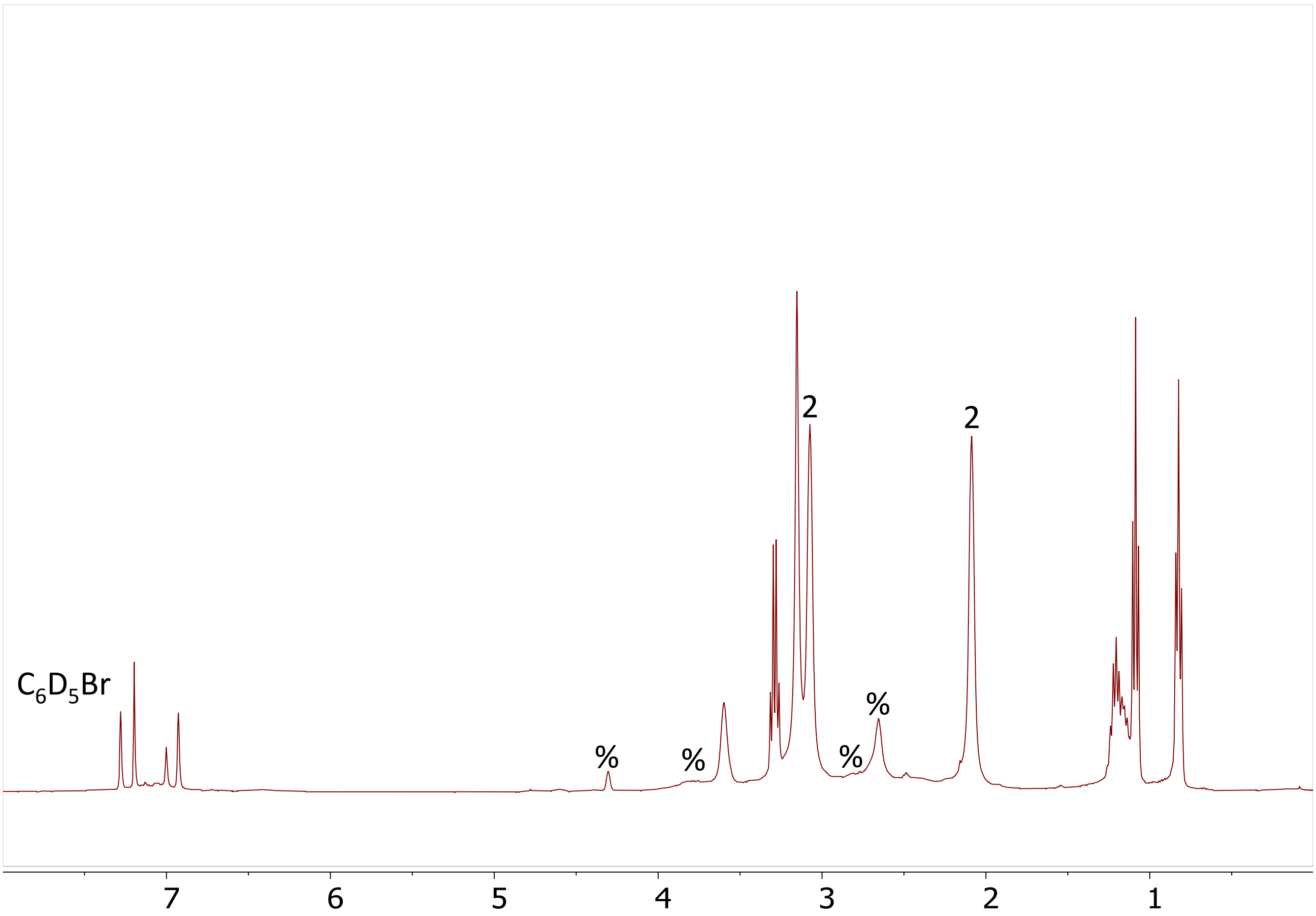

Figure S60. Crude ^{1}H NMR spectrum (400 MHz, C_6D_5Br, 25°C) resulting from the reaction between **1-NH$_2$K** and 4,7,13,16,21,24-hexaoxa-1,10-diazabicyclo[8.8.8]hexacosane (Kryptofix-222 = krypt) revealing a mixture of **1-NH** (%) and **2**.

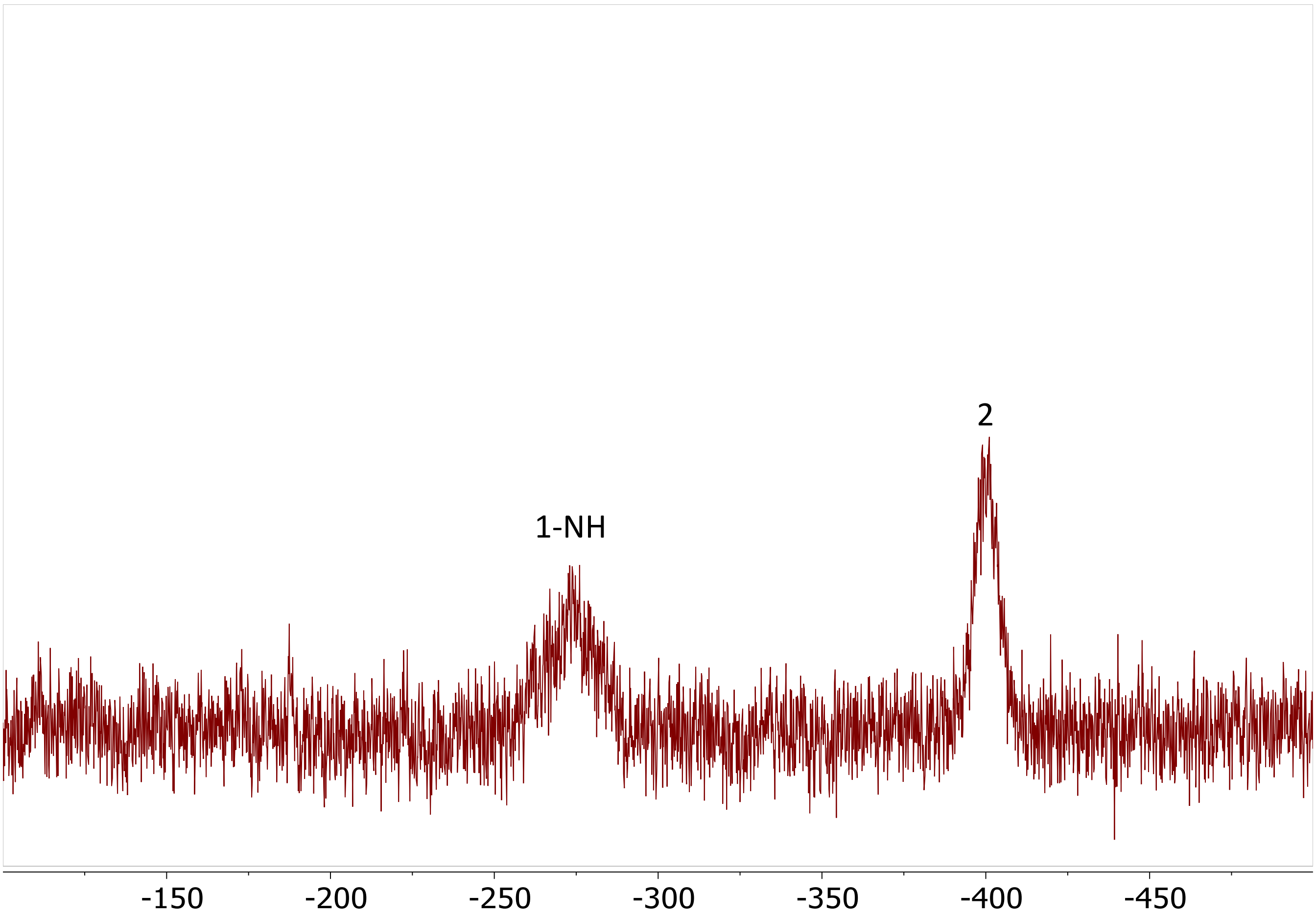

Figure S61. Crude ^{51}V NMR spectrum (105 MHz, C_6D_5Br, 25°C) resulting from the reaction between **1-NH$_2$K** and 4,7,13,16,21,24-hexaoxa-1,10-diazabicyclo[8.8.8]hexacosane (Kryptofix-222 = krypt) revealing mixture **1-NH** and **2**.

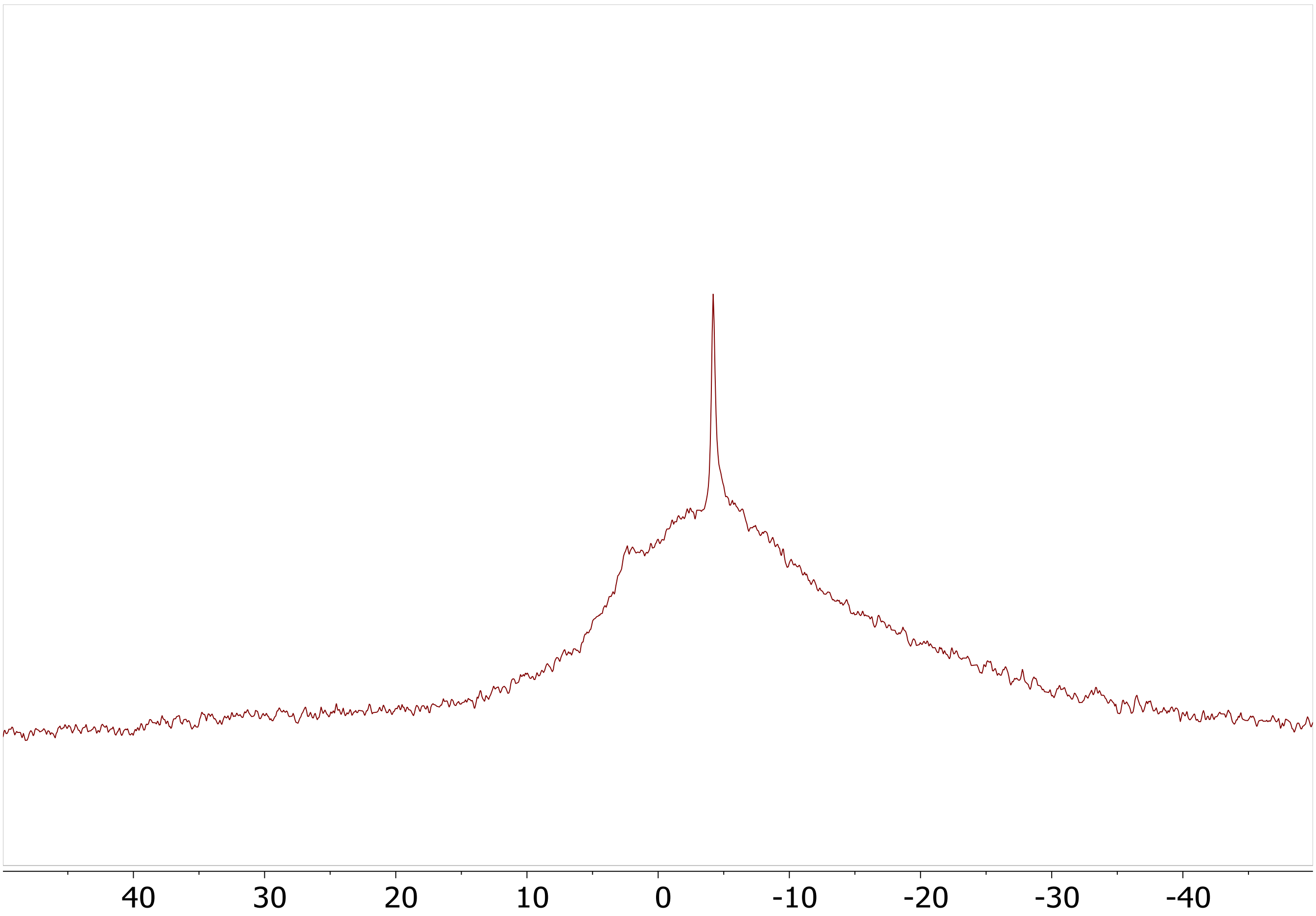

Figure S62. Crude ^{11}B NMR spectrum (128 MHz, C_6D_5Br, 25°C) resulting from the reaction between **1-NH$_2$K** and 4,7,13,16,21,24-hexaoxa-1,10-diazabicyclo[8.8.8]hexacosane (Kryptofix-222 = krypt) revealing a sharp resonance attributed to **1-NH**.

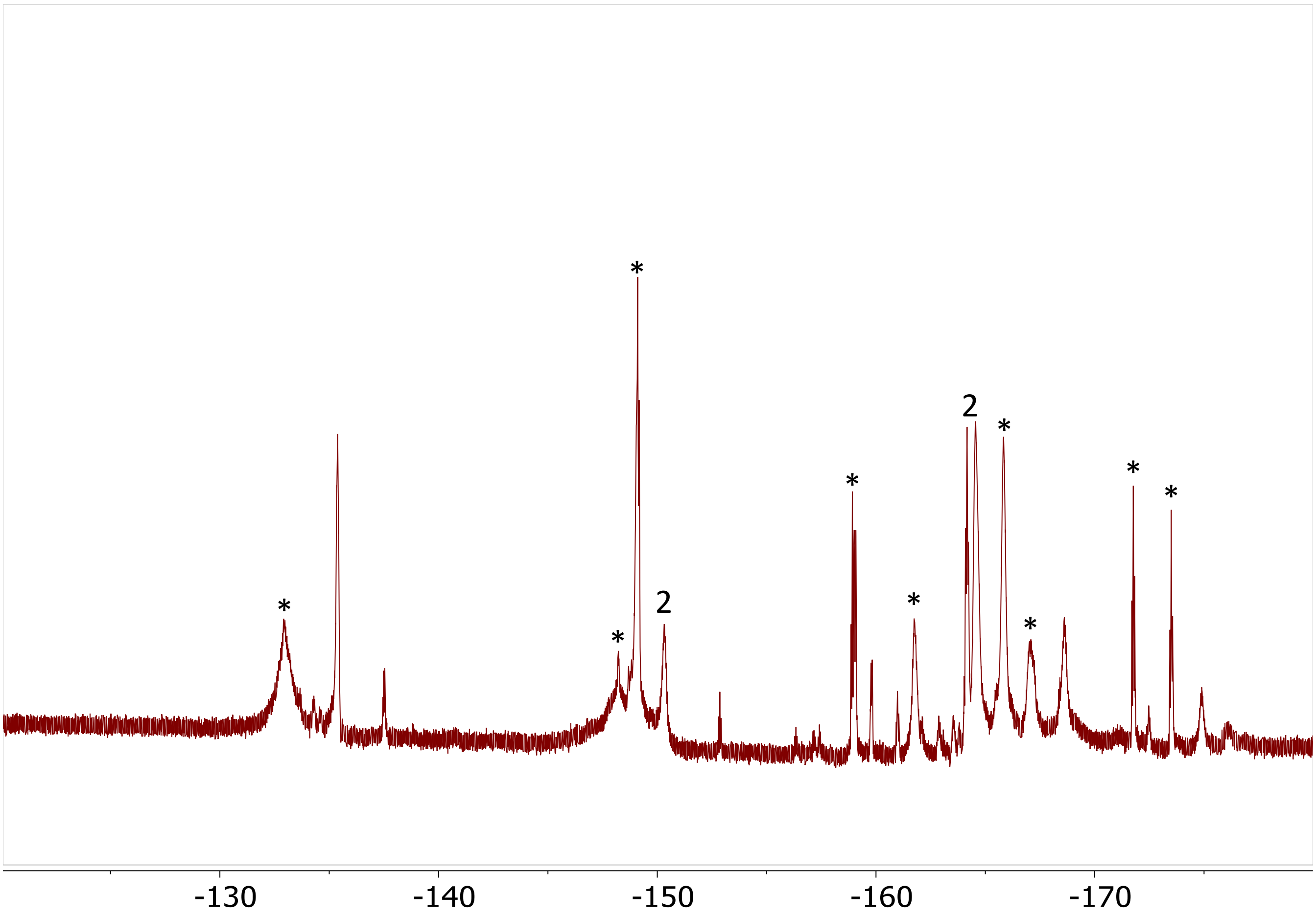

Figure S63. Crude ^{19}F NMR spectrum (376 MHz, C_6D_5Br, 25°C) resulting from the reaction between **1-NH$_2$K** and 4,7,13,16,21,24-hexaoxa-1,10-diazabicyclo[8.8.8]hexacosane (Kryptofix-222 = krypt) revealing mixture **1-NH** (*) and **2** as main products.

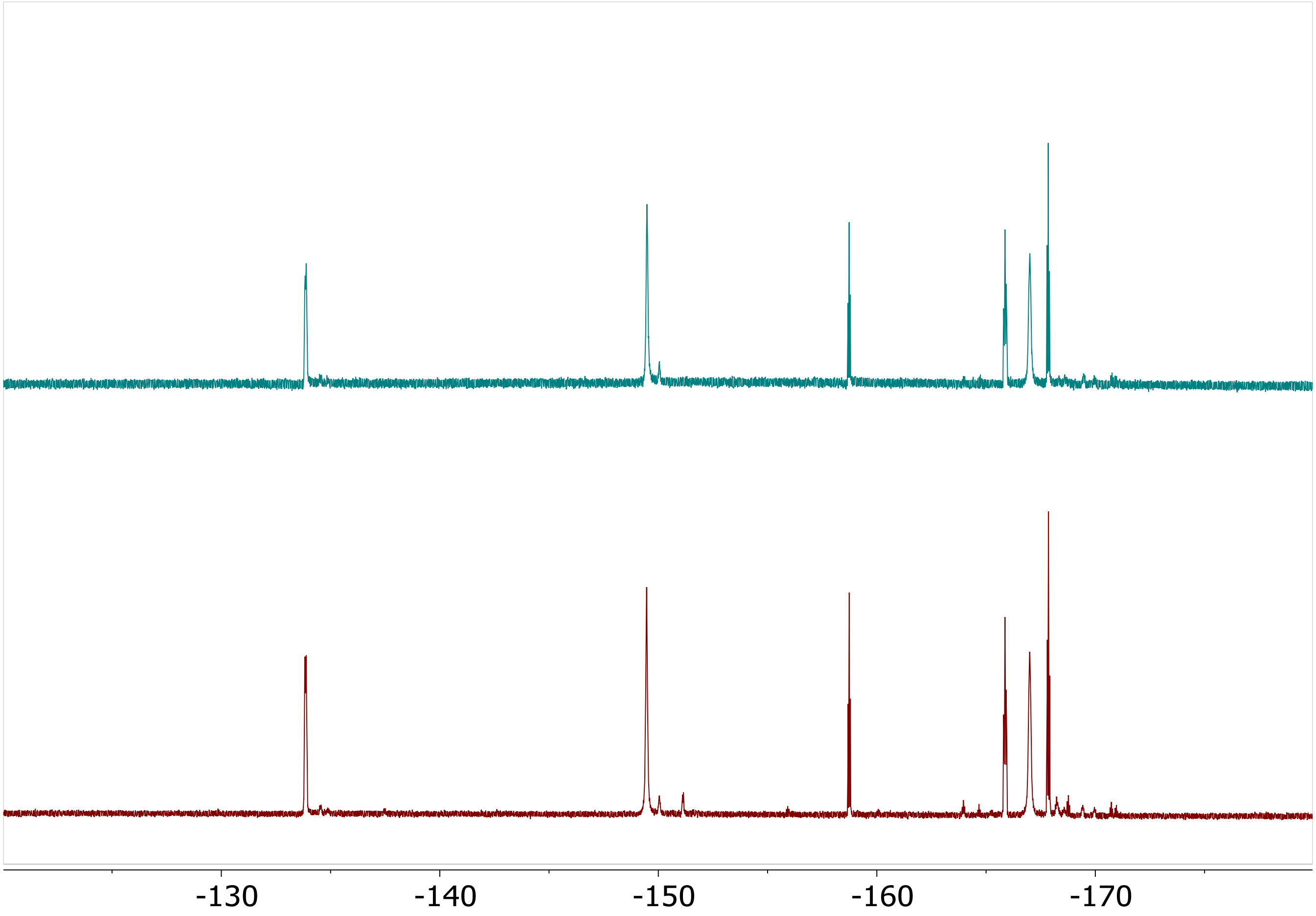

Figure S64. Crude ^{19}F NMR spectra (400 MHz, CD_3CN, 25°C) resulting from the combination of **1-NH$_3$** and piperidine in acetonitrile showing no reaction, which sets a lower **1-NH$_3$**(N–H) pK_a to be 19.35 (bottom). The ^{19}F NMR spectrum of isolated **1-NH$_3$** is provided for reference (top).

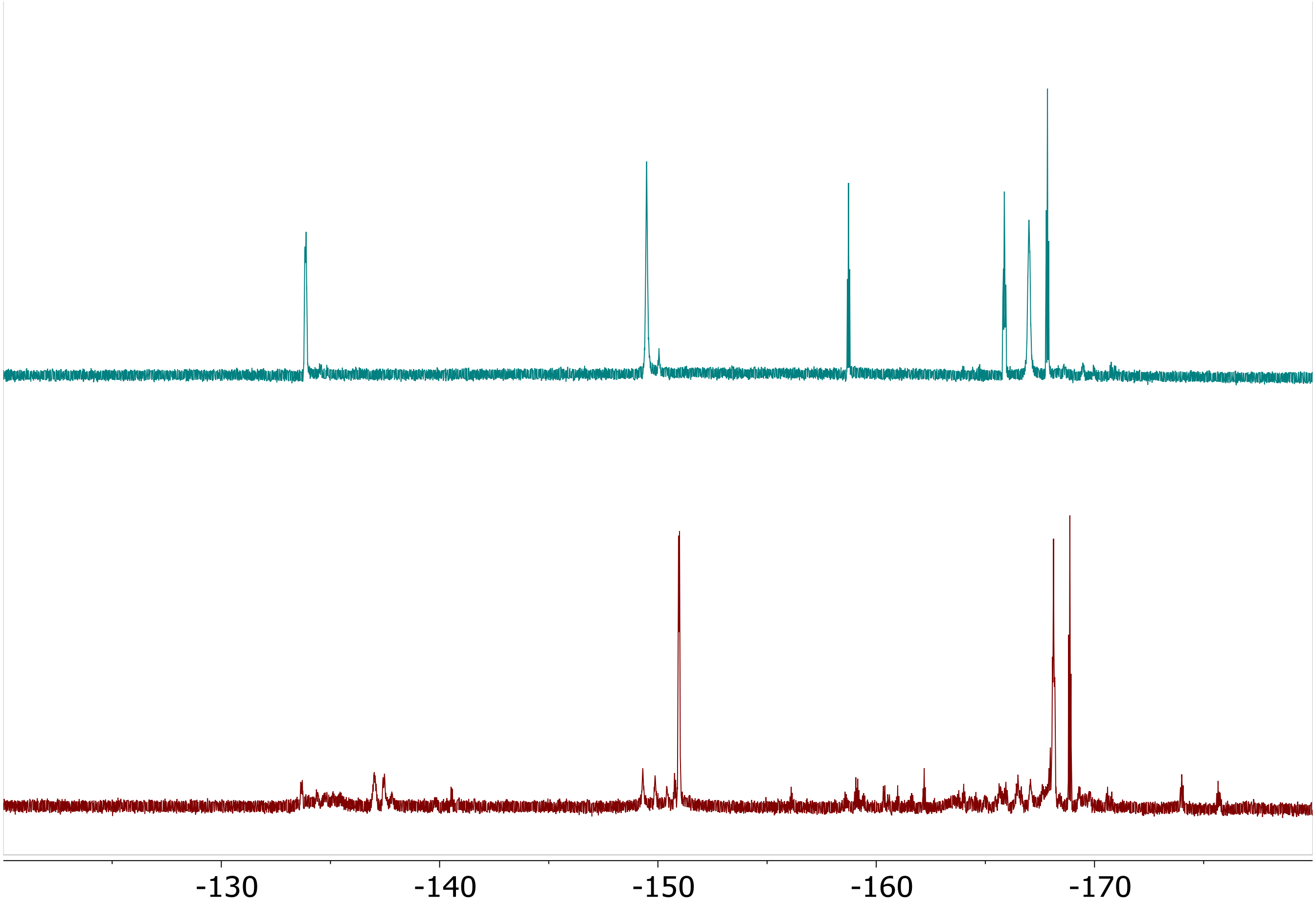

Figure S65. Crude ^{19}F NMR spectrum (400 MHz, CD_3CN, 25°C) resulting from the combination of **1-NH$_3$** and 1,8-Diazabicyclo[5.4.0]undec-7-ene (DBU) in acetonitrile showing the formation of **1-NH** and **2**, which sets an upper **1-NH$_3$**(N–H) pK_a to be 24.31 (bottom). The ^{19}F NMR spectrum of isolated **1-NH$_3$** is provided for reference (top).

4. Supplemental Figures for GC-TCD Experiments

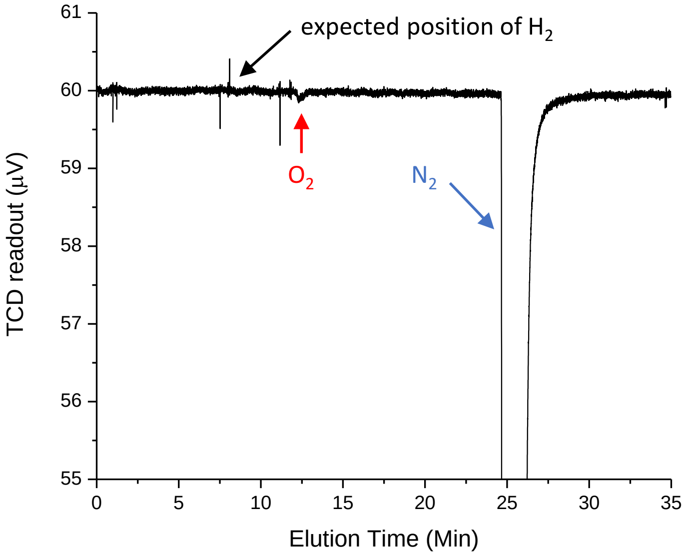

Figure S66. GC-TCD trace of the sampled headspace (100 μL) following the reaction between **1**$^-$ and PhSH in a sealed crimp-top vial revealing no H_2 gas formation consistent with the ^{1}H NMR spectrum (Fig. S47).

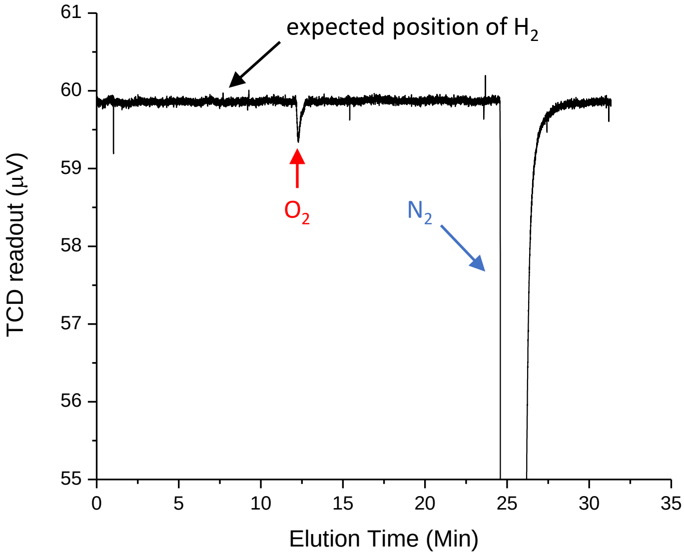

Figure S67. GC-TCD trace of the sampled headspace (100 μL) following the reaction between **1**$^-$ and C_6F_5OH in a sealed crimp-top vial revealing no H_2 gas formation consistent with the ^{1}H NMR spectrum (Fig. S48).

5. Supplemental Figures for X-ray crystallography

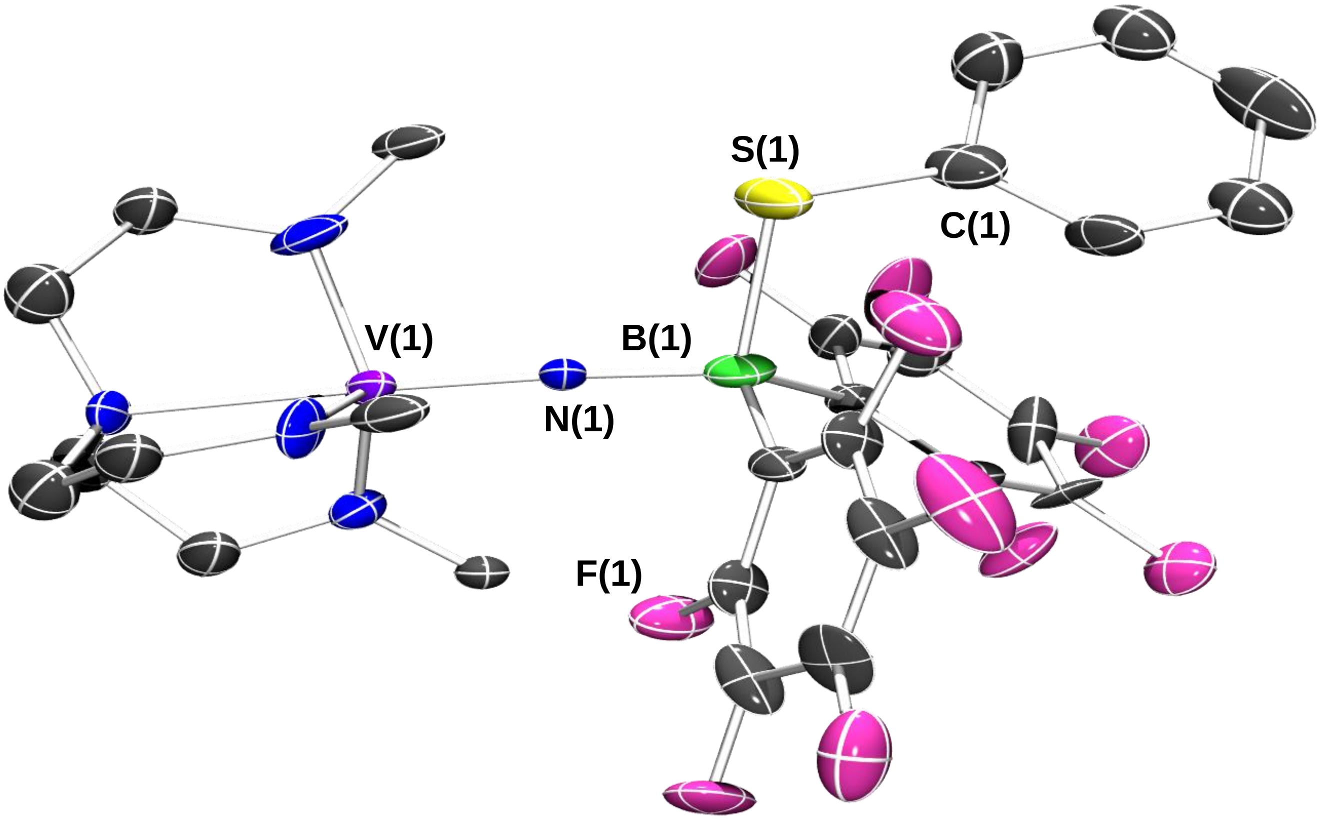

Figure S68. Solid-state structure of the anion of **1-SPh** (tren-based C_6F_5 groups (except *ipso* carbons), hydrogen atoms, $[\mathrm{CoCp}^*_2]^+$ counter-cation, and co-crystallized solvent molecules are omitted for clarity).

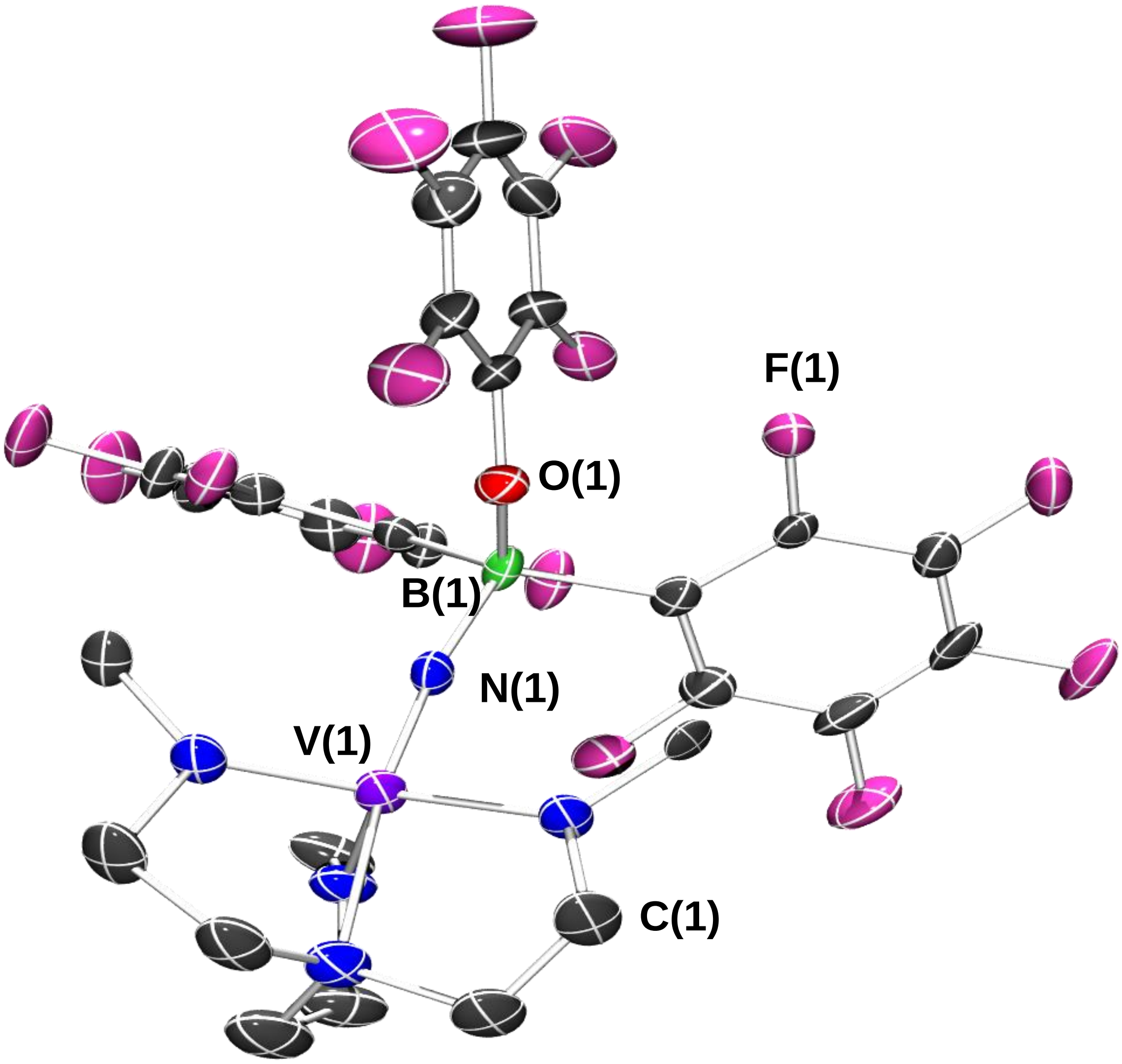

Figure S69. Solid-state structure of the anion of **1-OC$_6$F$_5$** (tren-based C$_6$F$_5$ groups (except *ipso* carbons), hydrogen atoms, $[\mathrm{CoCp}^*_2]^+$ counter-cation, and co-crystallized solvent molecules are omitted for clarity).

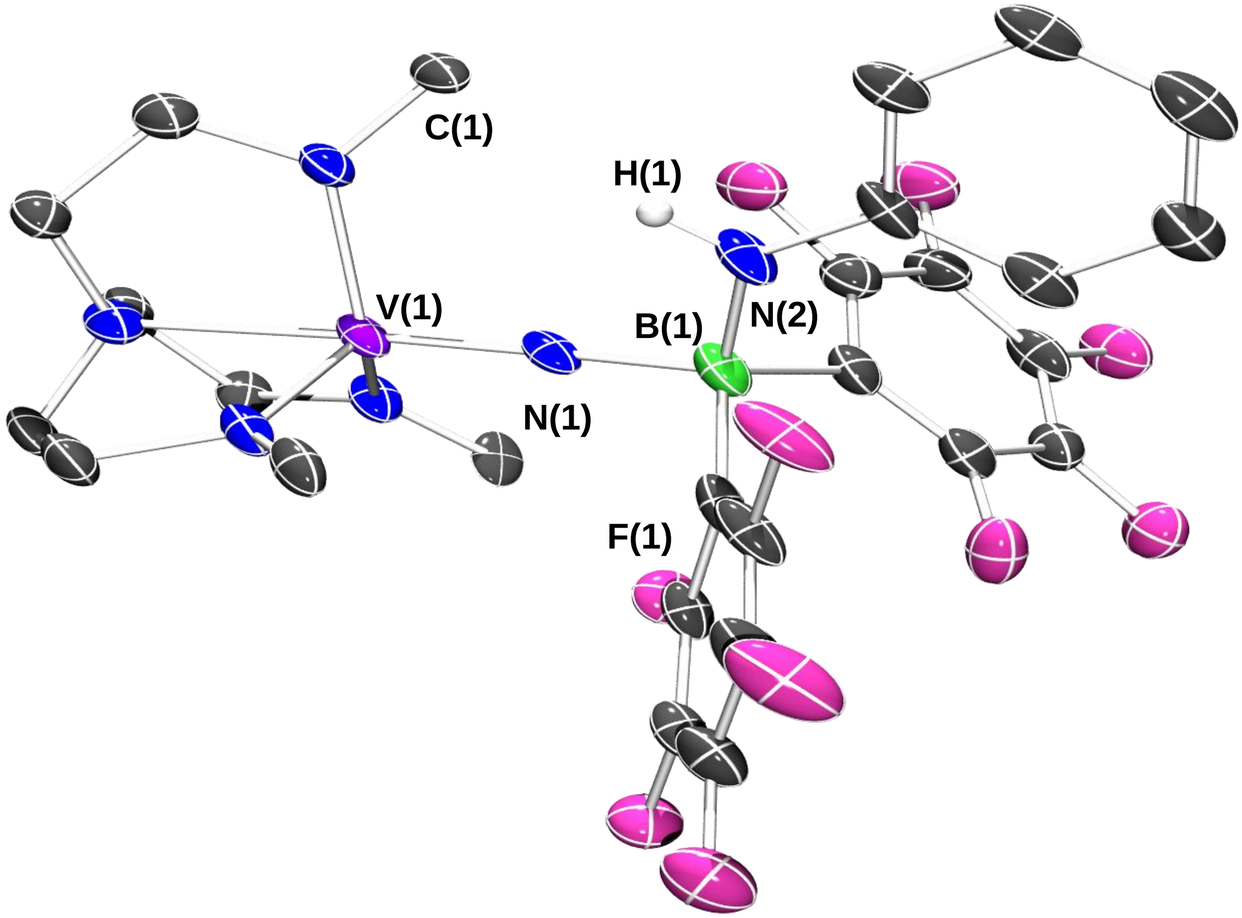

Figure S70. Solid-state structure of the anion of **1-NHPh** (tren-based C_6F_5 groups (except *ipso* carbons), hydrogen atoms (except NH), $[CoCp^*_2]^+$ counter-cation, and co-crystallized solvent molecules are omitted for clarity).

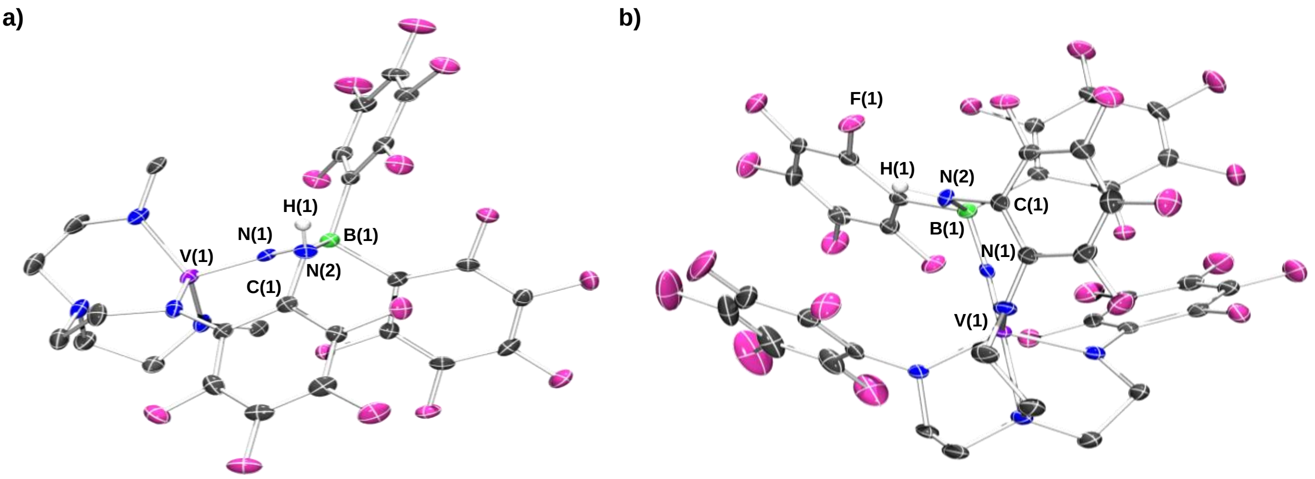

Figure S71. a) Solid-state structure of the anion of **1-NH** (all C_6F_5 groups (except *ipso* carbons and except the one undergoing S_NAr, hydrogen atoms (except NH), $[\mathrm{CoCp}_2^*]^+$ counter-cation, and co-crystallized solvent molecules are omitted for clarity). b) Solid-state structure of the anion of **1-NH** showing intramolecular π-π stacking (all hydrogen atoms (except NH), $[\mathrm{CoCp}_2^*]^+$ counter-cation, and co-crystallized solvent molecules are omitted for clarity).

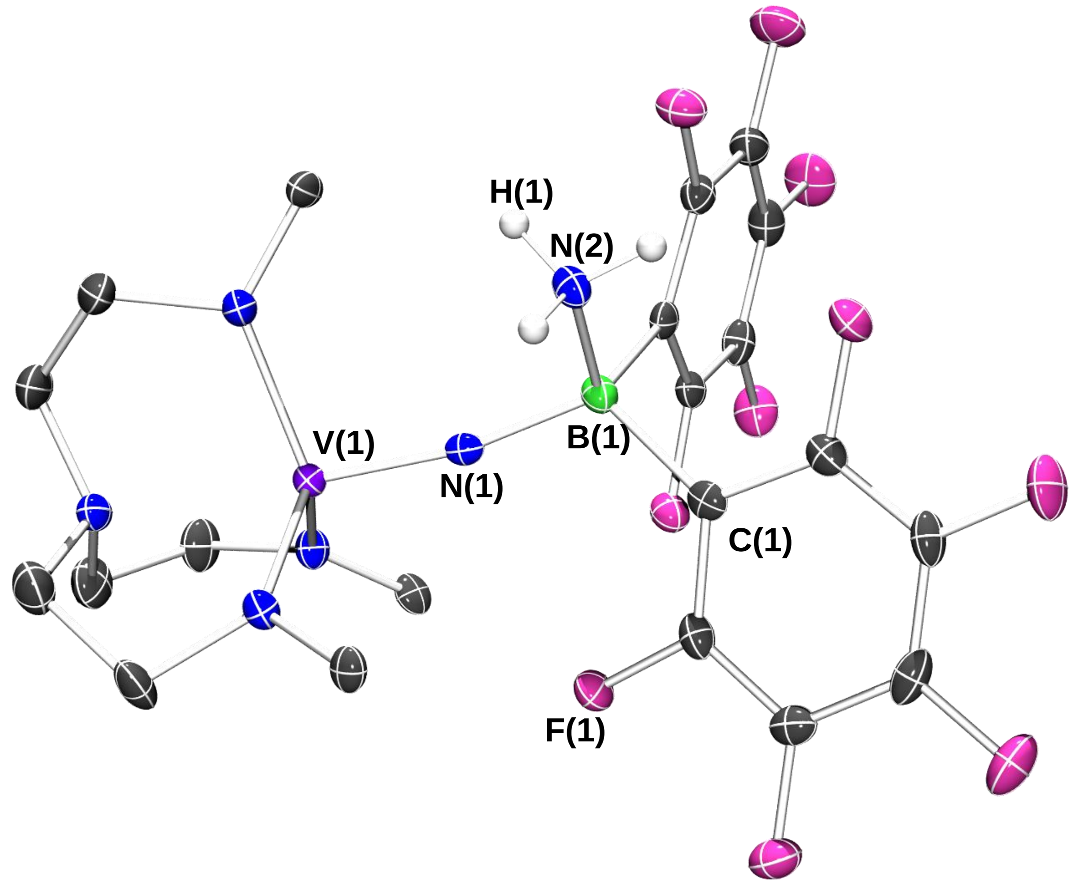

Figure S72. Solid-state structure of **1-NH₃** (tren-based C_6F_5 groups (except *ipso* carbons), hydrogen atoms (except NH), and co-crystallized solvent molecules are omitted for clarity).

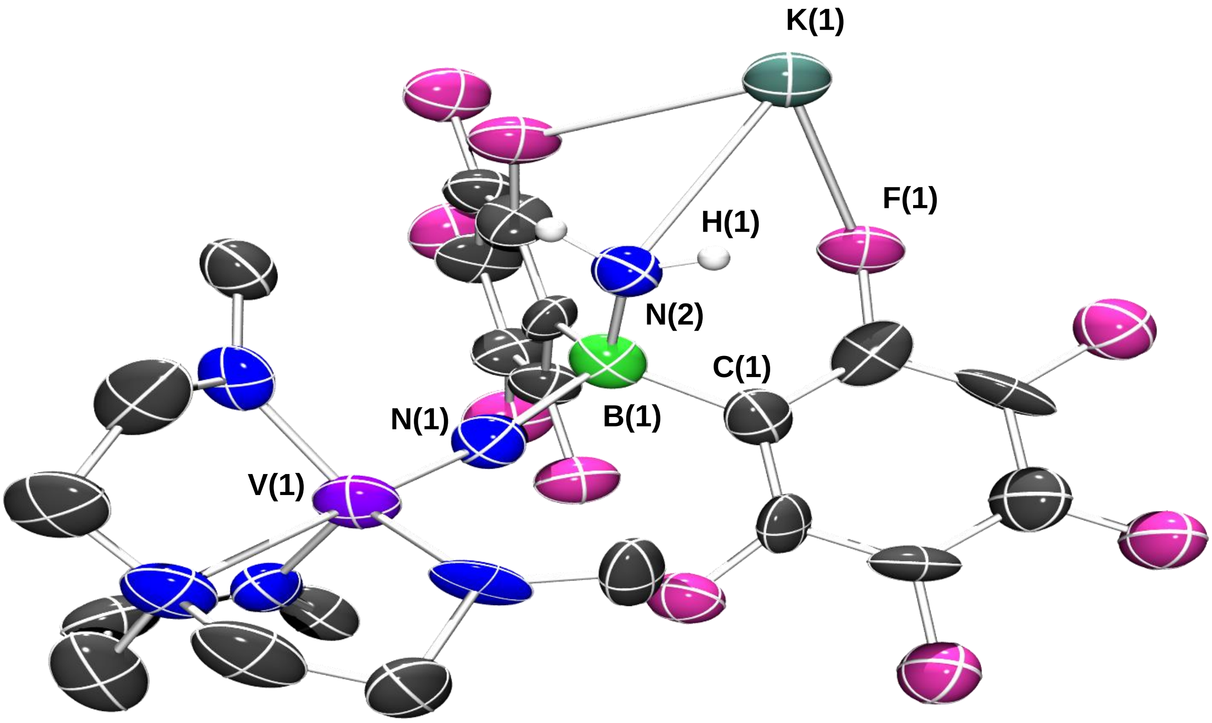

Figure S73. Solid-state structure of **1-NH$_2$K** (tren-based C_6F_5 groups (except *ipso* carbons), hydrogen atoms (except NH), and co-crystallized solvent molecules are omitted for clarity).

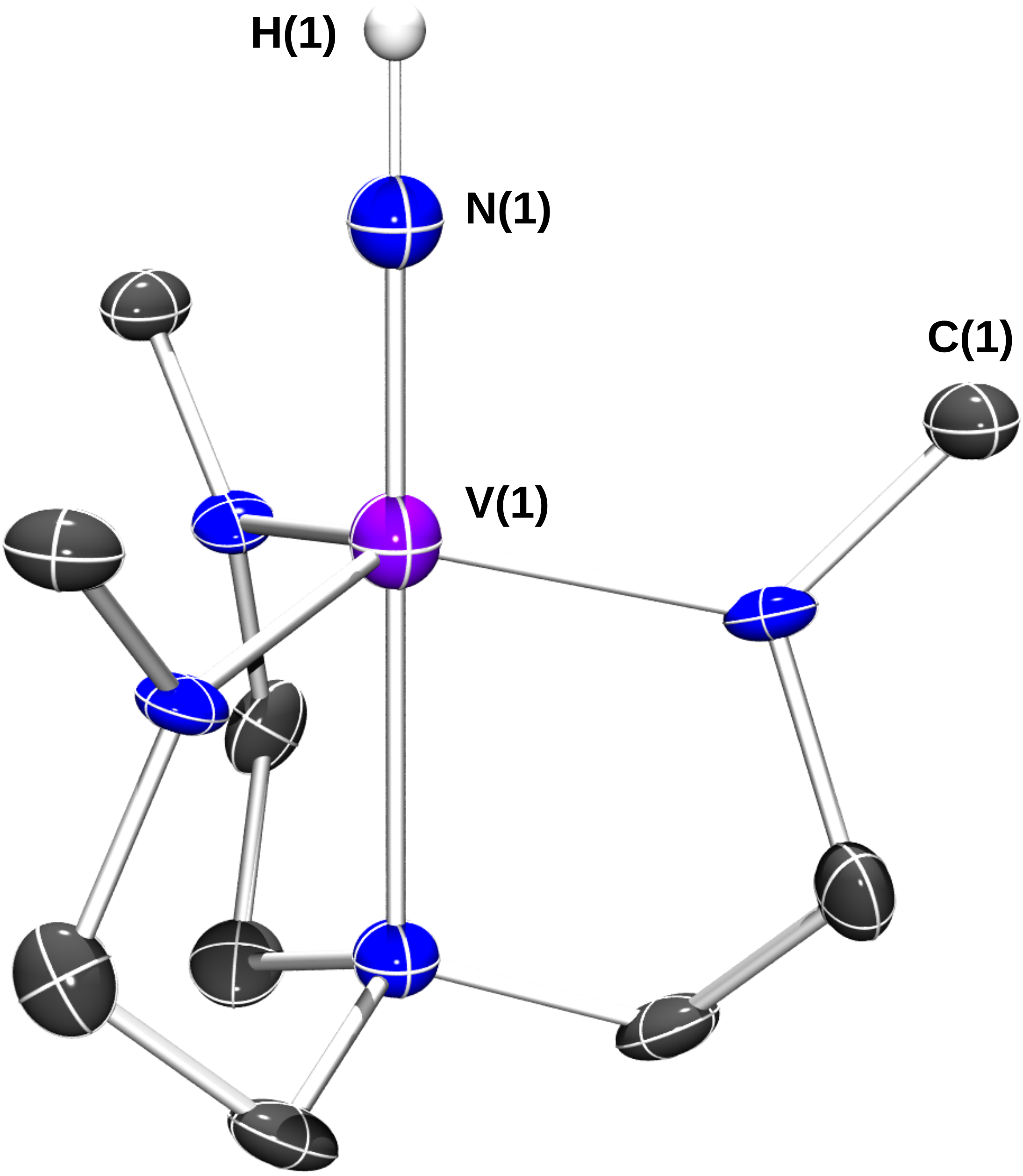

Figure S74. Solid-state structure of the anion of **2** (tren-based C_6F_5 groups (except *ipso* carbons), hydrogen atoms (except NH), and co-crystallized solvent molecules are omitted for clarity).

6. Supplemental Figures for Cyclic Voltammetry

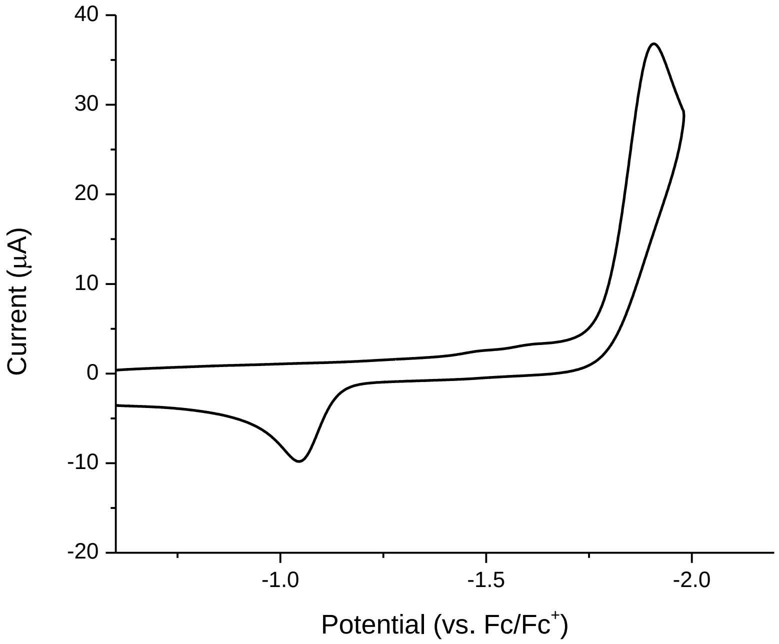

Figure S75. Cyclic voltammogram of **1-NH$_3$** in CH_3CN (1.5 mM) with 0.1 M $[Bu_4N][PF_6]$ electrolyte (glassy carbon working electrode, Ag wire pseudoreference, platinum wire counter, scan rate 250 mV/s, referenced to Fc/Fc$^+$). An irreversible reduction event is observed at -1.87 V vs. Fc/Fc$^+$.

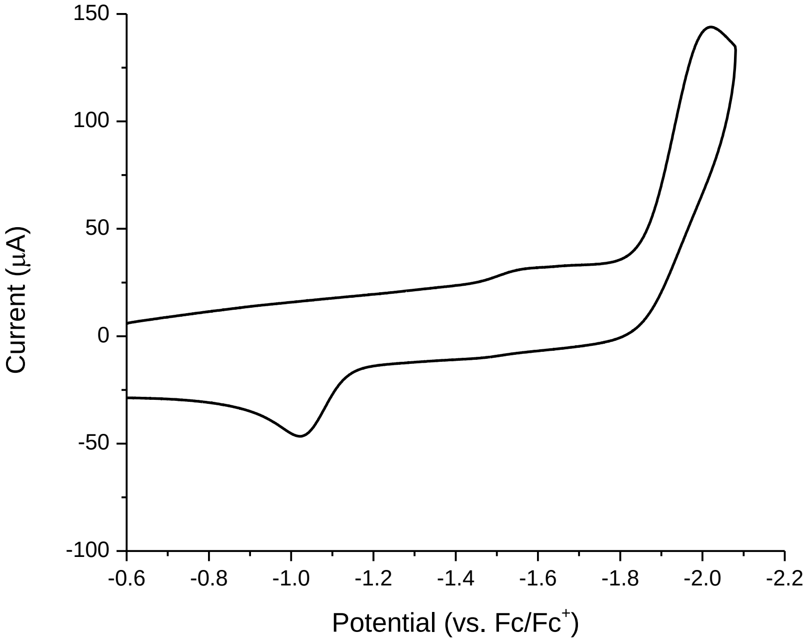

Figure S76. Cyclic voltammogram of **1-NH$_3$** in CH$_3$CN (1.5 mM) with 0.1 M [Bu$_4$N][PF$_6$] electrolyte (glassy carbon working electrode, Ag wire pseudoreference, platinum wire counter, scan rate 5,000 mV/s, referenced to Fc/Fc$^+$). No significant return oxidation event is observed upon fast scan rates consistent with the proposed intermediacy of **[1-NH$_3$]*** in the generation the S$_N$Ar product, **1-NH**.

7. DFT Methods and Results

DFT calculations were performed using Gaussian 09.2.[6] Geometry optimization of all the molecules were carried out using the uM062X/6-311++g(d,p) basis sets[7] in benzene using the conductor-like polarizable continuum model (CPCM)[8, 9] implemented in the Gaussian 09 software. Thermal energy corrections were extracted from the results of frequency analysis performed at the same level of theory. Frequency analysis of all the molecules contained no imaginary frequency showing that these are energy minima.

BDFE for C_6F_5OH = 78.91 Kcal/mol
BDFE for Ph_3CH = 71.66 Kcal/mol

Hydrogen radical
Zero-point correction= 0.000000 (Hartree/Particle)
Thermal correction to Energy= 0.001416
Thermal correction to Enthalpy= 0.002360
Thermal correction to Gibbs Free Energy= -0.010654
Sum of electronic and zero-point Energies= -0.498210
Sum of electronic and thermal Energies= -0.496794
Sum of electronic and thermal Enthalpies= -0.495850
Sum of electronic and thermal Free Energies= -0.508865

C_6F_5OH

C	-1.33627800	-0.41960600	0.00000000
C	-1.02885900	0.93262600	0.00000000
C	0.29118500	1.34962300	0.00000000
C	1.33292500	0.42748700	0.00000000
C	1.00315200	-0.92238800	0.00000000
C	-0.31257700	-1.35138800	0.00000000
O	2.60194300	0.87431000	0.00000000
H	3.21691500	0.13090600	0.00000000
F	0.56591600	2.65002300	0.00000000
F	-2.00652500	1.83003300	0.00000000
F	-2.60375100	-0.81713800	0.00000000
F	-0.59050300	-2.64924400	0.00000000
F	1.99822400	-1.81628600	0.00000000

Zero-point correction= 0.064872 (Hartree/Particle)
Thermal correction to Energy= 0.074879
Thermal correction to Enthalpy= 0.075823
Thermal correction to Gibbs Free Energy= 0.029612
Sum of electronic and zero-point Energies= -803.526021
Sum of electronic and thermal Energies= -803.516013
Sum of electronic and thermal Enthalpies= -803.515069
Sum of electronic and thermal Free Energies= -803.561281

C_6F_5O radical

C	0.00176200	-1.33835300	0.00000000
C	-1.22156100	-0.65281000	0.00000000
C	-1.23019300	0.71331100	0.00000000
C	-0.00186800	1.49450100	0.00000000

C	1.22838000	0.71615800	0.00000000
C	1.22338600	-0.65006200	0.00000000
O	-0.00333600	2.72430800	0.00000100
F	-2.37088600	1.36789900	0.00000000
F	-2.34513200	-1.35293500	0.00000000
F	0.00316300	-2.65139800	-0.00000100
F	2.34867300	-1.34749000	0.00000000
F	2.36721000	1.37381900	0.00000000

Zero-point correction= 0.051906 (Hartree/Particle)
Thermal correction to Energy= 0.061567
Thermal correction to Enthalpy= 0.062511
Thermal correction to Gibbs Free Energy= 0.016057
Sum of electronic and zero-point Energies= -802.890810
Sum of electronic and thermal Energies= -802.881149
Sum of electronic and thermal Enthalpies= -802.880205
Sum of electronic and thermal Free Energies= -802.926659

Ph_3CH

C	-1.41660900	3.90242100	-0.42867100
C	-1.96337300	3.25570100	0.67786500
C	-1.48325500	2.00977100	1.06216900
C	-0.45053400	1.38944100	0.35427000
C	0.09399300	2.04566900	-0.74839600
C	-0.38834300	3.29381100	-1.13908000
H	-1.91618400	1.50397600	1.91990200
H	-2.76223600	3.72340100	1.24148900
H	-1.78785800	4.87460200	-0.73048200
H	0.04537200	3.79029000	-1.99935000
H	0.90131800	1.58341000	-1.30562000
C	0.00067700	-0.00019600	0.78696400
H	0.00073700	-0.00026600	1.88274700
C	1.42970900	-0.30447700	0.35433400
C	2.48332100	0.28145500	1.06066600
C	1.72562900	-1.10672900	-0.74649500
C	3.80233300	0.07338100	0.67671100
H	2.26167300	0.91119900	1.91696800
C	3.04764900	-1.31404100	-1.13678300
H	0.92166500	-1.57632800	-1.30237100
C	4.08889500	-0.72626900	-0.42786000
H	4.60682700	0.53269600	1.23921100
H	3.26077600	-1.94009500	-1.99544600
H	5.11643300	-0.89175600	-0.72925800
C	-0.97770600	-1.08521400	0.35410900
C	-1.81604200	-0.94160900	-0.75023100
C	-1.00200600	-2.28876900	1.06351600
C	-2.65734800	-1.98210700	-1.14083100
H	-1.81630700	-0.01204500	-1.30867500
C	-1.84258900	-3.32633000	0.67927900
H	-0.34917100	-2.41097300	1.92248400

C	-2.67404200	-3.17587800	-0.42868700
H	-3.30250600	-1.85456700	-2.00232600
H	-1.85105000	-4.25127400	1.24409000
H	-3.33163700	-3.98245600	-0.73044900

Zero-point correction= 0.292201 (Hartree/Particle)
Thermal correction to Energy= 0.307137
Thermal correction to Enthalpy= 0.308081
Thermal correction to Gibbs Free Energy= 0.247246
Sum of electronic and zero-point Energies= -733.242591
Sum of electronic and thermal Energies= -733.227655
Sum of electronic and thermal Enthalpies= -733.226711
Sum of electronic and thermal Free Energies= -733.287546

Ph$_3$C radical

C	2.60549200	-3.39501400	-0.00000600
C	1.38565600	-3.44515300	-0.67188200
C	0.53761500	-2.34720900	-0.66930400
C	0.88907600	-1.15881500	0.00017100
C	2.12806600	-1.12657400	0.66936900
C	2.96927800	-2.22989800	0.67212200
H	-0.40241400	-2.39279600	-1.20680800
H	1.09744800	-4.34275500	-1.20649500
H	3.26506600	-4.25444900	-0.00001300
H	3.91097500	-2.18333200	1.20654600
H	2.41517900	-0.23045200	1.20712100
C	-0.00020000	0.00002000	-0.00016600
C	0.55902800	1.34940200	-0.00024900
C	1.76415900	1.63882000	-0.66947000
C	-0.08817300	2.40615900	0.66916200
C	2.29120300	2.92223800	-0.67198500
H	2.27344600	0.84723800	-1.20682100
C	0.44687800	3.68628600	0.67196800
H	-1.00808700	2.20664000	1.20640400
C	1.63818400	3.95352800	0.00013700
H	3.21301900	3.12092900	-1.20614100
H	-0.06416500	4.47856500	1.20647600
H	2.05320300	4.95425800	0.00035400
C	-1.44837600	-0.19051700	-0.00025600
C	-2.03990400	-1.27964100	0.66896600
C	-2.30186100	0.70853200	-0.66905900
C	-3.41605700	-1.45654900	0.67178100
H	-1.40728100	-1.97659500	1.20619900
C	-3.67687000	0.52290300	-0.67176800
H	-1.87159100	1.54574400	-1.20625700
C	-4.24333800	-0.55849600	0.00021100
H	-3.84644400	-2.29538500	1.20627900
H	-4.31002800	1.22189800	-1.20570500
H	-5.31746100	-0.69963800	0.00041600

```
Zero-point correction=                    0.279615 (Hartree/Particle)
Thermal correction to Energy=                 0.294213
Thermal correction to Enthalpy=                0.295157
Thermal correction to Gibbs Free Energy=        0.236320
Sum of electronic and zero-point Energies=         -732.621189
Sum of electronic and thermal Energies=           -732.606591
Sum of electronic and thermal Enthalpies=          -732.605647
Sum of electronic and thermal Free Energies=        -732.664484
```

8. References

1. A. Wong, J. Chu, G. Wu, J. Telser, R. Dobrovetsky and G. Ménard, *Inorg. Chem.*, 2020, **59**, 10343-10352.
2. E. S. Jang, C. L. McMullin, M. Käß, K. Meyer, T. R. Cundari and T. H. Warren, *J. Am. Chem. Soc.*, 2014, **136**, 10930-10940.
3. M. Gomberg, *J. Am. Chem. Soc.*, 1900, **22**, 757-771.
4. S. Kundu, S. Sinhababu, M. M. Siddiqui, A. V. Luebben, B. Dittrich, T. Yang, G. Frenking and H. W. Roesky, *J. Am. Chem. Soc.*, 2018, **140**, 9409-9412.
5. P. A. Chase, A. L. Gille, T. M. Gilbert and D. W. Stephan, *Dalton Trans.*, 2009, 7179-7188.
6. *Gaussian 09*, *Revision D.01*, M. J. Frisch, G. W. Trucks, H. B. Schlegel, G. E. Scuseria, M. A. Robb, J. R. Cheeseman, G. Scalmani, V. Barone, B. Mennucci, G. A. Petersson, H. Nakatsuji, M. Caricato, X. Li, H. P. Hratchian, A. F. Izmaylov, J. Bloino, G. Zheng, J. L. Sonnengerg, M. Hada, M. Ehara, K. Toyota, R. Fukuda, J. Hasegawa, M. Ishida, T. Nakajima, Y. Honda, O. Kitao, H. Nakai, T. Vreven, J. A. Montgomery Jr, J. E. Peralta, F. Ogliaro, M. Bearpark, J. J. Heyd, E. Brothers, K. N. Kudin, V. N. Staroverov, T. Keith, R. Kobayashi, J. Normand, K. Raghavachari, A. Rendell, J. C. Burant, S. S. Iyengar, J. Tomasi, M. Cossi, N. Rega, N. J. Millam, M. Klene, J. E. Knox, J. B. Cross, V. Bakken, C. Adamo, J. Jaramillo, R. Gomperts, R. E. Stratmann, O. Yazyev, A. J. Austin, R. Cammi, C. Pomelli, J. W. Ochterski, R. L. Martin, K. Morokuma, V. G. Zakrzewski, G. A. Voth, P. Salvador, J. J. Dannenberg, S. Dapprich, A. D. Daniels, Ö. Farkas, J. B. Foresman, J. V. Ortiz, J. Cioslowski and D. J. Fox, Gaussian, Inc., Wallingford CT, 2010.
7. Y. Zhao and D. Truhlar, *Theor. Chem. Acc.*, 2008, **120**, 215-241.
8. V. Barone and M. Cossi, *J. Phys. Chem. A*, 1998, **102**, 1995-2001.
9. M. Cossi, N. Rega, G. Scalmani and V. Barone, *J. Comput. Chem.*, 2003, **24**, 669-681.